AD-767 289

FUNDAMENTAL STUDIES OF SEMICONDUCTOR HETEROEPITAXY

ROCKWELL INTERNATIONAL CORP.

PREPARED FOR
ARMY MISSILE COMMAND
ADVANCED RESEARCH PROJECTS AGENCY

AUGUST 1973

DISTRIBUTED BY:

NTIS
National Technical Information Service
U. S. DEPARTMENT OF COMMERCE

AD

AD 767289

FUNDAMENTAL STUDIES OF SEMICONDUCTOR HETEROEPITAXY

FINAL REPORT

PART III, APPENDICES

DDC
RECEIVED
OCT 1 1973
C

ARPA Support Office
Research, Development, Engineering and Missile Systems Laboratory
United States Army Missile Command AMSMI RND
Redstone Arsenal
Huntsville, Alabama
Contract No. DAAH01-70-C-1311

Distribution of this document
is unlimited.

Sponsored by:
Advanced Research Projects Agency
ARPA Order No. 1585

DISTRIBUTION STATEMENT A
Approved for public release;
Distribution Unlimited
Reproduced by
NATIONAL TECHNICAL
INFORMATION SERVICE
US Department of Commerce
Springfield, VA. 22151

AD

FUNDAMENTAL STUDIES OF SEMICONDUCTOR HETEROEPITAXY

FINAL REPORT

PART III, APPENDICES

R. P. Ruth, A. J. Hughes, J. L. Kenty, H. M. Manasevit.
D. Medellin, A. C. Thorsen, Y. T. Chan, C. R. Viswanathan, and M. A. Ring

Research and Technology Division
Electronics Group
Rockwell International

August 1973

ARPA Support Office
Research, Development, Engineering and Missile Systems Laboratory
United States Army Missile Command AMSMI RND
Redstone Arsenal
Huntsville, Alabama
Contract No. DAAH01-70-C-1311

Distribution of this document
is unlimited.

Sponsored by:
Advanced Research Projects Agency
ARPA Order No. 1585

Security Classification

DOCUMENT CONTROL DATA - R & D

(Security classification of title, body of abstract and indexing annotation must be entered when the overall report is classified)

1. ORIGINATING ACTIVITY (Corporate author)
Rockwell International Corp., Electronics Group
Electronics Research Division
Anaheim, California

2a. REPORT SECURITY CLASSIFICATION
Unclassified

2b. GROUP

3. REPORT TITLE
Fundamental Studies of Semiconductor Heteroepitaxy, Part III

4. DESCRIPTIVE NOTES (Type of report and inclusive dates)
Final Report, June 1970 through June 1973

5. AUTHOR(S) (First name, middle initial, last name)
Ralph P. Ruth, A. James Hughes, Joseph L. Kenty, Harold M. Manasevit, Arthur C. Thorsen, Y. T. Chan, C. R. Viswanathan, Morey A. Ring

6. REPORT DATE
August 1973

7a. TOTAL NO. OF PAGES
155

7b. NO. OF REFS

8a. CONTRACT OR GRANT NO.
DAAH01-70-C-1311

b. PROJECT NO.

c.

d.

9a. ORIGINATOR'S REPORT NUMBER(S)
C71-86/501

9b. OTHER REPORT NO(S) (Any other numbers that may be assigned this report)

10. DISTRIBUTION STATEMENT
Distribution of this document is unlimited.

11. SUPPLEMENTARY NOTES

12. SPONSORING MILITARY ACTIVITY
Advanced Research Projects Agency
ARPA Order No. 1585
Washington, D.C.

13. ABSTRACT

The results of a three-year research program are described. The overall objective of the program was to carry out a fundamental study of nucleation and film growth mechanisms in heteroepitaxial semiconductor thin films. The specific technical objectives were 1) investigation of various aspects of the mechanisms of heteroepitaxial film growth, to establish technical guidelines for the preparation of better films; 2) preparation of improved, high-quality, device-grade heteroepitaxial films of Si and GaAs on insulating substrates by chemical vapor deposition (CVD) methods; 3) development of new or improved methods of characterizing heteroepitaxial semiconductor films; and 4) design and fabrication of selected thin-film devices taking advantage of the unique properties of heteroepitaxial films. The program involved both theoretical and experimental investigations of nucleation and growth mechanisms and development of improved techniques for film and substrate preparation and characterization. The CVD method of growing semiconductor films was emphasized because of its importance in the semiconductor device industry. Main emphasis was on the Si-on-Al_2O_3 system, with attention also given to the Si-on-$MgAl_2O_4$ and GaAs-on-Al_2O_3 systems. The work was divided among seven subtasks: 1) theory of epitaxy and heteroepitaxial interfaces; 2) deposition studies and film growth; 3) analysis and purification of CVD reactants; 4) preparation and characterization of substrates; 5) studies of *in situ* CVD film growth in the electron microscope; 6) evaluation of film properties; and 7) design and fabrication of special devices.

DD FORM 1 NOV 68 1473

Security Classification

Security Classification

14 KEY WORDS	LINK A		LINK B		LINK C.	
	ROLE	WT	ROLE	WT	ROLE	WT
Epitaxy						
GaAs						
Si						
Al_2O_3 (sapphire)						
$MgAl_2O_4$ (spinel)						
Chemical vapor deposition (CVD)						
In situ film growth						
Electron microscopy						
Epitaxy theory						
Heteroepitaxy						
Thin-film devices						
Semiconductors						
Film nucleation						
Transport properties						
Metalorganic compounds						
Physical vapor deposition (PVD)						
Substrate						
Polishing						
Gas-phase etching						
Anisotropy						
Thermally induced stress						
Piezoresistance						

Principal technical accomplishments include 1) experimental discovery and empirical characterization of significant anisotropy in the electrical properties of Si/Al_2O_3 films of several crystallographic orientations, and theoretical explanation of the effects in terms of a model that combines thermally-induced stresses due to expansion coefficient differences with the piezoresistance effect in Si; 2) delineation of preferred substrate orientations, deposition temperatures, film growth rates, and carrier gas atmosphere for optimized film properties in the Si/Al_2O_3 and $Si/MgAl_2O_4$ systems; 3) identification of the influence of surface-state conduction on measured electrical properties in Si films with carrier concentrations $<10^{16}cm^{-3}$; 4) identification of the role of the Al_2O_3 surface as a catalyst for the pyrolytic decomposition of SiH_4 in the formation of Si films by CVD; 5) development of gas-phase etching and improved mechanical polishing techniques for preparing surfaces of Al_2O_3 and $MgAl_2O_4$ substrates for the heteroepitaxial growth of semiconductor films; 6) development of an ion-beam sputtering technique for preparing ultrathin (<500Å) regions in Al_2O_3 substrates for transmission electron microscopy; 7) observation of the in situ growth of Si by physical vapor deposition (PVD) and CVD on Al_2O_3 and amosphous carbon substrates in the electron microscope; 8) observation and characterization of the transport of photoinjected electrons through single-crystal Al_2O_3; 9) measurement of carrier lifetimes in Si heteroepitaxial films on Al_2O_3 and correlation of lifetimes with various experimental parameters; 10) determination of surface-state density distributions in Si heteroepitaxial films on Al_2O_3; and 11) the successful fabrication in Si/Al_2O_3 of charge-coupled devices exhibiting good charge-transfer efficiency at high frequencies. Details of these and other results and investigations are given by means of data tabulations, graphs, photographs, and narrative. An extensive bibliography of electron microscope in situ film nucleation and growth studies is also included. The report is bound in three separate parts.

Security Classification

ABSTRACT

The results of a three-year research program are described. The overall objective of the program was to carry out a fundamental study of nucleation and film growth mechanisms in heteroepitaxial semiconductor thin films. The specific technical objectives were 1) investigation of various aspects of the mechanisms of heteroepitaxial film growth, to establish technical guidelines for the preparation of better films; 2) preparation of improved, high-quality, device-grade heteroepitaxial films of Si and GaAs on insulating substrates by chemical vapor deposition (CVD) methods; 3) development of new or improved methods of characterizing heteroepitaxial semiconductor films; and 4) design and fabrication of selected thin-film devices taking advantage of the unique properties of heteroepitaxial films.

The program involved both theoretical and experimental investigations of nucleation and growth mechanisms and development of improved techniques for film and substrate preparation and characterization. The CVD method of growing semiconductor films was emphasized because of its importance in the semiconductor device industry. Main emphasis was on the Si-on-Al_2O_3 system, with attention also given to the Si-on-$MgAl_2O_4$ and GaAs-on-Al_2O_3 systems. The work was divided among seven subtasks: 1) theory of epitaxy and heteroepitaxial interfaces; 2) deposition studies and film growth; 3) analysis and purification of CVD reactants; 4) preparation and characterization of substrates; 5) studies of *in situ* CVD film growth in the electron microscope; 6) evaluation of film properties; and 7) design and fabrication of special devices.

Principal technical accomplishments include 1) experimental discovery and empirical characterization of significant anisotropy in the electrical properties of Si/Al_2O_3 films of several crystallographic orientations, and theoretical explanation of the effects in terms of a model that combines thermally-induced stresses due to expansion coefficient differences with the piezoresistance effect in Si; 2) delineation of preferred substrate orientations, deposition temperatures, film growth rates, and carrier gas atmosphere for optimized film properties in the Si/Al_2O_3 and $Si/MgAl_2O_4$ systems; 3) identification of the influence of surface-state conduction on measured electrical properties in Si films with carrier concentrations $<10^{16}cm^{-3}$; 4) identification of the role of the Al_2O_3 surface as a catalyst for the pyrolytic decomposition of SiH_4 in the formation of Si films by CVD; 5) development of gas-phase etching and improved mechanical polishing techniques for preparing surfaces of Al_2O_3 and $MgAl_2O_4$ substrates for the heteroepitaxial growth of semiconductor films; 6) development of an ion-beam sputtering technique for preparing ultrathin (<500Å) regions in Al_2O_3 substrates for transmission electron microscopy; 7) observation of the *in situ* growth of Si by physical vapor deposition (PVD) and CVD on Al_2O_3 and amorphous carbon substrates in the electron microscope; 8) observation and characterization of the transport of photoinjected electrons through single-crystal Al_2O_3; 9) measurement of carrier lifetimes in Si heteroepitaxial films on Al_2O_3 and

correlation of lifetimes with various experimental parameters; 10) determination of surface-state density distributions in Si heteroepitaxial films on Al_2O_3; and 11) the successful fabrication in Si/Al_2O_3 of charge-coupled devices exhibiting good charge-transfer efficiency at high frequencies.

Details of these and other results and investigations are given by means of data tabulations, graphs, photographs, and narrative. An extensive bibliography of electron microscope *in situ* film nucleation and growth studies is also included. The report is bound in three separate parts.

PROGRAM SUMMARY

The overall objective of this three-year program was to carry out a fundamental study of nucleation and film growth mechanisms in heteroepitaxial semiconductor thin-film systems which would lead to new knowledge and understanding of these processes, and then to apply the results to the preparation of improved semiconductor thin films and thin-film devices on insulating substrates.

The specific technical objectives were the following: 1) investigation of various aspects of the mechanisms of heteroepitaxial film growth, to establish technical guidelines for the preparation of better films which could be applied to real situations; 2) preparation of improved, high-quality, device-grade heteroepitaxial films of Si and GaAs on insulating substrates by chemical vapor deposition (CVD) methods; 3) development of methods of characterizing heteroepitaxial films as to their suitability for subsequent device fabrication; and 4) design and fabrication of selected thin-film devices which take advantage of the unique properties of such films.

The plan for accomplishing these objectives involved the study of the fundamentals of heteroepitaxial semiconductor film growth on insulating substrates as the primary activity, with specialized device fabrication used as a means both of evaluating film properties and of exploiting certain unique properties of heteroepitaxial semiconductor-insulator systems. Both theoretical and experimental investigations were involved. The theoretical studies consisted of two types: 1) direct interaction with the experimental program, involving data analyses, suggestion of definitive experiments, and postulation of specific models to explain experimental observations; 2) development of original contributions to the theory of heteroepitaxial growth. The experimental investigations were also of two types: 1) fundamental explorations to delineate mechanisms and general empirical principles of the heteroepitaxial growth process; 2) practical device studies accompanying the fundamental investigations, so that new developments could be applied to the improvement of films and thin-film devices.

The chemical vapor deposition (CVD) method of growing semiconductor films was emphasized because of its importance in the semiconductor device industry. Main emphasis was on the Si-on-Al_2O_3 system, with attention also given to the Si-on-$MgAl_2O_4$ and GaAs-on-Al_2O_3 systems. The work was divided among seven subtasks: 1) theory of epitaxy and heteroepitaxial interfaces; 2) deposition studies and film growth; 3) analysis and purification of CVD reactants; 4) preparation and characterization of substrates; 5) studies of <u>in situ</u> CVD film growth in the electron microscope; 6) evaluation of film properties; and 7) design and fabrication of special devices.

The program was carried out primarily at facilities of the Electronics Group of the Rockwell International Corporation, by Rockwell personnel. Parts of three of the specific subtasks were performed by personnel of the University of California at Los Angeles (UCLA), in the Department of Electrical Sciences and Engineering and the Chemistry Department. Work on another subtask was done in part in the Department of Chemistry of California State University, San Diego (CSUSD). Both the UCLA and the CSUSD programs were supported by subcontracts from Rockwell.

The principal technical accomplishments of the program include the following: 1) experimental discovery and extensive characterization of significant anisotropy in the electrical properties of Si/Al_2O_3 films, and theoretical explanation of the effect in terms of a model that combines thermally-induced stresses with the piezoresistance effect in Si; 2) delineation of preferred substrate orientations, deposition temperatures, film growth rates, and carrier gas atmospheres for optimized film properties in the Si/Al_2O_3 and $Si/MgAl_2O_4$ systems; 3) identification of the influence of surface-state conduction on measured electrical properties in Si films with carrier concentrations $<10^{16}cm^{-3}$; 4) identification of the catalytic role of the Al_2O_3 surface in the heterogeneous pyrolytic decomposition of SiH_4 to form Si films by CVD; 5) development of gas-phase etching and improved mechanical polishing techniques for preparing surfaces of Al_2O_3 and $MgAl_2O_4$ for the heteroepitaxial growth of semiconductor films; 6) development of an ion-beam sputtering technique for preparing ultrathin (<500Å) regions in Al_2O_3 substrates for transmission electron microscopy; 7) observation of the in situ growth of Si by physical vapor deposition (PVD) and by CVD on Al_2O_3 and amorphous carbon substrates in the electron microscope; 8) observation and characterization of the transport of photoinjected electrons through single-crystal Al_2O_3; 9) measurement of carrier lifetimes in Si heteroepitaxial films on Al_2O_3; 10) determination of surface-state density distributions in Si heteroepitaxial films on Al_2O_3; and 11) the successful fabrication in Si/Al_2O_3 of charge-coupled devices exhibiting good charge-transfer efficiency at high frequencies.

A summary of the work of the contract program by subtask follows:

Subtask 1: Theory of Epitaxy and Heteroepitaxial Interfaces. Several separate investigations were carried out in attempts to model heteroepitaxial systems. An extension of the island alignment model using a Gaussian-atom Fourier-transform technique, the Frank-van der Merwe model, a Green's-function/Wannier-function approach, a contrived potential-energy model, and a molecular-orbital method for developing the heteroepitaxial interface were all critically reviewed for the purpose, and all were found inadequate for application to the real systems of interest. A two-body interatomic potential method, although also initially rejected, was finally adopted for modeling the Al_2O_3 lattice with Morse potentials and a suitable computer program; mechanical stability and surface reconstruction phenomena in Al_2O_3 were treated successfully by this method, involving relaxation of the several atomic planes nearest the Al_2O_3 surface. An electron-on-network method was also considered for determination of surface atom configurations and interfacial binding energies in situations where the surface structure is allowed to relax, but was also eventually found inadequate for realistic calculations in heteroepitaxial systems.

Extension of the modeling to the Si/Al_2O_3 composite was interrupted by the theoretical investigation of the effects on electrical properties of stresses in the Si films resulting from differential thermal contraction of substrate and film, prompted by the experimental observation of ~10% anisotropy in the carrier mobility in (001)Si/Al_2O_3 and ~40% anisotropy in (221)Si/Al_2O_3. A model combining thermal expansion stress and the piezoresistance effect, incorporating the anisotropies in substrate thermal expansion, Si elastic constants, and Si piezoresistance coefficients, was developed and applied to (001), (221) and (111)Si

films on Al_2O_3. Excellent agreement was obtained between theory and experiment in the first two cases; the amount of anisotropy and the directions (in the plane of the film) of maximum and minimum carrier mobility were correctly predicted. In (111)Si (on two different Al_2O_3 substrate orientations), however, the theoretically predicted effects were too small to account for the experimental observations, indicating that other (not yet identified) phenomena are more important in determining anisotropy in the (111)Si/Al_2O_3 system.

Extensive calculations were made for the general (xxl)Si orientation ($0 \leq x \leq \infty$), which defines all Si orientations along the zone that includes (001), (111), (221), and (110)Si and thus all of the Si/Al_2O_3 epitaxy modes of major interest. For n-type Si/Al_2O_3, the predicted stress effects ranged from a ~30% reduction for (001)Si to a ~25% enhancement in maximum mobility near (110)Si. For p-type Si films, the predicted stress effect is always a mobility enhancement, with the maximum mobility ranging from ~1.07μ_o for (001)Si to ~2.4μ_o for (110)Si, where μ_o is the zero-stress mobility. It is significant that the Si film orientation most used in commercial devices - (001) - is the one showing the lowest mobilities of all those investigated. Thus, considerable improvement in performance of certain types of devices could be realized by exploiting these predicted effects, which have major significance for heteroepitaxial device technology.

Subtask 2: Deposition Studies and Film Preparation. A major part of the work of this subtask consisted of preparing a variety of Si and GaAs heteroepitaxial film samples for use in other parts of the program. Experimental investigations of the effects of various deposition parameters upon the properties of Si and GaAs films continued throughout the program, including examination of the following: 1) dependence of electrical properties on growth temperature, growth rate, and crystallographic orientation of substrate (including the $(11\bar{2}0)$ orientation, not previously used for heteroepitaxy studies); 2) variations in Si film properties with thickness; 3) formation and properties of p-type Si/Al_2O_3 films; 4) effects of autodoping (at temperatures above ~1050C) in Si films on Al_2O_3 and $MgAl_2O_4$; 5) effects of reactor configuration on film properties; 6) characteristics of early-stage growth of Si films on Al_2O_3; 7) growth of Si films by SiH_4 pyrolysis at reduced pressures (1 to 10 torr); 8) growth of Si films in gaseous atmospheres other than pure H_2; 9) effects of annealing during growth on properties of Si films (no significant improvement in film properties observed); and 10) growth of GaAs films on Al_2O_3 and $MgAl_2O_4$. These studies revealed the strong interrelationships that exist among the various parameters involved in optimizing Si growth on insulators. Evaluation of the electrical properties of Si films on Al_2O_3 demonstrated that growth conditions (1) must be optimized for the particular substrate orientation chosen; (2) differ for those Al_2O_3 orientations which produce the same Si orientation; (3) are dependent upon reactor geometry and gaseous atmosphere; and (4) must be optimized for the particular film thickness desired.

Based on electrical properties of the films grown, the preferred substrate for Si heteroepitaxy was identified as one that produces (111)Si growth rather than (100)Si growth, namely $\sim(11\bar{2}0)Al_2O_3$ or $(111)MgAl_2O_4$, the highest mobilities being obtained on $(111)MgAl_2O_4$. Optimum growth temperatures varied with substrate orientation: (100)Si on $(01\bar{1}2)Al_2O_3$, 1050-1075C; (111)Si on $(10\bar{1}4)Al_2O_3$, 1075-1100C; (111)Si on $\sim(11\bar{2}0)Al_2O_3$, 1075-1100C; and (111)Si on $(111)MgAl_2O_4$, ~1025C. The preferred growth atmosphere appeared to be either H_2 or a $He-H_2$

mixture for growth on $(01\bar{1}2)Al_2O_3$ or ~$(11\bar{2}0)Al_2O_3$, but both $(10\bar{1}4)Al_2O_3$ and $(111)MgAl_2O_4$ apparently need a He-rich atmosphere (~90% He-10% H_2) for obtaining high quality films. For essentially every orientation studied, growth rates from ~2μm/min to ~4μm/min were found sufficient, although good growth was also achieved on $(01\bar{1}2)Al_2O_3$ at lower rates. These growth conditions are optimum for the reactor system used, but should be useful guides for CVD film growth in systems with other reactor geometries. These observations should lead to definite improvements in Si/Al_2O_3 film properties and thus to improved performance and reliability in Si/Al_2O_3 devices and circuits.

Subtask 3: Analysis and Purification of CVD Reactants. Since the impurity content of the various reactants used for CVD of Si and GaAs heteroepitaxial films probably provides the real limitation on the achievable impurity levels in the films themselves, a study was undertaken to attempt to identify and establish the concentrations of the principal impurities in the reactants that might influence the film properties if they were to become incorporated into the films during growth. During the first year, techniques of gas chromatography were developed for analysis of the reactants used for Si and GaAs heteroepitaxy by CVD, with silicone oil and polymer columns used for the chromatography. Several extraneous impurity peaks were observed in the chromatograms of SiH_4 samples, and diborane (B_2H_6) was tentatively identified as a significant impurity (~10 ppm), although not confirmed by mass spectrometer techniques. Small quantities of purified SiH_4, free of diborane, were prepared by successive injections in the chromatograph, but the quantities were too small for use in laboratory CVD experiments. Beginning in the second year of the program, samples of SiH_4 and of trimethylgallium (TMG) used for Si and GaAs CVD experiments were analyzed for impurity content by sensitive mass spectrometric techniques. Disilane and trimethylsilane, together with several other impurities of less concern, were found in the SiH_4 samples.

Significant impurity concentrations in some of the reactants (especially SiH_4) at times limited the accuracy of the study of the effects of deposition parameters on Si film properties. Cooperative efforts with vendors for preparation of improved-purity reactants continued throughout the program, as did analyses of reactants by mass spectrometer techniques. It was made clear that significant differences occurred in the purity of reactant materials; not only did they vary from supplier to supplier but also different tanks of the same material from the same supplier were not consistent in purity. Another problem was the lack of agreement in the analyses supplied by different analytical laboratories for the same tank of reactant and the differences in detection limits for the same element or compound that different laboratories possessed, making it difficult to determine which results were the most reliable and which supplier of gases was best. A "use test" still appears to be the most reasonable way of evaluating materials for the intended application. The analyses demonstrated the ultimate lack of understanding of the role of impurities in epitaxial film growth and the minimum requirements for the analytical methods that should be used in detecting these impurities. An extensive collaborative study involving the reactant supplier, the analytical laboratory, and the ultimate user is needed.

To examine some of the fundamentals of the chemistry and reaction kinetics of the CVD processes used for growing heteroepitaxial films of Si and GaAs, investigations of the reactions involved in the formation of Si by SiH_4 pyrolysis and of GaAs by the trimethylgallium (TMG)-AsH_3 reaction were undertaken. The influence of the Al_2O_3 surface on the mechanism of decomposition of SiH_4 as a function of temperature, and the decomposition modes and reaction products of TMG and

AsH_3 as functions of temperature, concentration ratio, and H_2 partial pressure (to attempt to determine the requirements for formation of optimum-quality GaAs) were examined. It was found that the surface of single-crystal Al_2O_3 does catalyze the thermal decomposition of SiH_4, whereas the pyrolysis is homogeneous over a Si surface. No effect of preheating the Al_2O_3 to temperatures as high as 1200C was found. A variety of observations made on the TMG-AsH_3 system included the following, among others: 1) GaAs does result from the reaction of TMG with AsH_3, and an excess of AsH_3 should be used in any application of the process; and 2) both CH_4 (methane) and H_2 are produced in the series of stepwise reactions leading to the final product. Further study of the reaction at high temperatures is recommended.

Subtask 4: Preparation and Characterization of Substrates. It was demonstrated that Al_2O_3 surfaces prepared by mechanical polishing techniques and used routinely for semiconductor heteroepitaxy typically had severe surface and subsurface damage, with many scratches often several microns deep yet often rendered invisible to close inspection because of amorphous or fine-grained debris embedded in the scratches in the final polishing stages. Early in the second year a much improved technique for mechanical polishing of $(10\bar{1}4)Al_2O_3$ was developed, and very good surfaces in this previously troublesome orientation were then obtained. Gas-phase etching/polishing procedures using SF_6 and various fluorinated halocarbons in the 1350 to 1500C temperature range were found to produce essentially scratch-free surfaces on $(01\bar{1}2)$ and near-$(11\bar{2}0)Al_2O_3$ substrates. Extensive gas-phase etch-rate data were obtained as a function of crystallographic orientation in this temperature range. The technique was further developed for (1) thinning Al_2O_3 substrates; (2) evaluating the effects of prolonged etching on $(01\bar{1}2)$, (0001), and ~$(11\bar{2}0)Al_2O_3$; and (3) assessing the subsurface damage caused by various mechanical polishing procedures. Evaluation of mechanical polishing methods for $MgAl_2O_4$ surfaces indicated that surface fill-in occurs for this material, just as for Al_2O_3. Some exploratory gas-phase etching experiments with $MgAl_2O_4$ surfaces were also carried out during the second year of the program.

Ion-beam sputtering techniques were developed for preparing ultra-thin (~200Å)Al_2O_3 wafers for use as substrates in the in situ CVD experiments with Si. Wafers successfully thinned to ~50μm or less by mechanical polishing techniques were subsequently thinned by ion etching to the point of perforation in some areas, resulting in adjoining regions of thicknesses suitable for transmission electron microscopy as applied in the in situ experiments. Three different Al_2O_3 orientations were successfully thinned by this method - (0001), $(10\bar{1}4)$, and $(01\bar{1}2)$. Considerable study of properties of the resulting thinned substrates was carried out, and improvements in the ion-thinning process were realized during the final year of the program, when the thinned substrates were used in the in situ CVD experiments (Subtask 5).

Mechanical lapping and polishing methods that produce good quality surfaces suitable for use as substrates for epitaxy were developed during the contract for several orientations of Al_2O_3 - (0001), $(01\bar{1}2)$, $(10\bar{1}4)$, $(11\bar{2}0)$, ~6 deg off $(11\bar{2}0)$ and $(11\bar{2}2)$. By means of etch-rate techniques developed for this

material it was possible to determine the apparent depth of damage in Al_2O_3 substrate wafers at various stages of preparation. At a given stage in the processing, the damage depth was found to increase for various orientations in the following order: $(10\bar{1}4)$, $(11\bar{2}0)$, $(01\bar{1}2)$, and (0001).

A technique utilizing the photoelectric process in a metal-insulator-semiconductor structure, consisting of an Al_2O_3 substrate with a Si or GaAs film grown on one surface and a semitransparent Al film on the other, demonstrated that photoexcited electrons from either the semiconductor or the metal film can be transported through single-crystal Al_2O_3 of several mils thickness. Further study of the charge transport process also established that (1) the Al_2O_3 used for substrates for growth of heteroepitaxial semiconductor films has trap levels approximately 0.18 eV below the conduction band; (2) the transport of photoinjected electrons occurs through the Poole-Frenkel conduction mechanism; and (3) the quantum efficiency for the photoelectric process is quite low, approximately 10^{-5}.

Routine characterization of substrate surfaces at various stages of preparation continued throughout the program, utilizing various standard techniques of x-ray and electron diffraction analysis and optical and electron (including scanning) microscopy.

Subtask 5: Studies of <u>in situ</u> Film Growth in the Electron Microscope.

In the first year of the program many of the modifications required in the transmission electron microscope for <u>in situ</u> observation of the nucleation and early-stage growth of CVD semiconductor films on insulating substrates were completed. Early in the second year a series of electron microscope modifications and tests was finished, culminating in the first series of successful PVD experiments inside the electron microscope. Al was deposited onto a heated carbon substrate and a sequence of micrographs was taken during the growth process, demonstrating the feasibility of performing <u>in situ</u> nucleation and growth studies in the equipment. Additional <u>in situ</u> PVD experiments were carried out in the second year, with both Al and Au deposited onto amorphous carbon substrates to delineate further the required techniques and experimental problems to be encountered in the later CVD experiments. Calculations and design for the CVD microchamber were also completed during the second year, and the fabrication of the microchamber and associated hardware was begun.

During the final year of the program the fabrication of the CVD microchamber and its mounting flange was completed, and a gas-handling manifold was installed on the electron microscope. Gas flow experiments were performed to determine the flow rate of gas through the microchamber as a function of pressure and to determine the maximum pressure attainable in the microchamber.

In addition, a number of <u>in situ</u> Si CVD experiments were performed resulting in the successful growth of Si films in the electron microscope by the pyrolysis of SiH_4. The nucleation and early growth of Si on both amorphous carbon and single-crystal Al_2O_3 substrates was observed, leading to the following conclusions: 1) the pyrolysis of SiH_4 to form Si films by CVD inside the electron microscope is feasible; 2) the <u>in situ</u> study by trans-

mission electron microscopy of the post-nucleation and early growth stages of a semiconductor film grown by CVD is feasible; 3) the nucleation and early growth processes for CVD Si are fundamentally similar to those of metal films grown by PVD, although some specific differences exist; 4) single-crystal Si growth on $(01\bar{1}2)Al_2O_3$ results primarily from the growth of nuclei of a preferred orientation at the expense of randomly oriented nuclei, and not from the large nucleation rate of these favorably oriented nuclei; 5) the ion-beam sputtering process can produce electron-transparent Al_2O_3 suitable for use as substrates for in situ CVD film growth experiments.

Subtask 6: Evaluation of Film Properties. From the beginning of the program, routine evaluation of film properties was carried out by established methods of x-ray and electron diffraction analysis, metallographic analysis, and electrical measurements of transport properties. A new technique for evaluating the characteristics of the interfacial region of heteroepitaxial films was developed, involving measurements of photoelectron emission from monochromatically-illuminated films in the MIS configuration on insulating substrates (see Subtask 4). Photocurrents due to electron transport through the single-crystal Al_2O_3 substrates were measured as a function of photon energy, permitting determination of various parameters in the Si/Al_2O_3 and $GaAs/Al_2O_3$ systems. These measurements gave values of 1.0eV for the electron affinity of Al_2O_3, 3.15eV for the barrier height at an Al_2O_3-Al interface, 4.50eV for the $Si-Al_2O_3$ interface barrier height, ~0.37eV for the band-bending in Si near the $Si-Al_2O_3$ interface, ~0.10eV for the band-bending in GaAs films near the Al_2O_3 interface, and electron escape lengths of at least 12μm in Si and 23μm in GaAs. Values for the work function of various metals were also determined by these measurements.

Determination of the energy spectrum of back-scattered proton or alpha-particle beams injected in channeling directions in heteroepitaxial semiconductor films was investigated as a means of measuring the density and the location of structural defects in the films. Experiments indicated that Si/insulator films have less imperfect interfacial regions than do GaAs/insulator films. The best structures of those examined were found in (100)Si films on $(01\bar{1}2)Al_2O_3$ substrates and in (111)Si films grown on near-$(11\bar{2}0)Al_2O_3$ substrates. Information on the early growth stages of Si on Al_2O_3 was also obtained by conventional transmission electron microscopy of very thin Si films grown on ion-thinned Al_2O_3 substrates in a conventional (atmospheric-pressure) vertical-flow CVD reactor. These experiments showed that the growth of a single-crystal Si film by CVD is the result of coalescence processes in the early growth stages and not of nucleation phenomena alone, producing films with a relatively higher incidence of defects and relatively lower carrier mobilities.

Rapid acquisition of data on electrical properties of the films was very important to the conduct of film growth experiments, especially in the second and third years; measurements of film conductivity type, resistivity, carrier concentration, and carrier mobility were made routinely on a majority of the epitaxial samples prepared on the program, utilizing either the van der Pauw method or the more accurate and conventional Hall-effect bridge method. These data were essential for the study of the effects of changes in deposition parameters on Si/Al_2O_3 and $Si/MgAl_2O_4$ film properties, and provided

considerable insight into the factors which most strongly influence film quality so that identification of the conditions for optimized film growth could be made.

It was determined that the electrical properties of undoped n-type heteroepitaxial Si films grown on various orientations of Al_2O_3 (and also $MgAl_2O_4$) by the pyrolysis of SiH_4 are dominated by surface-state conduction for carrier concentrations of $\sim 10^{16} cm^{-3}$ or below. It was found that there were inhomogeneities in the donor concentration of typical CVD Si/Al_2O_3 films over the film area, and that a concentration gradient existed from the center of the susceptor radially outward; films reflected this variation depending upon the placement of the substrate on the susceptor during CVD growth. Gas flow characteristics or a non-uniform temperature of the rf-heated pedestal (susceptor) were thought to account for the effect. Measurements were made of the variation of electrical properties of Si/Al_2O_3 with temperature, and some of the observed effects were attributed to high defect densities (e.g., deep-lying donor levels) or inhomogeneous strains in the films.

The most significant development to come from the film evaluation procedures was the observation of the anisotropy in electrical properties in Si/Al_2O_3 films. Mobility measurements as a function of azimuthal direction (every 18 deg) in the film plane indicated a maximum mobility in two directions and a minimum mobility in two directions, the latter displaced by 90 deg from the former. The mobility anisotropy factor A, defined as the ratio of the difference between the maximum and minimum values of mobility in the plane of the film to the average value of the mobility in that plane, was found to be about 40% for $(221)Si/(11\bar{2}2)Al_2O_3$ and about 9% for $(001)Si/01\bar{1}2)Al_2O_3$. Results of theoretical calculations (Subtask 1) agreed well with the experimental data. The calculations and the experimental results indicated that (221)Si exhibits higher electron mobilities than other more commonly used orientations. Measurements of anisotropy at 77K were also consistent with the corresponding increases in piezoresistance coefficients at that temperature. Data analyses predicted zero-stress mobilities significantly below bulk crystal values, however, indicating mechanisms other than thermally-induced stresses were dominant in reducing carrier mobilities in heteroepitaxial films. Extensive studies of $(111)Si$ on $(11\bar{2}0)Al_2O_3$ and on $(10\bar{1}4)Al_2O_3$ gave experimental anisotropies averaging 16% and 30%, respectively, much larger than theoretical predictions, again indicating the presence of other major influencing factors. There appeared to be an inverse relationship between anisotropy in (111)Si and the minimum or the average mobility, higher anisotropy corresponding to lower mobility. Attempts were made to correlate these results with reactor configuration (i.e., horizontal or vertical) and various deposition conditions. Measurements were also begun to examine the possibility of mobility anisotropy being present in the $Si/MgAl_2O_4$ system.

The surface-state density of thermally oxidized Si films on Al_2O_3 was determined late in the program using the MOS C-V technique. Evidence of both donor- and acceptor-type surface states was found; a peak in the acceptor-state density appeared at ~0.16eV below the conduction band, but the exact

location of the donor-state density peak could not be determined. Measurements of high-field transport properties of Si and GaAs heteroepitaxial films on Al_2O_3 were also undertaken, early in the program, to obtain drift mobility data for some of the films.

Subtask 7: Design and Fabrication of Devices. In the first year of the contract apparatus for determining minority carrier lifetime by pulsed C-V measurements in MOS structures was designed and constructed and tests were begun. A special MOS structure was designed for measurement of channel conductance, high- and low-field transport properties, and various interface characteristics of heteroepitaxial films. Initial attempts to fabricate Schottky-barrier diodes in Si/Al_2O_3 films as a means of evaluating their electrical properties were not successful and were not pursued further. In the second year the design of a Schottky-barrier type of FET was completed for use in fabricating experimental FET structures in GaAs/insulator films for operation at 1 GHz. Most of the device-oriented effort centered about the determination of carrier lifetimes using the MOS pulsed C-V technique (work which extended to the end of the program) and attempts to fabricate Schottky-barrier FET's in $GaAs/Al_2O_3$.

Recent device efforts produced Schottky-barrier diodes (in n-type Si/Al_2O_3 samples) having good reverse but unsatisfactory forward characteristics. The Schottky-barrier FET structures were still not satisfactory. Preliminary work on fabricating and evaluating Schottky-barrier photovoltaic cells using illumination from the back side was begun, and charge-coupled devices (CCD's) in Si/Al_2O_3 composites were successfully designed, fabricated, and tested.

The lifetime measurement method used has the important advantage that the actual carrier lifetime is magnified by the factor N/n_i, where N is the impurity concentration in the semiconductor and n_i is the intrinsic concentration, so that very short lifetimes typical of heteroepitaxial systems (10^{-10}-10^{-9}sec) could be measured. Carrier lifetimes and values of surface recombination velocity were obtained for As-doped n-type Si/Al_2O_3 samples and for As-doped n/n^+-type Si/Al_2O_3 samples grown by CVD on this contract, as well as for some commercially-obtained Si/Al_2O_3 samples that were P-doped. Lifetimes for As-doped (100)-oriented Si varied from $\sim 10^{-10}$ sec for films 1-3μm thick to $\sim 5 \times 10^{-9}$ sec for films ~10μm thick; the particular P-doped films measured exhibited lifetimes nearly an order of magnitude longer. No clear dependence of lifetime on As doping concentration or on Si orientation ((100) and (111) were studied) was detected. It was found that an underlying n^+ layer ($\sim 3 \times 10^{18} cm^{-3}$) significantly enhanced the lifetime in a 3μm top layer of As-doped ($\sim 10^{16} cm^{-3}$) Si for a given total film thickness, the enhancement being greater the greater the n^+ layer thickness ($\tau \sim 1\mu sec$ for 18μm total thickness); the n^+ sublayer evidently acts as a "getter" for the trapping centers that tend to lower the lifetime in the n-type material.

Since CCD's had previously been fabricated in Si and showed good charge transfer and since other Si/Al_2O_3 devices had exhibited good high-frequency and radiation-resistant characteristics it was determined that fabrication of CCD's should be undertaken in Si/Al_2O_3. The devices were successful, with good transfer

efficiency at high frequencies; four-phase 8-mil-per-cell CCD's were operated at 2MHz with 0.99 efficiency. Low-frequency operation, however, was found to be limited by the short carrier lifetime which allowed charge-up of the potential well.

PART III

APPENDIX 1

SURFACE SCIENCE 36 (1973) 580–593 © North-Holland Publishing Co.

WORK FUNCTIONS AND SURFACE DOUBLE LAYER POTENTIALS OF MONOVALENT METALS FROM A NETWORK MODEL*

P. K. RAWLINGS and H. REISS

Department of Chemistry, University of California, Los Angeles, California 90024, U.S.A.

Received 24 August 1972

The model described in this paper uses an electronic wave function which is defined to be nonzero only along the lines connecting first nearest neighbors in the metallic lattice. The electrons are assumed to move freely along the lines between nearest neighbors. No electron–electron or electron–nucleus force is included in the model calculations (except for forces arising from the Pauli exclusion principle). The work function is defined as the amount of energy required to move an electron from a point slightly inside the crystal to a point slightly outside. The contribution of the electronic double layer is included in the calculation of the work function as well as the dependence of the double layer potential on the surface geometry. Surface states, where the electron is localized in the neighborhood of the face of the crystal, are found to have energies sufficiently above the Fermi level to eliminate the possibility that they make any contribution to the double layer potential for the case of the (100) crystal plane. Consequently, surface states have been ignored in all the calculations. The surface double layer is assumed to be caused by the presence of a finite potential barrier at the surface of the crystal. Bulk electronic wave functions can penetrate this barrier and decay exponentially outside the crystal. The only parameters required by the model are the nearest neighbor distance for the lattice and the height of the potential barrier at the surface. The former quantity is fixed by the lattice structure (body centered cubic for the alkali metals) and by the density, while the latter quantity can be adjusted to give the best agreement between the model calculations and experiment. For the alkali metals, lithium through sodium, the best value of the barrier height is about 50% of the sum of the ionization potential energy, the heat of vaporization, and the calculated Fermi level for the corresponding metal. In addition, the value of the double layer potential for sodium agrees very well with a more sophisticated calculation by Bardeen and is reasonably close to the experimental measurement.

1. Introduction

The free electron molecular orbital method (FEMO) has been successfully applied by Kuhn[1]) and by Rudenberg and Scherr[2]) to the treatment of π-electron systems in conjugated molecular systems. As in the case of Hückel theory[3]), the free electron orbital method is directed towards the develop-

* Research supported under NSF Grant # GP-28722X and North American Rockwell Corporation PO # AOWV-521328M3.

ment of a "relative" internally consistent theory for these complicated systems. In the case of Hückel theory, parameters such as overlap integrals are determined by experiment in one molecule and are assumed to have the same magnitude in others. Strictly speaking, in the FEMO method there are no adjustable parameters (unless the distances between atoms are allowed to depart from the values actually observed in the molecule). Nevertheless, both methods provide a reasonable semi-quantitative picture of the electronic state of affairs within π-systems, and have been useful for making semi-quantitative estimates concerning the chemical and spectroscopic properties of π-systems.

Recently Montroll and his coworkers [1]) have expanded the FEMO method to include the treatment of local potentials due to individual atoms. The theory of course remains highly schematic, as well as parameterized, but it does allow relatively simple analytical solutions to be obtained for previously complicated problems. In this way, Montroll and his collaborators have been able to explore the qualitative features of many interesting solid state phenomena including the electronic properties of defects and surfaces. Since the original FEMO method proved useful in the semi-quantitative discussion of the electronic properties of molecules, it is interesting to see whether both the FEMO and Montroll's modification of it can be used in the semi-quantitative study of solids. We have in mind not only the examination of schematic relationships (Montroll and his collaborators have already done that), but also the development of an internally consistent parameterized theory in the same spirit as Hückel theory.

In order to study this question, we have elected to apply the network theory to the estimation of the work functions of monovalent metals, especially the alkalis. Our principal objective has been to determine the work function and its variation with crystal orientation. The approach is as simple as possible, involving a single adjustable parameter, namely the difference between the energy of a free electron in vacuum and the lowest level of the conduction band. This parameter is invariant to crystal orientation and could in principle be determined from measurements on a single crystal plane. All refinements, such as exchange and correlation effects, are explicitly ignored but should be implicitly involved within the barrier height which constitutes the adjustable parameter mentioned above. The detailed explicit treatment of these additional effects would be inconsistent with the severe approximations already contained within the theory. One would hope, however, that the network model would give a reasonable semi-quantitative account of the variation of work function with crystal orientation, once the adjustable parameter is determined, by using the experimental data available for one crystal plane. Furthermore, one would hope that there would be an

orderly relationship between the predictions of the theory for one alkali metal as compared to another.

2. The network model

Our treatment actually makes use of the FEMO method coupled with the Green's function approach developed by Montroll for the treatment of defects and surfaces in connection with his more elaborate network model. The one electron wave function is chosen to be nonzero only along the lines connecting the first nearest neighbors in the metallic lattice. This is equivalent to requiring that the potential be infinite everywhere within the crystal except on these lines. The electrons are assumed to move freely, i.e., we do not associate potential wells (as in the Montroll modification) with the individual atoms. To this extent, our model is more like the original FEMO method. However, we shall have to make use of the Bloch theorem[5]) in order to deal with the crystal and the Green's function approach will have to be used to treat the extended defect represented by the surface. The crystal symmetry enters the problem through the nodal conditions eqs. (3a) and (3b) below, and through the Bloch theorem.

The work function is defined as the amount of energy required to move an electron from the point slightly inside the crystal to a point slightly outside, and is effected by the electronic double layer[6]) which in turn depends on crystal surface. One of our main tasks will involve calculating the strength of this double layer.

As long as an electron remains on a line joining two nearest neighbor atoms inside the lattice, it has no force acting on it, and its potential energy may be set equal to zero. We assume that an abrupt change in potential occurs as the electron moves on to a dangling surface bond where it experiences a constant potential V_B ($V_B > 0$). The surface barrier V_B is the only parameter in the theory and will have to be determined through reference to some single experiment. In fact, the form of the potential barrier in the real crystal is not abrupt, but since we are searching for the simplest possible parameterized theory (and also because of the severe approximation already contained within the network model itself), we assume that it is abrupt. The dangling bonds for surface atoms have the same direction as if they were joined to another lattice site; but instead of being of length R (where R is the nearest neighbor distance), they extend all the way to infinity. The wave equation for this system may be expressed in the following form:

$$\nabla^2\psi = (\alpha^2 - k^2)\,\psi, \tag{1}$$

in which $\alpha^2 = 2mV/\hbar^2$, $k^2 = 2mKE/\hbar^2$, and ψ is the electronic wave function,

m the mass of the electron, KE the energy of the state described by ψ, V the potential, and h is Planck's constant divided by 2π. Clearly V (and α) equals zero for positions along bonds in the bulk, while $V = V_B$ on the dangling bonds. The solutions of eq. (1) for the surface and bulk bonds, respectively, are:

$$\psi_s = a_s \exp\{-(\alpha^2 - k^2)^{\frac{1}{2}} x\}, \qquad 0 \leqslant x < +\infty, \tag{2a}$$

$$\psi_B = a_B \cos\{kx + \delta_B\}, \qquad 0 \leqslant x \leqslant R, \tag{2b}$$

Each ψ is defined only on a particular bond and is zero elsewhere. Where several bonds meet at a lattice point, the wave functions associated with them must be equal. In addition, there are requirements associated with the conservation of momentum. These restrictions may be expressed as follows[2]):

$$\psi_1(0) = \psi_2(0) = \psi_3(0) = \ldots = \psi_n(0), \tag{3a}$$

$$\sum_{i=1}^{n} \left(\frac{\partial \psi_i}{\partial x}\right)_{x=0} = 0. \tag{3b}$$

In these equations n is the number of bonds meeting at a particular lattice site.

If the quantity $\phi(l, m, n)$ is the value of the wave function at the lattice site (l, m, n), eqs. (3a) and (3b) require, for a body centered cubic lattice, the following relationship:

$$\begin{aligned} 8\cos(kR)\,\phi(l, m, n) = {} & \phi(l+1, m+1, n+1) + \phi(l+1, m-1, n+1) \\ & + \phi(l-1, m+1, n+1) + \phi(l-1, m-1, n+1) \\ & + \phi(l+1, m+1, n-1) + \phi(l+1, m-1, n-1) \\ & + \phi(l-1, m+1, n-1) + \phi(l-1, m-1, n-1). \end{aligned} \tag{4}$$

In addition, for the bulk crystal we make use of periodic boundary conditions:

$$\phi(l, m, n) = \phi(l+N, m, n) = \phi(l, m+N, n) = \phi(l, m, n+N). \tag{5}$$

A possible solution to eqs. (4) and (5), which also satisfies Bloch's theorem, is:

$$\phi(l, m, n) = A \exp\left\{\frac{2\pi i}{N}(ls_1 + ms_2 + ns_3)\right\}, \tag{6}$$

where $s_1, s_2, s_3 = 1, 2, 3, \ldots, N$. Substitution of eq. (6) into (4), with appropriate collection of terms, yields:

$$\cos(kR) = \cos\left(\frac{2\pi s_1}{N}\right)\cos\left(\frac{2\pi s_2}{N}\right)\cos\left(\frac{2\pi s_3}{N}\right) = E. \tag{7}$$

Since the energy of an electron depends on k, and s_1, s_2, and s_3 are indices denoting possible states of the system, eq. (7) determines the density of states for network. The density of sets (s_1, s_2, s_3), satisfying eq. (7) in the range dE, has been derived, in another context, by Jelitto[7]) (see fig. 1). The density-of-states function is symmetric about $\cos(kR)=0$, and it follows that the Fermi

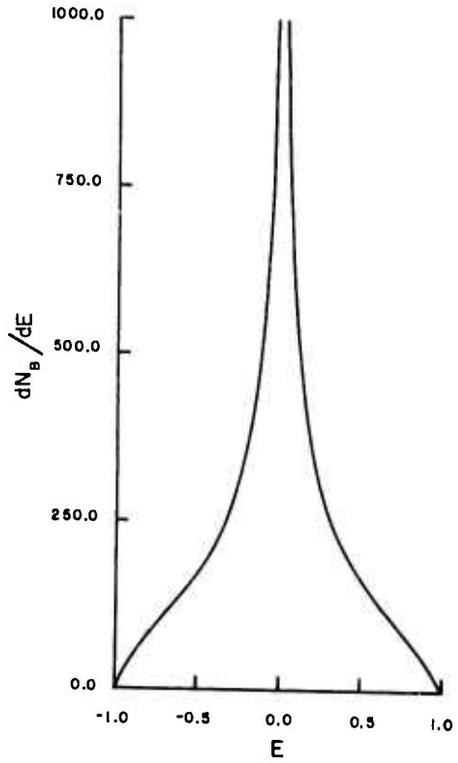

Fig. 1. The density of states, dN_B/dE, for a body centered cubic lattice plotted as a function of E, where E is defined to be the cosine of the reduced momentum wave vector, kR. This graph is given by Jelitto[7]).

level of the network corresponds to an energy level such that $kR=\frac{1}{2}\pi$. Therefore, the Fermi level is given by:

$$\mu_F = \hbar^2/32\, mR^2 . \tag{8}$$

In order to deal with surface states, we assume that the network is infinite in both the x and y directions, but has a finite thickness in the z direction. It is possible to write a general relationship [analogous to eq. (4)] which

applies to either bulk or surface sites. Thus, we have:

$$\begin{aligned} 8\cos(kR)\,\phi(l,m,n) &- \phi(l+1,m+1,n+1) - \phi(l+1,m-1,n+1) \\ &- \phi(l-1,m+1,n+1) - \phi(l-1,m-1,n+1) \\ &- \phi(l+1,m+1,n-1) - \phi(l+1,m-1,n-1) \\ &- \phi(l-1,m+1,n-1) - \phi(l-1,m-1,n-1) \\ &= H(l,m,n), \end{aligned} \tag{9a}$$

$$\phi(l+N,m,n) = \phi(l,m+N,n) = \phi(l,m,n), \tag{9b}$$

where

$$\begin{aligned} H(l,m,n) = {} & [\delta_{n,1} + \delta_{n,N_z}]\,[4\cos(kR) - 4A(kR)]\,\phi(l,m,n) \\ & - \delta_{n,1}\,[\phi(l+1,m+1,N_z) + \phi(l+1,m-1,N_z) \\ & + \phi(l-1,m+1,N_z) + \phi(l-1,m-1,N_z)] \\ & - \delta_{n,N_z}[\phi(l+1,m+1,1) + \phi(l+1,m-1,1) \\ & + \phi(l-1,m+1,1) + \phi(l-1,m-1,1)], \end{aligned}$$

$$A(kR) = \left[\frac{(\varkappa R)^2 - (kR)^2}{(kR)^2}\right]^{\frac{1}{2}} \sin(kR),$$

and the δ's are Kronecker delta functions. An equation of this general form was introduced by Montroll[4]) although he did not specifically treat the case in which an abrupt barrier of finite height V_B was located at the surface. We assume that the z-direction is the (001) direction and that the exposed surfaces are (001) surfaces having coordinates $z=1$ and $z=N_z$, respectively.

Because of the finite extent of the crystal in the z direction, we can no longer demand that ϕ satisfy the Bloch theorem in that direction. However, this requirement may still be applied to the x and y directions. A solution to eq. (9a), which satisfies the Bloch theorem in these directions, is:

$$\begin{aligned} \phi(l,m,n) &= A\exp\left\{\frac{2\pi i}{N}\,[s_1 l + s_2 m]\right\}\Phi(n), \\ s_1, s_2 &= 1, 2, 3, \ldots, N. \end{aligned} \tag{10}$$

If we substitute this into eq. (9) and collect terms, the result is

$$2F_B\Phi(n) - \Phi(n+1) - \Phi(n-1) = H_B(n), \tag{11}$$

in which

$$\begin{aligned} H_B(n) &= [\delta_{n,1} + \delta_{n,N_z}]\,\eta\Phi(n) - \delta_{n,1}\,\Phi(N_z) - \delta_{n,N_z}\,\Phi(1), \\ F_B &= \cos(kR)/[\cos(2\pi s_1/N)\cos(2\pi s_2/N)], \\ \eta &= [\cos(kR) - A(kR)]/[\cos(2\pi s_1/N)\cos(2\pi s_2/N)]. \end{aligned}$$

A differenee equation having the same form as eq. (11) has been solved by Montroll[4]) using an appropriate Green's funetion, $g(n)$. In terms of g, this solution may be expressed as:

$$\Phi(n) = \sum_{j=1}^{N_z} g(j-n)\, H_B(j), \tag{12}$$

where the Green's funetion is defined as:

$$g(n) = \frac{1}{2N_z} \sum_{s=1}^{N_z} \frac{\exp(2\pi i s n/N_z)}{F_B - \cos(2\pi s/N_z)}. \tag{12a}$$

For the $|F_B| > 1$, $\Phi(n)$ deeays exponentially as n refers to sites further from the surfaee, i.e., deeper in the bulk of the erystal. Therefore, this range of F_B is the range for surface states; and by substitution of the solution in this range baek into eq. (11), it may be shown that the following relation holds:

$$[\cos^2(kR) - A^2(kR)]^{\frac{1}{2}} = \cos(2\pi s_1/N)\cos(2\pi s_2/N). \tag{13}$$

This equation is, for surface states, the equivalent of eq. (7) for bulk states and, like eq. (7), determines the density of states.

The bulk wave funetions may be normalized as follows. First, the square of the wave funetion (square of the modulus) is integrated over eaeh individual bond, yielding a quantity proportional to the fraetion of eleetrons residing on the bond. This fraction is then summed over all bonds and the sum is set equal to unity. The fact that each state is oecupied by two eleetrons is then taken into aeeount at a later step by multiplying the density of states funetion, eq. (16), by 2. The integral for the square of the wave funetion on a dangling surfaee bond is, aecording to eq. (2a):

$$D_s = |\psi_s(0)|^2 \int_0^\infty \exp(-2\beta x)\, dx = \frac{|\psi_s(0)|^2}{2\beta}. \tag{14a}$$

In the above equation, $\beta = (\alpha^2 - k^2)^{\frac{1}{2}}$ and $|\psi_s(0)|$ is the value of the wave function at the surfaee node. The integral for the square of the wave function on a bond eonnecting two nearest neighbor lattice sites is, from eq. (26):

$$D_B = \int_0^R \cos^2(kx + \delta_B) = \frac{1}{2}\left\{R + \frac{\sin[2(kR + \delta_B)] - \sin(2\delta_B)}{2k}\right\}, \tag{14b}$$

where R is again the distance between nearest neighbors. It should be noted that although both the above integrals depend on the kinetic energy of the

electron, D_s is also a function of the surface barrier height, while D_B is a function of the distance R. In a body centered cubic lattice, each site has eight first nearest neighbors and therefore eight radiating bonds. However, for interior sites, each of these eight bonds is shared by one other lattice site and thus each interior site has only four bonds on the average.

In accordance with the prescription laid out above, we therefore write the following expression.

$$4D_B|a_B|^2 N^3 + \cdots + O(N^2) = 1, \tag{15a}$$

where N^3 is the number of sites in the lattice and N^2 is proportional to the number of surface sites. All terms on the left of eq. (15a), except the first, are of order N^2 or less; and since the size of the network can be thought of as being arbitrarily large, only the cubic term needs to be considered. Consequently, the following expression is obtained:

$$|a_B|^2 = 1/4D_B N^3. \tag{15b}$$

It turns out that for reasonable values of the barrier height, V_B, surface states on the (0, 0, 1) plane have energies above the Fermi level and are consequently unoccupied. As a result, surface states do not influence the surface double layer potential or the work function, at least not within the requirements of the network model. Thus, the properties of the surface states need not be included in the calculations for the double layer and work function which follow. We can therefore make full use of the density of states derivable by the method of Jelitto[7]).

This density of states in reduced momentum space is:

$$\rho(kR) = C_N \sin(kR) \frac{dN_B}{dE}, \tag{16}$$

where dN_B/dE has been expressed rigorously by Jelitto in terms of elliptic integrals. It may also be approximated using more elementary functions as follows:

$$\frac{dN_B}{dE} \approx 2[1 - |E|]^{\frac{1}{2}} \left[\ln\left(\frac{5.845}{|E|}\right)\right]^2 [16.679 + 3.6364|E| + 2.4880|E|^2];$$

an expression good to four significant figures over the range $0.005 \leqslant |E| \leqslant 1.0$; $E = \cos(kR)$ and C_N is a normalizing constant such that the total number of quantities in the region $0 \leqslant kR \leqslant \pi$ is N^3, i.e.,

$$\int_0^{\pi} \rho(kR)\, dkR = N^3.$$

Because the expression for $\rho(kR)$ is rather complicated, the above integral is evaluated most conveniently by numerical means. Unfortunately, the value of dN_B/dE is infinite for $|E|=0$, and the numerical integration cannot be performed over the entire integral even though the integral converges. The density of states function, $\rho(kR)$, is symmetric on the integral about the point $kR=\frac{1}{2}\pi$, and consequently the numerical integrations need only be performed from $kR=0$ to $kR=u$, where $u<\frac{1}{2}\pi$. There will be some uncertainty about the exact value of C_N, depending on the choice of upper limit for the integral. For the calculations in this paper, u has been set equal to $0.4985\,\pi$. This particular value was chosen for two reasons: (1) the approximation for dN_B/dE is known to be reasonably accurate over this range of integration, and (2) the value of C_N differs by only a few percent from the value assumed when the upper limit on the integral is changed from $0.485\,\pi$ to $0.49999\,\pi$.

3. Estimation of surface charge

The charge on each dangling surface bond may be calculated in a straightforward manner, being proportional to D_s. Multiplying this ratio by 2 to account for electron spin and finally integrating over all states (all possible values of momentum) gives the fraction of the total number of electrons residing on a surface bond. We call this quantity $G(\alpha R)$:

$$G(\alpha R)=\int_0^{\frac{1}{2}\pi} 2\rho(kR)\,D_s\,\mathrm{d}(kR)=\int_0^{\frac{1}{2}\pi}\frac{\cos^2(\delta_B)}{[(\alpha R)^2-(kR)^2]^{\frac{1}{2}}}\left(\frac{\rho(kR)}{2N^3}\right)\frac{\mathrm{d}(kR)}{1+\dfrac{\sin[2(kR+\delta_B)]-\sin(2\delta_B)}{2kR}}. \tag{17}$$

In this equation, D_s is defined by eq. (14a) and:

$$\tan(\delta_B)=\frac{\cos(kR)-1}{\sin(kR)}, \qquad |\psi_s(0)|^2=|a_B|^2\cos^2(\delta_B).$$

These two relations are derived from the requirement that the square of the modulus of the standing waves represented by eqs. (2a) and (2b) must be the same at all lattice sites for wave functions associated with the bulk energy states.

Because of the difficulties already discussed in connection with $\rho(kR)$, the actual upper limit of integration used in these calculations was $0.4985\,\pi$ instead of $\frac{1}{2}\pi$. The bulk wave functions are assumed to differ only by a phase factor from one lattice site to another even at the surface. Because $G(\alpha R)$ is normally a few tenths of an electron or less, and because the conductivity of the metal is high, all the positive charge, balancing the negative charge

located outside the lattice, is assumed to reside on the crystal surface. The total positive surface charge is therefore:

$$\sigma_s = n_s G(\alpha R) \left(\frac{N_s}{A_s}\right) e, \tag{18}$$

where n_s is the number of dangling surface bonds and (N_s/A_s) is the number of sites per unit area, while e is the charge on an electron.

4. Calculation of the double layer potential

The work required to move an electron from the surface to some point outside the crystal may be calculated using Gauss' theorem. Since the distribution of electric charge is uniform parallel to the crystal surface, the field acting on any electron is perpendicular to the surface and has an intensity:

$$F(x) = \sigma(x)/\varepsilon_0, \tag{19}$$

where $\varepsilon_0 = 8.85 \times 10^{-12}\ \mathrm{C^2/(N \cdot m)^2}$ and $\sigma(x)$ is the net amount of positive charge lying between the surface and the point x on the dangling bonds. The charge $\sigma(x)$ is evaluated from the expression:

$$\sigma(x) = n_s \left(\frac{N_s}{A_s}\right) e \int_0^{\frac{1}{2}\pi} \frac{\dfrac{\cos^2(\delta_B)\exp(-2\beta x)}{[(\alpha R)^2 - kR)^2]^{\frac{1}{2}}}}{1 + \dfrac{\sin[2(kR + \delta_B)] - \sin(2\delta_B)}{2kR}} \frac{\rho(kR)}{2N^3}\, \mathrm{d}(kR) \tag{20}$$

in which we have combined eq. (17) with (2a). The work performed against the double layer is then:

$$W_D = K_G \int_0^{x} F(l)\, \mathrm{d}l. \tag{21}$$

In this equation, $\mathrm{d}l$ represents distance along the direction of the surface bond, and K_G is a factor such that $K_G \mathrm{d}l$ is the distance normal to the surface. The integral in eq. (21) is most conveniently evaluated in terms of the reduced distance l/R, and the exact value of the upper limit is not very important because essentially all of the contribution to the double layer potential occurs within less than five times the nearest neighbor spacing from the surface. Thus, within the limitations of this model, changes in the double layer potential from one surface to another are determined by the variations in three factors: (1) the number of lattice sites per unit area of surface, (2) the number of dangling surface bonds at each site, and (3) the geometric factor K_G.

5. The work function

As indicated earlier, the work function is defined as work necessary to move an electron from the point just inside the lattice to a point just outside. The energy required for this process depends on the geometry of the surface through which the electron passes because of the contribution of the double layer. In keeping with the simplicity of the network model, the work function W_E is defined as:

$$W_E = V_B - \mu_F - W_D ; \tag{22}$$

whereas before V_B is the surface barrier, μ_F is the Fermi level, and now we denote the double layer potential by W_D. The first two quantities on the right of eq. (22) are independent of surface orientation, and the variation of work functions with surface is therefore due to W_D.

The double layer potential, eq. (21), can be expressed most conveniently in the following form:

$$W_D(\alpha R) = A_L I(\alpha R), \tag{23}$$

where

$$A_L = K_G R \binom{n_s}{4} \left(\frac{e}{\varepsilon_0}\right) \left(\frac{N_S}{A_S}\right),$$

and is only a function of the nearest neighbor distance and surface geometry, while $I(\alpha R)$ is an integral which depends only on the product αR. The values of $I(\alpha R)$ for various αR have been listed in table 1. In table 2, the densities of

TABLE 1

αR	$I(\alpha R)$	αR	$I(\alpha R)$
0.6	0.10553	1.2	0.01447
0.7	0.05890	1.3	0.01207
0.8	0.03944	1.4	0.01025
0.9	0.02879	1.5	0.00882
1.0	0.02215	1.6	0.00767
1.1	0.01765		

TABLE 2

Element	Density (g/cm³)	Nearest neighbor distance (Å)	A_L (001) (V)	A_L (011) (V)
Lithium	0.534	3.038	25.82	18.26
Sodium	1.007	3.666	21.39	15.12
Potassium	0.870	4.594	17.08	12.07
Rubidium	1.532	4.937	15.88	11.23
Cesium	1.873	5.349	14.67	10.37

TABLE 3

Element	ΔR	V_B (V)	μ_F (V)	$W_E(001)$ (V)	$W_D(001)$ (V)	$W_E(011)$ (V)	$W_D(011)$ (V)	$I - H - \mu_F$ (V)	$V_B/(I - H - \mu_F)$
Lithium	0.979	3.903	1.018	2.310	0.575	2.479	0.406	8.06	0.484
Sodium	1.107	3.426	0.699	2.355	0.372	2.464	0.263	6.95	0.493
Potassium	1.271	2.876	0.445	2.214	0.217	2.278	0.153	5.72	0.503
Rubidium	1.334	2.743	0.385	2.177	0.181	2.230	0.128	5.42	0.506
Cesium	1.344	2.373	0.328	1.881	0.164	1.929	0.116	5.03	0.472

the alkali metals and their first nearest neighbor distances are given, as well as the values of A_L for the (001) and (011) planes.

The surface barrier V_B may be estimated by the following expression:

$$V_B \approx I + H + \mu_F. \tag{24}$$

Here I is the ionization potential for an atom in gas phase, H is the heat of sublimation per atom, and μ_F the Fermi level which can be estimated from eq. (8). Eq. (24) approximates an equation given by Wigner and Bardeen[6]) and has its origin in comparing certain electronic integrals which occur in the expression for V_B with integrals which also occur in expressions for I and H. The barrier height may also be estimated by adjusting V_B so that the value predicted by the network theory agrees with experiment. This was done for the alkali metals using the work function calculated for the (001) plane. The experimental heats of vaporization, ionization potentials, and work functions have been compiled from various sources by Wigner and Bardeen[6]). In table 3, we compare the barrier heights estimated from eq. (24) with those obtained through adjustment of V_B to make the work function calculated by the network model agree with experiment. The best fit value obtained from the network model is always about one-half the value derived from eq. (24). On the other hand, eq. (24) is itself by no means precise. Considering the simplicity of the network model, the results are not very disparate. In fact, in the case of both Hückel theory and the FEMO method applied to molecules, the same order of magnitude is observed for the mismatch between theory and experiment.

Also included in table 3 are double layer potentials for two different surfaces. Bardeen[8]), using the free electron model, calculates that the surface double layer for the (110) plane of sodium is 0.4 V. The network model predicts a value of 0.37 V (using the value of V_B which brings the theoretical and experimental work functions into register) as compared with an experimental value[8]) of 0.15 V.

From these results, it appears as though the simple network model possesses about the same quantitative degree of validity with respect to surface state problems that the FEMO model possesses with respect to molecules. This suggests that it may be used to make ballpark estimates in a variety of solid state situations.

References

1) H. Kuhn, Helv. Chim. Acta **31** (1948) 1441; J. Chem. Phys. **18** (1948) 840; **22** (1954) 2098.
2) K. Ruedenberg and C. W. Scherr, J. Chem. Phys. **21** (1953) 1565;
C. W. Scherr, J. Chem. Phys. **21** (1953) 1582.
3) C. A. Coulson and H. C. Longuet-Higgens, Proc. Roy. Soc. (London) A **191** (1947) 39.

4) E. W. Montroll, J. Math. Phys. **11** (1970) 635;
R. G. J. Mills and E. W. Montroll, J. Math. Phys. **11** (1970) 2525;
E. W. Montroll, private communication to be published.
5) J. Callaway, *Energy Band Theory* (Academic Press, New York, 1965).
6) E. Wigner and J. Bardeen, Phys. Rev. **48** (1935) 84.
7) R. J. Jelitto, J. Phys. Chem. Solids **30** (1969) 609.
8) J. Bardeen, Phys. Rev. **49** (1936) 653.

Anisotropy in electrical properties of {001} Si/{01$\bar{1}$2} Al_2O_3 †

A. J. Hughes and A. C. Thorsen

North American Rockwell Corporation, 3370 Miraloma Avenue, Anaheim, California 92803
(Received 30 October 1972)

A detailed investigation of the Hall mobility has been carried out on a series of ≈2-μ-thick *n*-type {001} Si/{01$\bar{1}$2} Al_2O_3 films. A specially designed Hall bridge pattern has been used to obtain independent measurements of mobility as a function of current direction in the plane of the film. The data show an anisotropy in the mobility of approximately 9%, with a maximum in mobility occuring along the ⟨100⟩ Si direction that is parallel to the ⟨2$\bar{1}\bar{1}$0⟩ Al_2O_3 direction in the plane of the substrate. This behavior is found to be a consequence, through the piezoresistance effect, of the anisotropic thermal contraction of Al_2O_3 on cooling from the deposition temperature, which leads to an anisotropic thermally induced stress in the Si.

INTRODUCTION

The Hall mobility in epitaxial semiconductor films is usually considered to be a good criterion of film quality and has been used extensively in the optimization of the film growth process. It is therefore important that the properties of the film be homogeneous and uniform over the plane of the film if a realistic electrical parameter is to be deduced from a particular measurement. In most cases it is tacitly assumed that the mobility is isotropic in the plane of the film and does not depend upon the direction in which the measurement is made. We present results in this paper of a detailed investigation of the electrical properties of *n*-type {001} Si/{01$\bar{1}$2} Al_2O_3 and show that for this system an assumption of isotropy is not justified.[1] The mobility is found to vary with current direction in the plane of the film and has a maximum value along the particular ⟨100⟩ Si direction that is parallel to the ⟨2$\bar{1}\bar{1}$0⟩ Al_2O_3 direction in the plane of the substrate.

The experimental anisotropy in mobility reported in this paper will be explained theoretically in terms of the piezoresistance effect and anisotropic substrate-induced thermal stresses. While we believe this to be the principal mechanism behind the observed mobility anisotropy, phenomena associated with surface electric fields and surface quantization can often play a role in current conduction in some other measurement or device situations.

Surface quantization and surface transport in semiconductor inversion and accumulation layers are reviewed briefly by Stern[2] and a number of recent references are listed. Sato *et al.*[3] have investigated the mobility anisotropy of carriers in *p*-type and in *n*-type inversion layers on oxidized Si surfaces in MOSFET device configurations. These references compare field-effect mobilities in each of two perpendicular orientations for a number of different surface plane orientations. For some orientations, sizable anisotropies were reported. However, for the (001) Si orientation, the field-effect mobility is isotropic because of symmetry considerations.

The work of Sato *et al.* relates specifically to bulk Si and therefore did not consider any effects of substrate-induced stresses on the mobility. If there were a surface perturbation in the electrical conductivity of heteroepitaxial (001) Si/Al_2O_3 films, induced by surface charge and/or oxide layer impurities and taking the form of an accumulation or inversion layer, the resulting surface component of mobility would also be isotropic, except for the fact that there is an anisotropy in the film stresses. The mobility of a surface layer would therefore exhibit a small anisotropic effect which would be similar in relative magnitude to that found in bulk Si under similarly stressed conditions. It is unlikely therefore, that a small component of surface conductivity could contribute substantially to the total mobility anisotropy that would be measured in (001) Si/Al_2O_3 films.

The mobility anisotropy to be discussed in the present paper is believed not to be associated with either surface quantization or self-accumulation or inversion effects. There is no applied electric field normal to the surface and the oxide film formed during the after-growth annealing sequence is removed prior to the measurement of film properties. In addition, the high donor concentrations in the films tend to mask contributions to the electrical conduction from surface effects. To numerically assess the magnitude of any possible surface effects present under these conditions, however, would require the measurement of electrical properties in a MOS device configuration, and this has not been done in this work.

Collectively, the above arguments form the basis for our assumption that the mobility anisotropy reported here is a bulk effect and is due primarily to substrate-induced thermal stresses acting through the piezoresistance effect. The agreement between theory and experiment lends confidence to this interpretation.

THEORY

In order to explain the experimental observations discussed below, we have examined theoretically the effect of stress in the Si film on the electron transport properties of the film. As is well known, transport properties such as resistivity and mobility can be related to applied stresses through the piezoresistance effect. Numerous studies of the piezoresistance effect in bulk Si have been reported in the literature over a number of years. Much less attention has been paid to stress and its effect on the transport properties of epitaxial films.

Stress in Si films on sapphire (Al_2O_3) has been examined by Dumin,[4] and in Si films on spinel substrates both by Schlötterer[5] and by Robinson and Dumin.[6] Schlötterer presents formulae for the fractional change in resistiv-

Copyright © 1973 American Institute of Physics

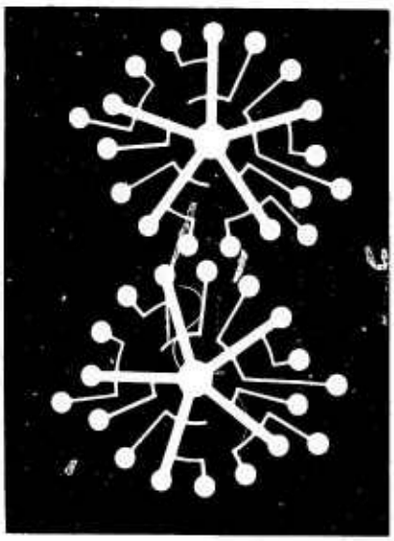

FIG. 1. Specially designed Hall bridge pattern permitting an independent measurement of electrical properties every 18 deg in the plane of the film.

ity ($\Delta\rho/\rho_0$) in terms of piezoresistance coefficients π_{11}, π_{12}, π_{44} and an assumed isotropic stress σ_f in the Si film due to differential thermal contraction between film and substrate. Since he was dealing with spinel substrates, it was assumed that the thermal stress and the induced changes in resistivity were isotropic in the plane of the film. In this section we treat the anisotropy in stress and piezoresistivity and present formulae which are applicable to the anisotropic case.

Before presenting the theoretical results obtained, we will briefly sketch the method. A more detailed theoretical discussion will be given elsewhere.[7] The theoretical determination of the effect of thermally induced stresses on film resistivity and mobility can be divided into three parts: (a) calculation of the piezoresistance effect in terms of stresses; (b) calculation of these stresses in terms of the various coefficients of thermal expansion; and (c) successive transformations of film and substrate coordinate systems to achieve the proper relative crystallographic orientation and to include anisotropy in the plane of the Si film.

The resistivity and stress are related through the equation[8] $E_i = \rho_{ij} J_j + \pi_{ijkl} J_j T_{kl}$, where E is the electric field, J the current density, ρ the zero-stress resistivity tensor, T the stress tensor, and π the piezoresistance tensor. For cubic crystals such as Si, ρ_{ij} is both diagonal and isotropic and equal to $\rho_0\delta_{ij}$, where ρ_0 is the zero-stress resistivity. This tensor equation is commonly contracted to a single-subscript notation for ρ and T and to a double-subscript notation for π.[8] In this notation, T can be written as a 6-component column vector and π as a 6×6 matrix. Referred to the Si crystal axes, π has only three independent coefficients: π_{11}, π_{12}, and π_{44}; however, all 36 π coefficients may be nonzero when referred to a Cartesian coordinate system having an arbitrary orientation with respect to the Si crystal axes.

We first consider the so-called longitudinal piezoresistance effect for the case in which there is only one component of current (J_1), and the field E_1 is in the direction of the current flow. Then $E_1/J_1 = \rho_0(1 + \pi_{1k}T_k)$, where ρ_0 is the zero-stress Si resistivity and k is summed from 1 to 6. Defining E_1/J_1 as ρ_1, the longitudinal piezoresistance is then given by

$$\Delta\rho_1/\rho_0 = (\rho_1 - \rho_0)/\rho_0 = (E_1/J_1\rho_0) - 1 = \pi_{1k}T_k. \quad (1)$$

The longitudinal piezoresistance effect can thus be calculated if the π coefficients and the Si film stresses T_k are known. For a Cartesian coordinate system with axes along the Si crystal axes, the π_{1k} are particularly simple and the sum involves only $\pi_{11}T_1 + \pi_{12}(T_2 + T_3)$. For an arbitrary orientation of axes, which is of primary interest to us here, "rotated" π coefficients are given by Pfann and Thurston.[9] These transformed π coefficients are given in terms of the direction cosines of the arbitrary coordinate system with respect to the Si crystal axes. The determination of π coefficients appropriate to an arbitrary coordinate system is straightforward but is laborious.

We next consider the determination of stresses in the Si film for the case of (001) Si on (01$\bar{1}$2) Al_2O_3. A state of compressive stress arises in the Si film due to the relative thermal contraction of the Si and the Al_2O_3 substrate. In order to calculate this stress, we consider the case of a thin film on a relatively (say 100–150 times) thicker substrate so that bending of the composite can be neglected, and assume that the strain induced in the Si is proportional to the difference in thermal contraction between the two materials. In addition, the thermal contraction is assumed to take place over a

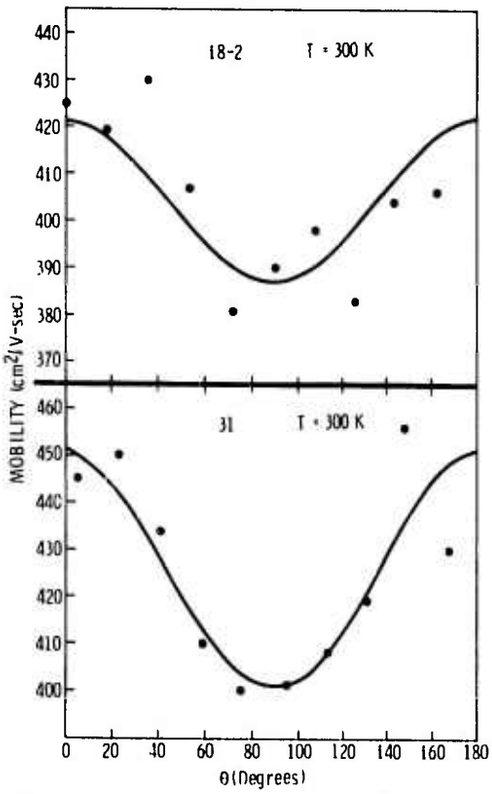

FIG. 2. Typical room-temperature mobility data for two (001) Si/(01$\bar{1}$2) Al_2O_3 samples. The solid curves are least-squares theoretical fits to the experimental points. The maximum mobility is at $\theta = 0°$ and is along the [100] Si direction and the minimum is at $\theta = 90°$ along the [010] Si direction.

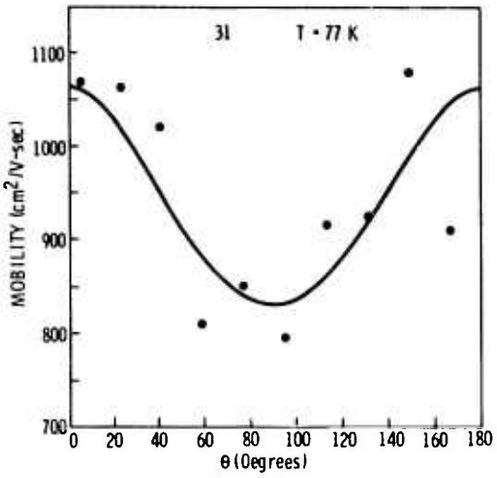

FIG. 3. Low-temperature (77 K) mobility data for one (001) Si/(01$\bar{1}$2) Al_2O_3 sample and corresponding least-squares theoretical curve.

temperature range from room temperature to the growth temperature.[10]

The Cartesian coordinate system employed is defined as follows. The z axis is normal to the surface of the Si film and thus is perpendicular to (001) Si and also perpendicular to (01$\bar{1}$2) Al_2O_3. The x and y axes are in the plane of the film with $x \parallel [100]$ Si and $\parallel [2\bar{1}\bar{1}0]$ Al_2O_3, and $y \parallel [010]$ Si and $\parallel [01\bar{1}\bar{1}]$ Al_2O_3.

The six stresses $T_1, T_2, T_3, T_4, T_5, T_6$ (= $T_{xx}, T_{yy}, T_{zz}, T_{yz}, T_{xz}, T_{xy}$, respectively) completely define the stress in the Si film. The stresses T_3, T_4, and T_5 are zero at the free surface of the Si film and if we further assume that the film is thin enough that all stresses are uniform in the z direction, then $T_3 = T_4 = T_5$ are zero everywhere in the film. T_6 is in general nonzero, but for the relative orientation of film and substrate under consideration is identically zero. Thus only T_1 and T_2 are nonzero. Denoting the elastic constants of Si by C_{ij} and the stiffness coefficients by S_{ij}, we find the following implicit relations for the stresses T_1 and T_2:

$$\begin{aligned}\tfrac{1}{2}(T_1+T_2) &= [(C_{11}^2 + C_{11}C_{12} - 2C_{12}^2)/2C_{11}][1.287(\alpha_s-\alpha_1) \\ &\quad + 0.713(\alpha_s-\alpha_2)]\Delta T \\ &= [1/2(S_{11}+S_{12})][1.287(\alpha_s-\alpha_1) \\ &\quad + 0.713(\alpha_s-\alpha_2)]\Delta T, \end{aligned} \tag{2}$$

and

$$\begin{aligned}\tfrac{1}{2}(T_1-T_2) &= (-0.713)\tfrac{1}{2}(C_{11}-C_{12})(\alpha_1-\alpha_2)\Delta T \\ &= -0.713[S_{11}/2(S_{11}-S_{12})(S_{11}+2S_{12})](\alpha_1-\alpha_2)\Delta T. \end{aligned} \tag{3}$$

Here α_s is the (isotropic) Si thermal expansion coefficient and α_1 and α_2 are thermal expansion coefficients for the Al_2O_3 substrate, perpendicular to the c axis of Al_2O_3 and parallel to the c axis of Al_2O_3, respectively. ΔT is the temperature difference between growth and room temperatures and in Eqs. (2) and (3) is understood to be a positive number. In the limit $\alpha_1 = \alpha_2$, T_1 and T_2 are equal, and Eq. (2) reduces to that given by Schlötterer.[5] The thermal stresses in the Si film due to the substrate and required for calculation of the piezoresistance effect have now been obtained.

We next return to the longitudinal piezoresistance effect and to Eq. (1). The stresses calculated above relate to the coordinate system and parallel Si/Al_2O_3 relations given. Using the results of Ref. 9, the π_{1k} coefficients in Eq. (1) are then transformed to the same coordinate systems used for the stress. The piezoresistance $(\Delta\rho_1'/\rho_0)$ thus obtained represents the change in resistivity due to stress for a current J_1 and field E_1 in the x direction $\parallel [100]$ Si. We are, however, interested in the piezoresistance as a function of angle in the plane of the film. A second transformation on both the π's and the stresses is then performed which represents a rotation about the z axis. The angle θ of this rotation is measured from the x axis and is positive toward the y axis. The longitudinal piezoresistance effect corresponding to current flow at an angle θ from the [100] Si direction then becomes

$$\begin{aligned}\Delta\rho_1/\rho_0 &= E_1/J_1\rho_0 - 1 \\ &= \tfrac{1}{2}(T_1+T_2)(\pi_{11}+\pi_{12}) + \tfrac{1}{2}(T_1-T_2)(\pi_{11}-\pi_{12})\cos 2\theta, \end{aligned} \tag{4}$$

where T_1 and T_2 are given in Eqs. (2) and (3). To avoid ambiguity in orientation, we repeat that the angle θ is measured from that $\langle 100\rangle$ Si direction in the plane of the film that is parallel to the $\langle 2\bar{1}\bar{1}0\rangle$ Al_2O_3 direction in the plane of the substrate. Note that the term depending on θ, which determines the amount of orientational aniso-

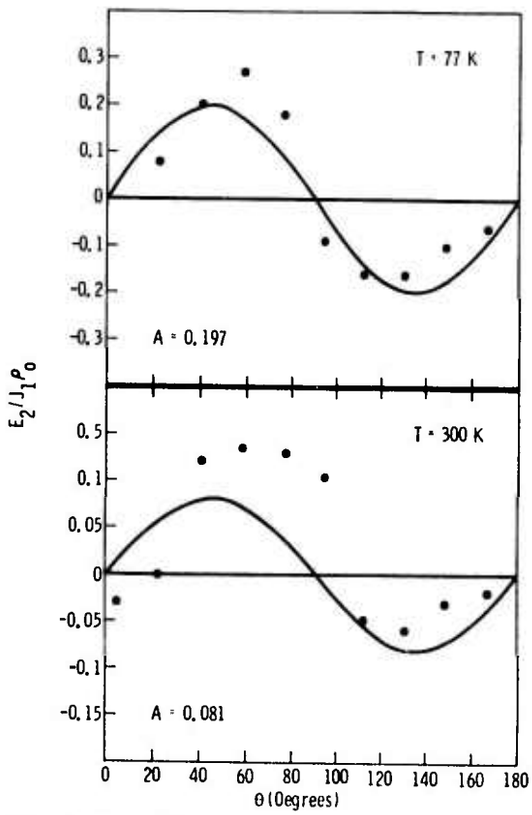

FIG. 4. Plots of the normalized transverse field $(E_2/J_1\rho_0)$ for one sample at 77 and at 300 K. The transverse field E_2 is at right angles to the current flow J_1 and both are in the plane of the film. The least-squares theoretical fits to the data are shown as the solid curves.

TABLE I. Anisotropy data for {001} Si/{01$\bar{1}$2} Al_2O_3.

Sample	μ_{max}	μ_{min}	μ_A	A(%)	rms error (%)	μ_0
Room-temperature data						
102	446	408	427	8.9	1.6	615
18-1	432	397	415	8.6	1.4	598
15	472	425	449	10.5	2.5	648
3412-3	513	472	493	8.2	1.9	711
3411-1	516	478	497	7.6	2.1	717
18-2	422	387	405	8.6	2.5	584
31	451	401	426	11.3	2.2	614
13	443	394	419	11.7	2.9	604
(average)	(462)	(420)	(441)	(9.5)		(636)
Liquid-N_2 temperature (77 K) data						
18-1	1014	797	906	24	5.7	1305
31	1063	832	948	24	7.0	1367

tropy in resistivity and mobility, also depends directly on $\alpha_1 - \alpha_2$. That is, the anisotropy in piezoresistance in the (001) Si plane depends directly on the anisotropy in thermal expansion coefficients of the Al_2O_3 substrate. Using $\alpha_3 = 3.9\times10^{-6}/°C$,[5] $\alpha_1 = 8.31\times10^{-6}/°C$, $\alpha_2 = 9.03\times10^{-6}/°C$,[11] $\Delta T = 1100\,°C$, and the known elastic constants of Si,[12] Eqs. (2) and (3), yield stresses of

$$\tfrac{1}{2}(T_1 + T_2) = -0.9206\times10^{10}\ \text{dyn/cm}^2, \qquad (5)$$

$$\tfrac{1}{2}(T_1 - T_2) = +0.2852\times10^{9}\ \text{dyn/cm}^2.$$

Substituting values of piezoresistance coefficients for n-type Si from Smith,[13,14] Eq. (4) becomes

$$\Delta\rho_1/\rho_0 = 0.44192 - 0.04449\cos2\theta. \qquad (6)$$

Since the mobility μ can be related to the resistivity ρ_1 by $\mu = R_H/\rho_1$, where R_H = the Hall constant, the theoretical anisotropy in mobility can be written

$$\mu/\mu_0 = [1 + (\Delta\rho_1/\rho_0)]^{-1} = (1.44192 - 0.04449\cos2\theta)^{-1}, \qquad (7)$$

where μ_0 is the zero-stress mobility. From Eq. (7), we note that the mobility will be a maximum along the [100] Si direction and will be a minimum 90° away along the [010] Si direction.

The amount of anisotropy can be described conveniently by a parameter A which we define as $A \equiv (\mu_{max} - \mu_{min})/\mu_A$, where $\mu_A \equiv \frac{1}{2}(\mu_{max} + \mu_{min})$ is an approximate average mobility in the plane.[15] The predicted mobility anisotropy is found to be $A = 6.2\%$ and the average mobility is found to be $\mu_A = 0.694\,\mu_0$. Thus we find a 6.2% anisotropy in mobility superimposed on a substantial 30% over-all theoretical reduction in mobility for n-type Si.

The theory also predicts a transverse piezoresistance effect corresponding to an electric field E_2 in the plane of the film and orthogonal to the current J_1 direction. This transverse piezoresistance effect is also found to depend upon orientation and is given by

$$E_2/J_1\rho_0 = -\tfrac{1}{2}(T_1 - T_2)(\pi_{11} - \pi_{12})\sin2\theta = +0.04449\sin2\theta, \qquad (8)$$

and is zero along the [100] Si direction and is of maximum magnitude along the [010] Si direction. The sign convention employed here is that E_2 is positive if $J_1 \times E_2$ is out of the plane of the film and is thus in the $+z$ direction.

The transverse piezoresistance ($E_3/J_1\rho_0$) associated with a field E_3 normal to the Si film was also examined and for (001) Si on (01$\bar{1}$2) Al_2O_3, is found to be identically zero.

Although the results described above were obtained explicitly for n-type Si, the formalism is also valid for p-type Si providing that appropriate values for the π coefficients are used. The quantity $\pi_{11} - \pi_{12}$, which is important for the anisotropic effect, is found to be approximately a factor of 20 less for p-type Si. As a result, little anisotropy would be expected in the Si orientation under discussion, although other orientations can in general show pronounced effects.

EXPERIMENTAL

The films used for this study were grown by chemical vapor deposition techniques in two different reactor systems. One of these is a vertical system[16] and the other is a horizontal system. In both cases the films were formed from the thermal decomposition of silane (SiH_4), with H_2 used as a carrier gas. Intentional doping to concentrations of $(1-6)\times10^{16}$ cm^{-3} was achieved with the use of arsine (AsH_3). Growth temperatures ranged from 955 °C in the horizontal system to 1075 °C in the vertical system, and film thicknesses varied from 1.5 to 1.8 μ.

After growth the samples were annealed at 1100 °C in O_2 for 30 min followed by a N_2 anneal for 2 h at 1100 °C in order to stabilize film properties and electrically neutralize any Al impurities in the film.[17] The resulting oxide film was removed prior to making electrical measurements.

Measurements of resistivity and Hall effect were made on each film using a specially designed Hall bridge pattern etched in the epitaxial layers. This pattern, shown in Fig. 1, consists of two wheel-shaped bridges. The five arms of a single bridge are separated by 72 deg from each other, and the arms of one bridge are rotated by 18 deg with respect to those of the other bridge. This allows an independent measurement of electrical properties (Hall coefficient and resistivity) every 18 deg in the plane of the film.

Electrical data were taken on eight samples of {001} Si/{01$\bar{1}$2} Al_2O_3. For every sample, the orientation of each leg of the Hall pattern was determined with respect to one of the Si directions of the form ⟨100⟩ in the plane of the film. This was accomplished by obtaining a Laüe back-reflection x-ray pattern for each substrate and from this locating a ⟨2$\bar{1}\bar{1}$0⟩ Al_2O_3 direction in the plane of the substrate that is parallel to a ⟨100⟩ Si direction in the film plane. The mobility in each leg can then be plotted versus the angle θ between the current direction and that particular ⟨100⟩ Si axis. Typical room-temperature mobility data from two samples are shown plotted in Fig. 2. The mobility can be seen to vary with angle and appears to approach a maximum at $\theta = 0°$ and a min-

imum at $\theta \approx 90°$. This is consistent with the behavior predicted by Eq. (7) and suggests that the theoretical form of the mobility could be used to fit the experimental results.

The theory leading to Eq. (7) predicts that the mobility anisotropy should be of the form

$$\mu/\mu_0 = (a - b\cos 2\theta)^{-1}, \tag{9}$$

where a and b are constants. Equation (9) cannot be employed directly in analyzing the experimental results in that the zero-stress mobility μ_0 is not known and would be expected to be a function of growth conditions and to vary slightly from sample to sample or run to run. Accordingly, we have fitted the experimental results by the method of least squares to a theoretical curve of the form

$$\mu = (a' - b'\cos 2\theta)^{-1}. \tag{10}$$

The numerical curves thus determined are shown by the two solid curves in Fig. 2 for two samples. The anisotropy parameter A is independent of μ_0 and is equal to $2b/a = 2b'/a'$.

The electrical data taken on the eight samples of {001} Si/{01$\bar{1}$2} Al_2O_3 were all fitted by least squares and analyzed in terms of Eq. (10). The maximum mobility μ_{max}, minimum mobility μ_{min}, average mobility μ_A, and anisotropy parameter A were calculated. These four quantities are tabulated in Table I for the samples measured. It can be seen that the anisotropy A varies from approximately 7.6% to 11.7% with an average value of 9.5%.

The scatter in the mobility data, as evidenced by the results shown in Fig. 2, is probably due primarily to inhomogeneities in film properties over the surface of the film. For example, carrier concentrations measured on the separate areas of the Hall pattern on a given film are found to vary an average of ±7%. Even though these differences are taken into account in calculating the mobility in each arm of the bridge, slight errors may be introduced since the spatial extent over which the resistivity is measured is much larger than that over which the Hall constant (carrier concentration) is measured (see configuration of bridge in Fig. 1).

The rms error (%) between the experimental points and the fitted theoretical curve for each sample is shown in Table I. The error in all cases is sufficiently small compared with the anisotropy to indicate that the fit, and hence the correlation between theory and experiment, is statistically significant.

Measurements were taken at 77 K on two selected samples and these results are also tabulated in Table I. Representative data for one sample are shown in Fig. 3. The parameters deduced from the curve-fitting procedure for this data are also shown in Table I. The anisotropy A is found to increase in going from room temperature to 77 K by roughly a factor of 3 for those samples measured. Correlation of this increase in anisotropy with theory would require information on the variation of the Si piezoresistance coefficients π_{11} and π_{12} with temperature. Data for π_{11} as a function of temperature are available in the literature[18] and indicate that π_{11} increases by a factor close to 3 in going from room temperature to 77 K. Data on π_{12} as a function of temperature do not appear to be available; however, it is not unreasonable to assume that the temperature dependence of both coefficients is the same. If this is the case, then the experimental increase in anisotropy at low temperature is consistent with theory.

The last column in Table I lists values of μ_0, the zero-stress mobility. As mentioned earlier, μ_0 cannot directly be determined from experimental data but must be obtained from a combination of theory and experiment. The relationship between zero-stress mobility μ_0 and the average mobility μ_A may be written as [15]

$$\mu_0 = \mu_A(a^2 - b^2)/a \approx \mu_A a. \tag{11}$$

We then assume that Eq. (7) holds and that $a = 1.44192$. The values of μ_0 thus determined are given in the last column of Table I and range from a high of 717 to a low of 584, with an average of 636.

The rather low value of μ_0 compared with bulk mobilities in Si (> 1000 cm^2/V sec at these carrier concentrations) should be noted and strongly suggests that a considerable mobility reduction results in these films from causes other than thermal stress.

We next consider the transverse piezoresistance effect described in Eq. (8). We have attempted to measure the transverse piezoresistance voltage appearing across appropriate terminals of the Hall bridge. However, the small size of the voltage makes this determination extremely difficult. The voltage is measured across the same terminals as the Hall voltage, with no magnetic field. As a consequence, any misalignment in the terminals would result in an "offset" voltage which would tend to mask the transverse voltage and introduce errors. In addition, inhomogeneities in bridge-arm thickness and width also introduce some ambiguity.

Notwithstanding the above difficulties, some experimental transverse-effect data have been obtained. In obtaining these data, the sense of the transverse voltage must be properly accounted for since Eq. (8) predicts a negative voltage over some range of angles. The sign convention employed is that the transverse field is taken positive if the current direction crossed into the transverse field yields a vector out of the plane of the film.

Representative data on one sample taken at 300 K are shown in Fig. 4. A least-squares fit of these data to a $\sin 2\theta$ term as suggested by Eq. (8) is shown by the solid curve in Fig. 4. The resulting coefficient of the $\sin 2\theta$ term is approximately equal to 0.08, which is larger than predicted from Eq. (8); however, the fit of the experimental points is not good. The value of ρ_0 used in Eq. (8) is the value of ρ_0 determined from the longitudinal mobility measurements described above.

The transverse voltage also becomes substantially larger at 77 K, and low-temperature data are also plotted in Fig. 4. The magnitude of the increase is a factor of between 2 and 3, similar to the increase found for the longitudinal effect. Note that the least-squares fit to a theoretical $\sin 2\theta$ term is much better at 77 than at 300 K, due probably to the larger signal.

SUMMARY AND CONCLUSIONS

Detailed studies of the electrical properties of {001} Si/{01$\bar{1}$2} Al_2O_3 have shown the existence of a significant anisotropy in mobility. This anisotropy can be accounted for through the piezoresistance effect in terms of a simple model of thermally induced stress taking into account the difference in thermal expansion coefficients of Al_2O_3 parallel and perpendicular to the c axis. Both longitudinal and transverse piezoresistance effects were considered and theoretical formulae developed which account for the anisotropic effects.

The theory for the longitudinal piezoresistance effect predicts an anisotropy in mobility of about 6.2% and for the transverse piezoresistance effect predicts a $\sin 2\theta$ anisotropy coefficient of about 0.044 for the normalized transverse electric field. The value of each of these quantities is strongly dependent upon the data used for the thermal expansion of Al_2O_3. Recent measurements[19] at this laboratory using a differential technique have given a difference in thermal expansion coefficients $\alpha_1 - \alpha_2$ of $(-1.08 \pm 0.12) \times 10^{-6}$/°C for the Al_2O_3 substrate. Using this value for $\alpha_1 - \alpha_2$ leads to a predicted mobility anisotropy of 9.3%[20] and a transverse electric field anisotropy factor of 0.067 which are in good agreement with the experimental results.

A few concluding points suggested by our investigation of the electrical properties of {001} Si/{01$\bar{1}$2} Al_2O_3 should be mentioned. The first is simply that the anisotropy in mobility reported here must be taken into account in the evaluation and/or optimization of film-growth processes. Previous practice has apparently been to ignore the orientation of current flow in the plane of the film, and thus mobility data for various {001} Si films could possess a built-in ≈10% scatter due to this anisotropy. Such scatter renders the task of definitively evaluating changes in film-growth processes somewhat difficult.

Second, for some Si film applications in which the mobility is important it would be desirable to orient the current flow (along the ⟨100⟩ Si direction ∥ ⟨2$\bar{1}\bar{1}$0⟩ Al_2O_3 direction) to obtain the maximum mobility.

The third and final point concerns the interpretation of the origin of the mechanisms determining mobility in these heteroepitaxial films. The excellent agreement between theory and experiment for the mobility anisotropy suggests that the anisotropy can be substantially accounted for in terms of thermal stresses induced by the Al_2O_3 substrate.

In principle, residual growth stresses in the Si due to lattice mismatch and effects of dislocation distributions in the films could also lead to anisotropies in carrier mobility. Our results, however, indicate that the anisotropy can be adequately explained without recourse to these effects. On the other hand, the rather low average value (≈636 cm²/V sec) deduced for the zero-stress mobility μ_0 from analysis of the theoretical and experimental data indicates that thermally induced stress is not the dominant mechanism in lowering the over-all average film mobility from bulk Si values. Thus, defect structures, such as dislocations, would appear to play an important role in determining heteroepitaxial Si film mobilities.

At any rate, these studies of mobility anisotropy have yielded more detailed information than has previously been available from studies of mobility. This also suggests that additional detailed investigations, which examine the variation of anisotropy with film thickness, growth conditions, and temperature, may well prove valuable in better understanding and improving Si/Al_2O_3 films.

ACKNOWLEDGMENTS

The authors wish to thank H. M. Mansevit, F. M. Erdmann, and R. Harada for providing the samples used for this study, J. P. Wendt for carrying out the electrical measurements, R. E. Johnson for performing the photolithographic processing, and R. P. Ruth for a critical review of the manuscript.

---

[1]Supported in part by ARPA under Order No. 1585, monitored by USAMICOM, Redstone Arsenal, AL, under Contract No DAAH01-70-C-1311.

[1]Similar but larger anisotropic effects have also been observed in the (221) Si/(1122) Al_2O_3 system and are reported by A. C. Thorsen and A. J. Hughes, Appl. Phys. Lett. **21**, 579 (1972).

[2]F. Stern, J. Vac. Sci. Technol. **9**, 752 (1972).

[3]H. Sato, Y. Takeishi, and H. Hara, Jap. J. Appl. Phys. **8**, 588 (1969); Phys. Rev. B **4**, 1950 (1971)

[4]D. J. Dumin, J. Appl. Phys. **36**, 2700 (1965).

[5]H. Schlötterer, Solid-State Electron. **11**, 947 (1968).

[6]P. H. Robinson and D. J. Dumin, J. Electrochem. Soc. **115**, 75 (1968).

[7]A. J. Hughes (unpublished).

[8]W. P. Mason and R. N. Thurston, J. Acoust. Soc. Am. **29**, 1096 (1957).

[9]W. G. Pfann and R. N. Thurston, J. Appl. Phys. **32**, 2008 (1961).

[10]This procedure may overestimate the elastic stress at room temperature since it ignores plastic relaxation and generation of dislocations. On the other hand, the basic piezoresistance formula, Eq. (1), which is linear in the stress may, for large stresses, tend to underestimate the effect of stress on resistivity. For example, Schlötterer (Ref. 5) included a term quadratic in the stress to calculate piezoresistivity in his isotropic calculations. Arguments for a numerical correction term of this nature have not been explored adequately and we believe inclusion of such a term would be largely illusory. For definiteness, we have therefore employed the model described above.

[11]J. B. Austin, J. Am. Ceram. Soc. **14**, 795 (1931).

[12]R. F. S. Hearmon, *Landolt-Börnstein Numerical Data and Functional Relationships in Science and Technology, New Series*, edited by K. H. Hellwege (Springer-Verlag, New York, 1969), Vol. III/2, p. 3. The values of elastic constants employed in the text were $C_{11} = 16.5 \times 10^{11}$, $C_{12} = 6.4 \times 10^{11}$, and $C_{44} = 7.93 \times 10^{11}$ dyn/cm².

[13]C. S. Smith, Phys. Rev. **94**, 42 (1954).

[14]The values of piezoresistance coefficients employed in the text for n-type Si were $\pi_{11} = -102 \times 10^{12}$, $\pi_{12} = +54 \times 10^{12}$, and $\pi_{44} = -14 \times 10^{12}$ cm²/dyn. The assumption implicit here is that the bulk piezoresistance coefficients can be employed for these ≈2-μ-thick Si films. This is reasonable for this application but may be incorrect for narrow channel FET devices in which carrier quantization and altered piezoresistance coefficients would both have to be considered.

[15]For a mobility variation of the form $\mu/\mu_0 = (a + b\cos 2\theta)^{-1}$, it can be shown that the true rotational average value is $\bar{\mu}/\mu_0 = (a^2 - b^2)^{-1/2}$, compared with $\mu_A/\mu_0 = a/(a^2 - b^2)$. For the numerical parameters of Eq. (7), these two averages are identical to three significant figures.

[16]H. M. Manasevit, D. H. Forbes, and I. B. Cadoff, Trans. Am. Inst. Min. Eng. 236, 275 (1966).

[17]E. C. Ross and G. Warfield, J. Appl. Phys. **40,** 2339 (1969).
[18]O. N. Tufte and E. L. Stelzer, Phys. Rev. A **133,** A1705 (1964); F. J. Morin, T. H. Geballe, and C. Herring, Phys. Rev. **105,** 525 (1957).
[19]S. B. Austerman (private communication).

[20]In view of the approximations in the theoretical model, such close agreement for the mobility anisotropy between theory (9.3% for $\alpha_1 - \alpha_2 = -1.08 \times 10^{-6}/°C$) and the average experimental value (9.5%) is fortuitous.

APPENDIX 3

Anisotropy in the electrical properties of *n*-type (221) Si/(11$\bar{2}$2) Al_2O_3 †

A.C. Thorsen and A.J. Hughes

North American Rockwell Corporation Electronics Group, 3370 Miraloma Avenue, Anaheim, California 92803

(Received 3 August 1972; in final form 11 October 1972)

Studies of the resistivity and Hall effect in *n*-type (221) Si/(11$\bar{2}$2) Al_2O_3 films have shown that the electron mobility is a strong function of azimuthal direction in the plane of the film. Typical variations in mobility between high- and low-mobility directions are approximately 40%. The anisotropy in mobility is explained on the basis of piezoresistance effects in Si, due to stresses induced by the differential thermal contraction between the Si and the Al_2O_3 substrate.

An implicit assumption that is usually made in the electrical characterization of silicon heteroepitaxial films on sapphire (Al_2O_3) substrates is that the electrical properties are isotropic in the plane of the film. Although this assumption is approximately correct in the (100) Si growth plane, [1] we report results in this letter showing that the electrical properties are extremely anisotropic in the (221) Si plane. It is shown that the anisotropy can be explained on the basis of the piezoresistance in Si associated with stresses induced by the differential thermal contraction between the Si and the Al_2O_3 substrate.

The (221) orientation of Si is of particular interest since the piezoresistance effect leads to the prediction that there will be directions in the plane of an *n*-type film for which the carrier mobility exceeds that of bulk Si, and other directions for which the mobility is less than the bulk value. As a consequence, it is possible to separate the contribution to mobility degradation in the Si/Al_2O_3 system, due to differential thermal expansion stresses from degradation due to other causes. The results indicate that differences in thermal expansion are not in themselves sufficient to explain the reduced mobility in Si/Al_2O_3 films.

The data reported in the present paper are from measurements taken on Si grown by chemical vapor deposition on a Al_2O_3 orientation ~3° from the (11$\bar{2}$2) plane, although nearly identical effects are observed on the (11$\bar{2}$2) plane or on other planes near the (11$\bar{2}$2) plane. Previous orientation studies[2] have shown that (221) Si ∥ (11$\bar{2}$2) Al_2O_3 and that [$\bar{1}$10] Si ∥ [1$\bar{1}$00] Al_2O_3 in the plane of the film. The reactor system and methods of growth are similar to those described previously, [3] and utilize the pyrolysis of silane (SiH_4).

For this experiment, As-doped films, having thicknesses from 1.9 to 2.5 μm and net donor concentrations of $(2-7)\times10^{16}$ cm^{-3}, were grown at 1100 °C at a growth rate of approximately 2 μm/min. After growth the samples were annealed at 1100 °C in O_2 for 30 min, followed by a N_2 anneal for 2 h at 1100 °C in order to stabilize film properties and electrically neutralize any Al impurities present in the film. [4] After removal of the resulting oxide film, electrical measurements were carried out on a specially designed double-Hall-bridge pattern etched in the Si film by the use of photolithographic techniques. The bridge allows an independent measurement of Hall mobility (μ) every 18° in the plane of the film.

Plots of Hall mobility (μ) vs angle (θ) measured from the [1$\bar{1}$0] Si direction are shown for representative samples in Fig. 1. For each sample, a least-squares fit of the data to the equation $(\mu)^{-1} = a + b\cos2\theta$ was obtained (see below). An anisotropy factor A can be defined according to $A = 100(\mu_{max} - \mu_{min})/\mu_A = 200b/a$, where μ_{max} and μ_{min} are the maximum and minimum mobilities determined from the least-squares fit, respectively, and $\mu_A \equiv \frac{1}{2}(\mu_{max} + \mu_{min})$. Table I shows the values of these parameters for a number of samples. The observed anisotropy is seen to be appreciable, as evidenced by an average room-temperature anisotropy factor of approximately 39%.

In order to explain this behavior, we have calculated the reduction in mobility due to the piezoresistance effect resulting from the difference in thermal expansion coefficients of Si and Al_2O_3. For the sake of completeness, we have also taken into account the difference in thermal expansion coefficients in Al_2O_3 parallel and perpendicular to the [0001] axis. The details of the calculations will be given in a more complete account of this work[5]; however, using the data of Smith[6] for the piezoresistance coefficients ($\pi_{11} = -102\times10^{-12}$, $\pi_{12} = 54\times10^{-12}$, $\pi_{44} = -14\times10^{-12}$, in units of cm^2/dyn), values of elastic constants ($C_{11} = 16.5\times10^{11}$, $C_{12} = 6.4\times10^{11}$, $C_{44} = 7.93\times10^{11}$, in units of dyn/$cm^2$) from Hearmon, [7] the thermal expan-

TABLE I. Anisotropy parameters of several (221) Si/(11$\bar{2}$2) Al_2O_3 films.

Sample No.	Temperature (°K)	A (%)	μ_{max} (cm^2/V sec)	μ_{min} (cm^2/V sec)	μ_0 (cm^2/V sec)	rms error (%)
HJ-1	300	30.4	671	494	597	2.7
HJ-58	300	32.2	700	506	615	3.3
HJ-58	77	84.9	1900	769	1250	3.8
HJ-16	300	35.5	690	483	600	2.3
HJ-15	300	39.5	686	460	585	2.8
HJ-0	300	40.1	679	452	575	2.6
HJ-6	300	46.2	737	460	607	3.4
HJ-25	300	48.6	708	431	575	3.5
HJ-25	77	108.6	1680	497	900	6.0

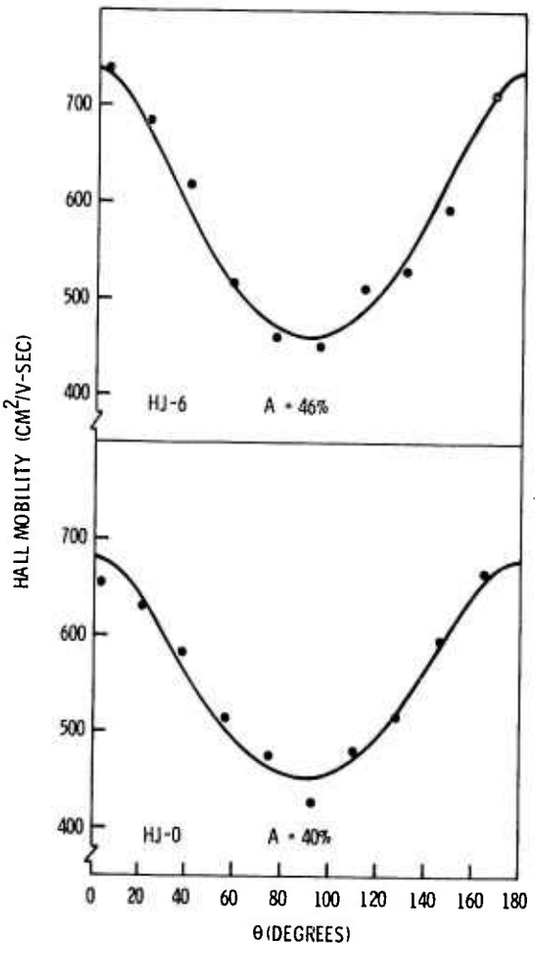

FIG. 1. Variation of Hall mobility with angle from the [1$\bar{1}$0] Si direction for two (221) Si/(11$\bar{2}$2) Al_2O_3 films.

sion coefficients $\alpha_{Si} = 3.9 \times 10^{-6}/°C$,[8] $\alpha_{Al_2O_3}$ ($\|c$) $= 9.03 \times 10^{-6}/°C$, $\alpha_{Al_2O_3}$ ($\perp c$) $= 8.31 \times 10^{-6}/°C$,[9] and a temperature difference of 1100 °C, over which the thermal contraction takes place, we find that $(\mu/\mu_0)^{-1} = 1.06375 - 0.21891 \times \cos 2\theta$, where μ_0 is the mobility in the absence of stress and θ is defined as above. The theory predicts an anisotropy factor of 41%, in good agreement with the experimental values given in Table I.

An interesting feature of the piezoresistance in this plane is that the mobility is predicted to be larger than the unstressed mobility for $0° \leq \theta < 37°$, and smaller than the unstressed mobility for $37° < \theta \leq 90°$ (if we consider only the first quadrant). The theory predicts at 37° the effect of thermal stress on the mobility is zero, so that $\mu(37°) = \mu_0$, the unstressed mobility. The difference between the bulk mobility and the value of mobility measured at this angle thus represents the mobility degradation due to the causes other than thermally induced stress. The fact that the value of $\mu_0 \approx 600$ cm²/V sec is much smaller than the bulk mobility[10] strongly suggests that thermally induced stress is not the dominant mechanism in lowering the mobility.

The piezoresistance theory also predicts an electric field orthogonal to the current direction independent of any externally applied magnetic field. This transverse field (E_T) is given theoretically by $E_T/j\rho_0 = 0.21227 \times \sin 2\theta$, where j is the current density and ρ_0 is the resistivity in the absence of stress. Accordingly, we have measured this transverse field (across the same terminals used to measure the Hall voltage), and show the quantity $E_T/j\rho_0$ plotted for two samples in Fig. 2. The quantity ρ_0 is found from $\rho_0 = R_H/\mu_0$, where R_H is the Hall constant and μ_0, as before, is the mobility at $\theta = 37°$. A least-squares fit of the data to the predicted equation yields an average value for the coefficient of $\sin 2\theta$ of 0.2, in good agreement with theory.

The temperature dependence of the anisotropy has not been examined in detail, although measurements on selected samples at 77 °K show a much larger anisotropy, as evidenced by the data in Table I. Such an increase is consistent with what might be expected for the variation of piezoresistance with temperature. Although detailed measurements of all of the piezoresistance coefficients have not been carried out, π_{11} appears to be an order of 3 times greater at 77 °K than at 300 °K.[11] If it is assumed that all of the coefficients vary by the same amount, it can be shown that the anisotropy factor A would be expected to be an order of 2.7 times greater at 77 °K. The data on two samples show an average increase of a factor of 2.4, consistent with that predicted.

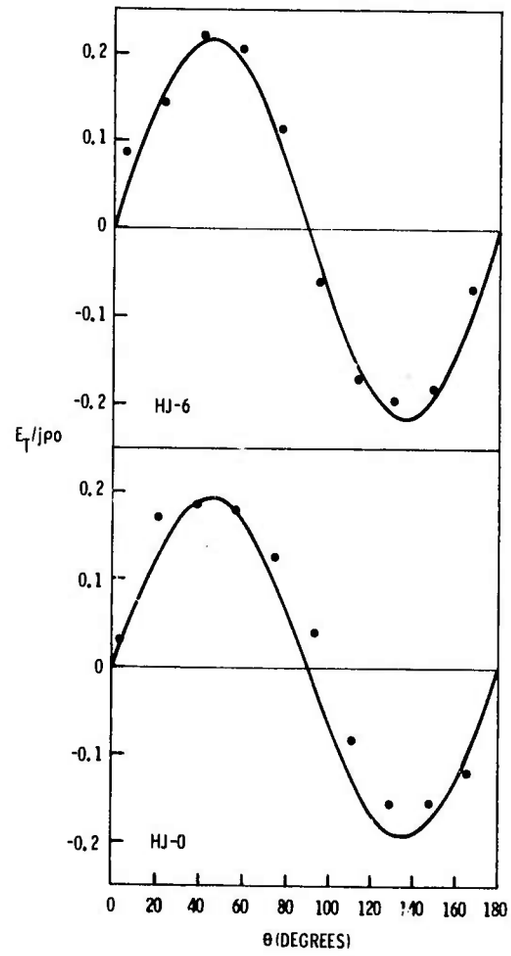

FIG. 2. Variation of transverse field E_T with angle from the [1$\bar{1}$0] Si direction.

The enhanced mobility predicted for some current directions suggests that the (221) plane of Si/Al_2O_3 may yield superior electron mobilities. In comparison with (100) Si and (111) Si grown at this laboratory, the (221) plane has indeed yielded higher mobilities. It would be expected that some types of devices would show improved performance if oriented in such a way as to take advantage of the improved mobility. In MOS devices the stress-induced anisotropy would have to be considered in conjunction with the anisotropies previously found in n- and p-channel devices,[12] which are a consequence of surface quantization effects in the channel resulting from the high electric field at the surface.

The mobility anisotropy discussed in this letter is believed not to be associated with surface quantization since there is no applied electric field normal to the surface and the oxide film formed during the aftergrowth annealing sequence has been removed prior to the measurement of film properties. In addition, the high donor concentrations in the films tend to mask contributions to the electrical conduction from surface effects. Experimentally, we have seen no significant effect of ambient or surface chemical treatments on the conductivity. However, to quantitatively assess the magnitude of possible surface effects would require the measurement of electrical properties in an MOS-device configuration under flat-band conditions.

The good agreement found between the experimentally determined mobility anisotropy and the calculated piezoresistance lends confidence to the assumption that the anisotropy is related primarily to thermally induced stress. If this is indeed the case, further experiments which examine the variation of anisotropy with film thickness, growth conditions, or other variables may well prove valuable in determining the relation of stress to these variables.

The authors wish to thank H.M. Manasevit and F.M. Erdmann for providing the Si samples used for this study, J.P. Wendt for carrying out the electrical measurements, and R.E. Johnson for performing the photolithographic processing. The authors also acknowledge L. Moudy for many helpful discussions regarding the orientation and parallel relationships in the Si/Al_2O_3 system under consideration, and R.P. Ruth for a critical review of the manuscript.

---

†Research supported in part by the Advanced Research Projects Agency under Order No. 1585, and monitored by the U.S. Army Missile Command, Redstone Arsenal, Alab., under Contract No. DAAH 01-70-C-1311.

[1]A.C. Thorsen and A.J. Hughes, Second National Conference on Crystal Growth, Princeton, N.J., 1972 (unpublished). For a substrate with isotropic thermal expansion, there will theoretically be no thermal stress-induced anisotropy in mobility for Si epitaxial films having the (100) or (111) orientation. This result is a consequence of the crystal symmetry of the Si. Since Al_2O_3 substrates have an anisotropic thermal expansion, a small anisotropy in mobility (less than 10%) is predicted in the (100) $Si/(01\bar{1}2)$ Al_2O_3 system on the basis of the model presented in this letter.

[2]H.M. Manasevit, R.L. Nolder, and L.A. Moudy, Trans. AIME **242**, 465 (1968).

[3]H.M. Manasevit, D.H. Forbes, and I.B. Cadoff, Trans. AIME **236**, 275 (1966).

[4]E.C. Ross and G. Warfield, J. Appl. Phys. **40**, 2339 (1969).

[5]A.J. Hughes (unpublished).

[6]C.S. Smith, Phys. Rev. **94**, 42 (1954).

[7]R.F.S. Hearmon in *Landolt-Bornstein Numerical Data and Functional Relationships in Science and Technology, New Series*, edited by K.H. Hellwege (Springer-Verlag, New York, 1969), Vol. III/2, p. 3.

[8]H. Schlötterer, Solid-State Electron. **11**, 947 (1968).

[9]J.B. Austin, J. Am. Ceram. Soc. **14**, 795 (1931).

[10]S.M. Sze and J.C. Irvin, Solid-State Electron. **11**, 599 (1968).

[11]O.N. Tufte and E.L. Stelzer, Phys. Rev. **133**, A1705 (1964); F.J. Morin, T.H. Geballe, and C. Herring, Phys. Rev. **105**, 525 (1957).

[12]T. Sato, Y. Takeishi, and H. Hara, Phys. Rev. B **4**, 1950 (1971); D. Coleman, R.T. Bate, and J.P. Mize, J. Appl. Phys. **39**, 1923 (1968); F. Stern, J. Vacuum Sci. Technol. **9**, 752 (1972).

APPENDIX 4

PREPRINT

STRESS INDUCED ANISOTROPY IN THE ELECTRICAL PROPERTIES OF $Si/A\ell_2O_3$*

A. J. Hughes
Rockwell International Corporation
3370 Miraloma Avenue
Anaheim, California 92803

ABSTRACT

The effect of stress on the electrical properties for a number of orientations of $Si/A\ell_2O_3$ has been theoretically determined. The stress model developed and employed is based upon the differential in thermal expansion between Si film and $A\ell_2O_3$ substrate. The anisotropy in substrate thermal expansion coefficients and in Si film stresses is rigorously included and treated within the framework of a thin-film thick-substrate approach. The phenomenological piezoresistance formalism is used to determine the effect of stress on resistivity which is then in turn related to the carrier mobility. In calculating the mobility change due to thermal stress, it is assumed that bulk piezoresistance coefficients can be employed. Mobility calculations were performed for the common Si orientations - (001), (111) and (221) - and for a number of orientations not yet grown and investigated experimentally. For all $Si/A\ell_2O_3$ orientations and modes of epitaxy treated, an anisotropy in mobility is predicted with two directions of maximum mobility and two directions of minimum mobility in the plane of the Si film. For n-type Si the mobility is either reduced or enhanced depending upon mode of epitaxy and orientation. For p-type Si the mobility is always enhanced and for some orientations by a significant factor. Experimental data are reviewed for n-type (001)Si and (221)Si and found to agree with the theoretically predicted mobility anisotropy, lending confidence to the use of the thermal stress-piezoresistance model.

---

*Supported in part by ARPA under Order 1585, monitored by USAMICOM, Redstone Arsenal, AL, under contract DAAH01-70-C-1311

I. INTRODUCTION

The principal objective of the present investigation has been the determination of the effect of thermal expansion stress on the carrier mobility in n- and p-type $Si/A\ell_2O_3$ films. The theoretical analysis of mobility and mobility anisotropies and the responsible physical mechanisms began as a response to the recent experimental discovery at this laboratory that a mobility anisotropy was present in (001)Si[1], (221)Si[2] and (111)Si[3] heteroepitaxial films grown on $A\ell_2O_3$ and would probably occur in all orientations of $Si/A\ell_2O_3$. It was recognized that different physical mechanisms which could produce some form of mobility anisotropy would, in general, be expected to lead to different magnitudes of anisotropy and to different orientations for the mobility maxima and minima in the plane of the film. Thus, detailed studies of the mobility anisotropy could, in principle, provide a more powerful means than has previously been available for determining the role of various phenomena in establishing the carrier mobility in $Si/A\ell_2O_3$ films.

$Si/A\ell_2O_3$ epitaxy has been actively pursued for a number of years now and is of considerable practical and commercial significance for certain classes of devices. However, a fundamental understanding and adequate theoretical models capable of delineating quantitatively the various physical phenomena, and their possible role in producing a mobility anisotropy, are almost completely lacking. Since stresses in $Si/A\ell_2O_3$ are known experimentally to be on the order of 10^9-10^{10} dyn/cm^2 [4,5] and since Si is a strongly piezoresistive material, it was felt that a piezoresistance-effect anisotropy model would be a useful theoretical tool and should

relate substantially to experimental mobility anisotropies. It is our view that the room temperature stress in $Si/A\ell_2O_3$ films is predominantly due to thermal expansion mismatch stress rather than to lattice-constant mismatch or other growth stresses. This view, coupled with the fact that thermal stresses appear much more amenable to theoretical treatment than do growth stresses, dictated that an investigation in terms of a model combining thermal expansion stresses and piezoresistance effects would be a useful step in better understanding and improving $Si/A\ell_2O_3$ films. This is the basic approach of the paper.

II. MATHEMATICAL DESCRIPTION OF HETEROEPITAXIAL ORIENTATION RELATIONS

In the present paper, the treatment of the piezoresistance effect for $Si/A\ell_2O_3$ heteroepitaxial films will require that various physical property tensors, e.g., piezoresistance π, elastic constant C, stress T, and strain ϵ, be transformed for rotated coordinate systems in the Si and in the $A\ell_2O_3$ which correctly embody the relative orientations of the film and substrate for the different growth modes of $Si/A\ell_2O_3$ heteroepitaxy. A rigorous mathematical formalism for this has been developed which facilitates treating an arbitrary Si film orientation and which is applicable to all the major growth modes of $Si/A\ell_2O_3$ heteroepitaxy.

The experimental description of a mode of epitaxy is accomplished by employing x-ray diffraction (using back-reflection Laue and full-circle goniometer techniques) to determine the relative crystallographic relationships between film and substrate. The relative crystallographic relationship between a Si film and the $A\ell_2O_3$ substrate can be completely and uniquely specified by giving two non-collinear directions in the substrate which are parallel, respectively, to two film directions. This information for the four major growth modes for $Si/A\ell_2O_3$ is presented in Table I and is taken from the work of Manasevit, Nolder and Moudy[6]. The relationships shown for $(221)Si//(11\bar{2}2)A\ell_2O_3$ in Table I were not given in Ref. 6 and have been recently obtained by Moudy[7]. Note that Table I presents both parallel plane and parallel direction information. For Si, the direction [a,b,c] is normal to the plane (a,b,c) having the same indices. For $A\ell_2O_3$, the direction [h,k,i,ℓ] is not normal to the plane (h,k,i,ℓ) unless ℓ is zero.

The information in Table I allows at least two sets of two parallel directions to be obtained for each of the modes of epitaxy. From these given directions, two sets of three parallel directions can be constructed which are mutually orthogonal. The resulting orthogonal direction vectors will be denoted by $D_1^{>f}$, $D_2^{>f}$, $D_3^{>f}$ for the Si film (f) and these are parallel, respectively, to $D_1^{>s}$, $D_2^{>s}$, $D_3^{>s}$ in the $A\ell_2O_3$ substrate (s). $D_1^{>f}$, $D_2^{>f}$, $D_3^{>f}$ are mutually orthogonal and form a right-handed set. The same is true of the set $D_1^{>s}$, $D_2^{>s}$, $D_3^{>s}$ in the substrate. Thus far, the $D_1^{>f}$, $D_2^{>f}$, $D_3^{>f}$ and $D_1^{>s}$, $D_2^{>s}$, $D_3^{>s}$ are abstract vectors. In order to proceed further toward a mathematical theory of epitaxial orientation relations, specific coordinate systems in both Si and $A\ell_2O_3$ must be defined and employed.

Thus, let a Cartesian set of axes (unit vectors) be defined in the film and denoted by (X_f^o, Y_f^o, Z_f^o). In Si, these are referenced to the cubic crystal axes. Let a similar Cartesian set be defined in the substrate and be denoted by (X_s^o, Y_s^o, Z_s^o). The Cartesian set of axes (X_s^o, Y_s^o, Z_s^o) is referenced to the $A\ell_2O_3$ hexagonal axes $a_1^>$, $a_2^>$, $a_3^>$, $a_4^>$, with X_s^o along the $a_1^>$ axes; Y_s^o 90 deg from the $a_1^>$ axis and toward the $a_2^>$ axis; and Z_s^o along the C (or $a_4^>$) axis. In general, (X_f^o, Y_f^o, Z_f^o) and (X_s^o, Y_s^o, Z_s^o) differ in relative orientation. The relative orientation between these two coordinate systems embodies the experimental parallel relation information of Table I and determines the relative crystallographic orientation of Si film and $A\ell_2O_3$ substrates. The important determining constraint is that $D_i^{>f}$ in the Si film be parallel to the $D_i^{>s}$ in the substrate for i = 1,2,3.

Let (SF) denote the matrix transformation between (X_s^o, Y_s^o, Z_s^o) and (X_f^o, Y_f^o, Z_f^o). Consider the coordinate axes to be spatially coincident; (SF) will, therefore, simply be a rigid body rotation matrix. The matrix (SF), therefore, is orthogonal and $(\widetilde{SF}) = (SF)^{-1}$ We then have

$$\begin{pmatrix} X_s^o \\ Y_s^o \\ Z_s^o \end{pmatrix} = (SF) \begin{pmatrix} X_f^o \\ Y_f^o \\ Z_f^o \end{pmatrix} \quad \text{and} \quad \begin{pmatrix} X_f^o \\ Y_f^o \\ Z_f^o \end{pmatrix} = (\widetilde{SF}) \begin{pmatrix} X_s^o \\ Y_s^o \\ Z_s^o \end{pmatrix} . \qquad (1)$$

Now let the parallel direction vectors $D_i^{>f}$ and $D_i^{>s}$ for i = 1,2,3 be expressed in Cartesian components relative to their respective coordinate systems. We then form the matrices (lmn) and (LMN):

$$(lmn) = \begin{pmatrix} l_1 & m_1 & n_1 \\ l_2 & m_2 & n_2 \\ l_3 & m_3 & n_3 \end{pmatrix} \quad \text{and} \quad (LMN) = \begin{pmatrix} L_1 & M_1 & N_1 \\ L_2 & M_2 & N_2 \\ L_3 & M_3 & N_3 \end{pmatrix} , \qquad (2)$$

where $l_1, m_1, n_1 \equiv D_{1x}^f, D_{1y}^f, D_{1z}^f$; $L_1, M_1, N_1 \equiv D_{1x}^s, D_{1y}^s, D_{1z}^s$, etc. Thus, (lmn) is comprised of row vectors relating to the Si film and (LMN) is comprised of row vectors relating to the $A\ell_2O_3$ substrate. In forming the matrices (lmn) and (LMN), the vectors $D_i^>$ have been assumed to be orthogonal and normalized to unit magnitude.

The matrices (lmn) and (LMN) then define new primed coordinate systems (X_f', Y_f', Z_f') and (X_s', Y_s', Z_s')

$$\begin{pmatrix} X_f' \\ Y_f' \\ Z_f' \end{pmatrix} = (lmn) \begin{pmatrix} X_f^o \\ Y_f^o \\ Z_f^o \end{pmatrix} \quad \text{and} \quad \begin{pmatrix} X_s' \\ Y_s' \\ Z_s' \end{pmatrix} = (LMN) \begin{pmatrix} X_s^o \\ Y_s^o \\ Z_s^o \end{pmatrix}. \tag{3}$$

The primed vectors (X_f', Y_f', Z_f') must be parallel and thus equal to the primed vectors (X_s', Y_s', Z_s'). Using Eqn. (1), we have

$$(lmn) \begin{pmatrix} X_f^o \\ Y_f^o \\ Z_f^o \end{pmatrix} = (LMN)\ (SF) \begin{pmatrix} X_f^o \\ Y_f^o \\ Z_f^o \end{pmatrix}, \tag{4}$$

which yields the following relation between (lmn) and (LMN) matrices,

$$(lmn) = (LMN)\ (SF) \text{ and } (LMN) = (lmn)\ (\widetilde{SF}), \tag{5}$$

which must be obeyed by an (lmn) matrix and an (LMN) matrix in order to be consistent with the parallel relations associated with a given mode of epitaxy. If (lmn) and (LMN) are known, then (SF) can be determined from

$$(SF) = (\widetilde{LMN})\ (lmn) \text{ and } (\widetilde{SF}) = (\widetilde{lmn})\ (LMN). \tag{6}$$

Next, suppose we operate on (X_s', Y_s', Z_s') and (X_f', Y_f', Z_f') in Eqn. (3) with the same transfomation matrix (α) yielding

$$\begin{pmatrix} X_f'' \\ Y_f'' \\ Z_f'' \end{pmatrix} = (\alpha) \begin{pmatrix} X_f' \\ Y_f' \\ Z_f' \end{pmatrix} \quad \text{and} \quad \begin{pmatrix} X_s'' \\ Y_s'' \\ Z_s'' \end{pmatrix} = (\alpha) \begin{pmatrix} X_s' \\ Y_s' \\ Z_s' \end{pmatrix}. \tag{7}$$

The matrix (α) thus yields new (lmn) and (LMN) matrices

$$(lmn)' = (\alpha)\ (lmn) \text{ and } (LMN)' = (\alpha)\ (LMN)\ . \tag{8}$$

Since (X_f', Y_f', Z_f') were parallel, respectively, to (X_s', Y_s', Z_s'), (X_f'', Y_f'', Z_f'') must also be parallel, respectively to (X_s'', Y_s'', Z_s''). We obtain

$$\begin{aligned}(SF)' &= (\widetilde{LMN})'\ (lmn)' = (\widetilde{LMN})\ (\widetilde{\alpha})\ (\alpha)\ (lmn) \\ &= (\widetilde{LMN})\ (lmn) = (SF).\end{aligned} \tag{9}$$

Thus, a rotation (α) simultaneously applied to both (X_s', Y_s', Z_s') and (X_f', Y_f', Z_f') yields new matrices $(LMN)'$ and $(lmn)'$ which leave (SF) unaltered and thus relate to the same mode of epitaxy as the original (LMN) and (lmn) matrices. Extensive use of the rotation (α) and Eqn. (8) will be made in subsequent sections. There (lmn) will relate to reference axes in the plane of the Si film and (α) will represent a rotation in the plane of the film.

We next want to consider a different class of operation -- symmetry operations -- which does not change the mode of epitaxy but which does change the form of the transformation matrix (SF). New (lmn), (LMN), and (SF) matrices, physically equivalent by symmetry but not identical in form to the original matrices, can readily be obtained. Let (α_f) represent a point group symmetry operation for Si and let (α_s) represent a symmorphic symmetry operation for Al_2O_3. Initially (α_f) can be considered to operate on (X_f^o, Y_f^o, Z_f^o) and (α_s) to operate only on (X_s^o, Y_s^o, Z_s^o). Analogous to Eqn. (3) we obtain

$$\begin{pmatrix} X_f'' \\ Y_f'' \\ Z_f'' \end{pmatrix} = (lmn)\ (\alpha_f) \begin{pmatrix} X_f^o \\ Y_f^o \\ Z_f^o \end{pmatrix} \quad \text{and} \quad \begin{pmatrix} X_s'' \\ Y_s'' \\ Z_s'' \end{pmatrix} = (LMN)\ (\alpha_s) \begin{pmatrix} X_s^o \\ Y_s^o \\ Z_s^o \end{pmatrix}. \tag{10}$$

Letting $(SF)'$ be the transformation which now connects (X_f^o, Y_f^o, Z_f^o) and (X_s^o, Y_s^o, Z_s^o), we have

$$(SF)' = (\tilde{\alpha}_s)\ (\tilde{LMN})\ (lmn)\ (\alpha_f) = (\tilde{\alpha}_s)\ (SF)\ (\alpha_f). \qquad (11)$$

In general, $(SF)'$ will be different from (SF) originally adopted, but on general principles must correspond to a physically equivalent relative orientation of film and substrate and, thus, to the same mode of epitaxy.

By considering (α_f) to post-multiply (lmn) rather than (X_f^o, Y_f^o, Z_f^o) and (α_s) to similarly post-multiply (LMN), we have the result from Eqn. (10) tha (lmn) (α_f) is symmetry-equivalent to (lmn) and (LMN) (α_s) is symmetry-equivalent to (LMN). A prescription has thus been given for obtaining all equivalent sets of (lmn), (LMN) and (SF) matrices from an original arbitrarily chosen set.

In general, the existence of symmetry-equivalent parallel directions and relative orientations of film and substrate presents no problems. However, in particular cases an internal consistency problem of practical significance can arise. Suppose, for example, that parallel relations for a given mode of epitaxy have been established. This amounts to having arbitrarily labeled a few principal x-ray reflections which then fixes the coordinate systems and directions.

Next, suppose that a substrate yielding this mode of epitaxy is cut a few degrees "off-orientation." X-ray studies providing the required characterization of the substrate and film surfaces can then lead to different but equivalent pole diagrams. However, only one of these pole diagrams is mathematically consistent with the previously determined parallel relations. The inconsistency here

is, in effect, the simultaneous use of different coordinate systems.

The reason for emphasizing equivalent film/substrate orientations is that information obtained from crystallographers characterizing a mode of epitaxy and the film/substrate surfaces can lead to confusion. From the point of view of crystallography, a direction and its equivalent are equally acceptable. However, equivalence is not adequate for mathematical consistency.

One final type of operation will now be discussed which will be used in subsequent sections of the paper to treat piezoresistance for Si films grown on $A\ell_2O_3$ substrates of arbitrary surface orientation. We shall identify the third row of the (LMN) and (lmn) matrices with directions normal to the substrate and film surfaces, respectively. Thus, if a substrate is cut "off-orientation," a modified set of matrices is required. Suppose the direction vector characterizing the original substrate surface is taken from the third row of the (LMN) matrix and written as a column vector. Then a matrix operation (γ) acting on this vector yields a new vector characterizing the off-orientation substrate surface. Thus,

$$\begin{pmatrix} L_3 \\ M_3 \\ N_3 \end{pmatrix}' = (\gamma) \begin{pmatrix} L_3 \\ M_3 \\ N_3 \end{pmatrix} . \qquad (12)$$

The $(LMN)'$ matrix associated with this substrate surface orientation is then given by

$$(LMN)' = (LMN)\ (\tilde{\gamma}). \tag{13}$$

Now let a similar sort of transformation be defined for the Si film,

$$(lmn)' = (lmn)\ (\tilde{\beta}), \tag{14}$$

with the proviso that (γ) and (β) are to be compatible and preserve the original (identical, not merely equivalent) mode of epitaxy. Therefore,

$$(lmn)' = (LMN)'\ (SF), \tag{15}$$

where (SF) is the transformation matrix defined for the original on-orientation case.

From Eqns (13), (14), and (15), we find that

$$(\tilde{\beta}) = (\tilde{SF})\ (\tilde{\gamma})\ (SF) \tag{16}$$

and (β) and (γ) are related by a similarity transformation.

The utility of the above relationship between (lmn), (LMN), and (γ) and (β) lies in the fact that, for an arbitrary substrate orientation, the crystallographic zones in film and substrate are not exactly parallel in general. Thus, in particular cases, the substrate (film) orientation may be more accurately and umambiguously determined than the film (substrate) surface orientation. The procedure would then be to employ the more accurate determination, assume a given mode of epitaxy based upon earlier work, and then calculate $(lmn)'$ and $(LMN)'$ matrices as indicated above.

Since the operations (γ) and (β) in Eqns. (13) and (14) preserve the original identical mode of epitaxy, it must be possible to represent both of them in terms of an operation (α) as in Eqns. (7) and (8):

$$(\alpha)\ (LMN) = (LMN)\ \widetilde{(\gamma)};\ \alpha = (LMN)\ \widetilde{(\gamma)}\ \widetilde{(L\bar{M}N)}$$
$$(\alpha)\ (\bar{l}mn) = (lmn)\ \widetilde{(\beta)};\ \alpha = (lmn)\ \widetilde{(\beta)}\ \widetilde{(l\bar{m}n)}. \qquad (17)$$

Using Eqn. (16), we find that Eqns. (17) are consistent and an operation (α) can be defined which is operationally identical to $\widetilde{(\gamma)}$ and $\widetilde{(\beta)}$ as indicated.

The parallel relations assumed and the transformation matrices (SF), which have been developed for the four $Si/A\ell_2O_3$ modes of major interest, are presented in Table II. One mode of Si epitaxy on spinel ($MgA\ell_2O_4$) is also treated in Table II.

In Table II, the Z_f' and Z_s' parallel directions are given in terms of normals to film and substrate planes. X_f', Y_f' and and X_s', Y_s' are given explicitly in terms of direction vectors. This distinction is convenient in subsequent sections which will focus attention on film and substrate surface planes. The parallel directions (planes) for the $A\ell_2O_3$ substrate are given both in a hexagonal four-index notation and in Cartesian coordinates.

The orientation relations $(111)Si//(11\bar{2}4)A\ell_2O_3$ and $(221)Si//(11\bar{2}2)A\ell_2O_3$ were both determined experimentally and in Table II are identified as belonging to the identical mode of epitaxy (Mode II). The basis for this is the following. The $(111)Si//(11\bar{2}4)A\ell_2O_3$ parallel directions and transformation matrix (SF) for Mode II were assumed. The (111)Si surface plane was then

transformed to a (221)Si surface plane. The associated (LMN) matrix for (221)Si//$(11\bar{2}2)A\ell_2O_3$ was then calculated, employing the formulae given in this section, and compared with that obtained directly from the experimental data. The two (LMN) matrices were found to be substantially identical. For example, Z_s' for (221)Si//$(11\bar{2}2)A\ell_2O_3$ is $\perp(11\bar{2}2)$ while the transformed Z_s' derived from (111)Si//$(11\bar{2}4)A\ell_2O_3$ is $\perp(1,1,\bar{2}, 2.03412)$. The angle between these two planes is equal to 0.31506 deg and is smaller than the experimental error in either the (111)Si or (221)Si orientation determinations. We shall, based on a low-index argument, assume that the (111)Si orientation relation is the more fundamental and take this Si/$A\ell_2O_3$ case as the "natural" defining growth for Mode II epitaxy. (221)Si is then in the same mode of epitaxy but is "rotated" following the mathematical formalism given in this section.

III. STRESS AND STRAIN IN $Si/A\ell_2O_3$ EPITAXIAL FILMS

The principal objective of the present paper is the theoretical determination of stress-induced anisotropies in carrier mobility for $Si/A\ell_2O_3$ films. In this section we shall discuss briefly the origin of stress and strain in $Si/A\ell_2O_3$ films and then describe the stress model we have employed to calculate thermal expansion mismatch stresses for use in the piezoresistance-effect studies.

The origin of stress and strain in various epitaxial films has been discussed by Hoffman[8] and by Chopra[9]. These authors both divide the stresses in epitaxial films into two categories: (1) intrinsic stresses and (2) thermal stresses.

For the case of $Si/A\ell_2O_3$ epitaxial films, our view is that the probable major origin of intrinsic stress is lattice misfit or mismatch between film and substrate. However, it is not presently possible to actually calculate the lattice-mismatch intrinsic stress. In general, this intrinsic stress is probably of less importance in establishing the total room temperature stress level in the films than is the thermal stress to be discussed subsequently. Intuitively this seems a reasonable assumption, in that the films are grown at elevated temperatures and the lattice mismatch or growth stress can be relieved by the generation of dislocations. High dislocation densities in Si films have been observed, consistent with this assumption.

Let us next consider the second category of stresses in epitaxial films, thermal stresses. Thermal stress in $Si/A\ell_2O_3$ is due to the combined constraints of strong film-substrate bonding

and dissimilar coefficients of thermal expansion and contraction for film and substrate.

One formula often quoted[9] is

$$T_{th} = (\alpha_F - \alpha_s)\Delta T E_F, \tag{18}$$

where T_{th} is the thermal stress, α_f an average film expansion coefficient, and α_s an average substrate expansion coefficient. ΔT is the temperature differential between growth and room temperature and E_F is an appropriate Young's modulus of the film.

Equation (18) has been rather widely used as a means of estimating film stresses due to thermal expansion mismatch. However, there are several qualifications and remarks which pertain to this equation.

First, the equation is valid only for the thin-film thick-substrate case. Jefkins[10] has presented formulae for the stress in Si films on $A\ell_2O_3$ substrates based on an isotropic simple elastic model. These formulae indicate that for films of interest [~2μm-thick Si, 10-20mil-thick $A\ell_2O_3$] the stress relief due to bending is slight and the isotropic (average) stress calculated using Eqn.(18) agrees to within about 1½%. This small difference would justify the use of the thin-film thick-substrate approximation for calculation of the average stress in a thin film.

The second point to be noted about Eqn. (18) concerns the question of anisotropy. Anisotropy is generally defined as the dependence of a given physical property upon crystallographic orientation. Thus Eqn. (18) is anisotropic in that Young's modulus E_f depends upon the Si film orientation and is different for, say,

(001) and (111)Si films. However, in the context of this paper, anisotropy will be taken to refer primarily to the dependence of a given physical property upon angular orientation in the plane of a given film/substrate composite. In this sense the model of Eqn. (18) is isotropic and yields no information on anisotropic stresses in epitaxial films.

The question of anisotropy has apparently not been treated in the literature. Schlötterer[11] employed a formula similar to Eqn. (18) in treating stress in Si films on $MgA\ell_2O_4$ substrates. The film orientation was properly taken into account in calculating the appropriate Young's modulus E_F. However, the applied thermal strains and the resulting stress were isotropic as is appropriate for (001) and (111)Si on $MgA\ell_2O_4$. The case of $A\ell_2O_3$ with a built-in thermal stress anisotropy was not treated.

$A\ell_2O_3$ substrates, in general, yield a thermal strain which is intrinsically anisotropic because of an anisotropy in thermal expansion. The thin-film thick-substrate model which we have employed explicitly treats substrate induced anisotropy.

Our model is based upon the relative thermal expansion between Si film and $A\ell_2O_3$ substrate and the strain in particular directions which this expansion induces. Following Nye[12], the thermal expansion for both Si and $A\ell_2O_3$ is described by second-rank symmetric tensors referenced to Cartesian coordinate systems.

Let α_s be the expansion coefficient for Si and let α_1 and α_2 be the thermal expansion coefficients respectively perpendicular and parallel to the (0001) axis (or c-axis) for $A\ell_2O_3$. The relative thermal expansions between film and substrate are then

$$\begin{pmatrix} \alpha_s & 0 & 0 \\ 0 & \alpha_s & 0 \\ 0 & 0 & \alpha_s \end{pmatrix} \Delta T - \begin{pmatrix} \alpha_1 & 0 & 0 \\ 0 & \alpha_1 & 0 \\ 0 & 0 & \alpha_2 \end{pmatrix} \Delta T = \begin{pmatrix} (\alpha_s-\alpha_1) & 0 & 0 \\ 0 & (\alpha_s-\alpha_1) & 0 \\ 0 & 0 & (\alpha_s-\alpha_2) \end{pmatrix} \Delta T \qquad (19)$$

for a temperature difference ΔT. Here, Cartesian axes in Si are along the cubic axes. For $A\ell_2O_3$ the x-axis is parallel to $\hat{a_1}$, the y-axis is at 90 deg from the $\hat{a_1}$ axis and toward the $\hat{a_2}$ axis. The z-axis is parallel to the $A\ell_2O_3$ c (or $\hat{a_4}$)-axis.

Equation (19) is written in terms of the so-called tensor thermal expansions α_{ij}. For convenience we now switch to the so-called "engineering" thermal expansions[12] ε_i given by $\varepsilon_1 = \alpha_{11}$, $\varepsilon_2 = \alpha_{22}$, $\varepsilon_3 = \alpha_{33}$, $\varepsilon_4 = 2\alpha_{23}$, $\varepsilon_5 = 2\alpha_{13}$, and $\varepsilon_6 = 2\alpha_{12}$. In this contracted single index notation, Eqn. (19) yields $\varepsilon_1 = (\alpha_s-\alpha_1)\Delta T$, $\varepsilon_2=(\alpha_s-\alpha_1)\Delta T=\varepsilon_1$, $\varepsilon_3=(\alpha_s-\alpha_2)\Delta T$, $\varepsilon_4=0$, $\varepsilon_5=0$, and $\varepsilon_6=0$.

For application to the $Si/A\ell_2O_3$ system we shall require the thermal expansions for an arbitrary film/substrate orientation. Let (X',Y',Z') represent a new set of Cartesian axes with X' and Y' in the plane of the film (substrate) surface and Z' normal to the film (substrate) surface plane. The coordinate transformation effecting this change of axes would then be obtained from Eqn. (3) of Section II. The Si thermal expansion matrix is invariant to an arbitrary (lmn) coordinate transformation. Therefore the relative thermal expansion matrix on the right hand side of Eqn. (19) may be transformed directly using only the (LMN) matrix appropriate to the substrate.

Thus, let the coordinate transformation matrix for the substrate be

	x	y	z
x'	L_1	M_1	N_1
y'	L_2	M_2	N_2
z'	L_3	M_3	N_3 .

(20)

The engineering thermal expansions in the arbitrary surface plane (X' and Y' in the plane, Z' normal to the plane) are then given by

$$\begin{aligned}
\varepsilon_1' &= (1-N_1^2)\varepsilon_1 + N_1^2\varepsilon_3 \\
\varepsilon_2' &= (1-N_2^2)\varepsilon_1 + N_2^2\varepsilon_3 \\
\varepsilon_3' &= (1-N_3^3)\varepsilon_1 + N_3^2\varepsilon_3 \\
\varepsilon_4' &= -2N_2N_3(\varepsilon_1-\varepsilon_3) \\
\varepsilon_5' &= -2N_1N_3(\varepsilon_1-\varepsilon_3) \\
\varepsilon_6' &= -2N_1N_2(\varepsilon_1-\varepsilon_3)
\end{aligned} \tag{21}$$

We emphasize that the above are thermal expansions and have not yet been identified as strains per se.

The film and substrate are assumed to be firmly bonded across the interface and constrained in the X' and Y' coordinate directions in the plane of the interface. Thus, the thermal expansions ε_1', ε_2' and ε_6' given in Eqn. (21) are to be regarded as applied strains. There are no other components of applied thermal strain since the film/substrate materials are free to expand or contract in these other directions. However, the ε_1', ε_2' and ε_6' applied thermal strains do act to produce other components of strain through Poisson-type effects.

The stress model will now be developed in terms of the applied thermal strains ε_1', ε_2' and ε_6'. The model

will be in terms of the engineering stresses as given by Nye (13), where $T_1=T_{11}=T_{xx}$, $T_2=T_{22}=T_{yy}$, $T_3=T_{33}=T_{zz}$, $T_4=T_{23}=T_{yz}$, $T_5=T_{13}=T_{xz}$ and $T_6=T_{12}=T_{xy}$. The matrix of elastic constants also is assumed in the form given by Nye.

The essence of the model is simply that the applied thermal strains ε_1', ε_2' and ε_6' are assumed applied to the Si film. These strains interact through the elastic properties of the Si to produce stresses in the Si. In this model the only role of the substrate is to produce the initial applied strains, and the elastic properties of the substrate need not be considered.

The stresses in the Si film T_i', are then given in terms of the Si elastic constant matrix elements C_{ij}' and the strains ε_i' by

$$\begin{pmatrix} T_1' \\ T_2' \\ T_3' \\ T_4' \\ T_5' \\ T_6' \end{pmatrix} = \begin{pmatrix} C_{11}' & C_{12}' & C_{13}' & C_{14}' & C_{15}' & C_{16}' \\ C_{12}' & & & & & \cdot \\ C_{13}' & & & & & \cdot \\ C_{14}' & & & & & \cdot \\ C_{15}' & & & & & \cdot \\ C_{16}' & \cdot & \cdot & \cdot & \cdot & C_{66}' \end{pmatrix} \begin{pmatrix} \varepsilon_1' \\ \varepsilon_2' \\ \varepsilon_3' \\ \varepsilon_4' \\ \varepsilon_5' \\ \varepsilon_6' \end{pmatrix}, \qquad (22)$$

where ε_1', ε_2', ε_6' are the applied thermal strains and ε_3', ε_4', ε_5' are Poisson reaction strains to be determined by boundary conditions.

The Si film surface is a free surface and must have no stresses on the z surface. Thus T_3, T_4, T_5 are all zero at the free surface of the Si film. Since the film is thin, we assume the stresses are approximately constant in the z direction. Continuity then allows us to set these three stresses to zero throughout the Si film. This is the second basic assumption of the model.

The Si elastic constants C'_{ij} (i=1, 6; j=1,6) for the arbitrary Cartesian coordinate system can be obtained from those for the original crystallographic system along the Si cubic axes by suitable transformation. Wortman and Evans[14] have worked out the tedious transformation based upon the fourth rank elastic tensor properties and we have employed their results for the Si matrix elements C'_{ij}.

Assuming the C'_{ij} to be known for the desired coordinate system, and the applied thermal strains ε'_1, ε'_2 and ε'_6 to be known from Eqn. (21), the reaction strains ε'_3, ε'_4, ε'_5, not given by Eqn. (21) can be determined by matrix inversion. The determination of the thermal expansion stresses T'_1, T'_2 and T'_6 required for the carrier mobility-piezoresistance study can then be carried out.

This summarizes the stress model which is basic to the present work. Within the framework of what is essentially a thin-film thick-substrate model, the anisotropy in thermal expansion coefficients and the anisotropy in the Si stresses have been rigorously included and treated.

The stress model developed is a very simple model. Our present opinion is that for the $Si/A\ell_2O_3$ films of interest (1.5-2μm-thick Si, 10-20mil-thick $A\ell_2O_3$) any limitations in application of the stress formula will be due in large measure to features which lie outside the framework of the elastic theory, rather than in the level of rigor employed in working this particular problem.

IV. THE PIEZORESISTANCE EFFECT IN Si

The basic phenomenological formalism for the linear piezoresistance effect in a thin "bulk" Si film has been established for some time now. However, there has previously been no development and application to heteroepitaxial substrate-induced mobility anisotropies. In this section the formal equations which we have employed in calculations of mobility anisotropy are discussed. Most of the emphasis is upon a linear model but non-linear corrections of interest for the high stress levels in $Si/A\ell_2O_3$ films are also presented and employed.

The linear piezoresistance effect has been discussed by various authors[15,16,17]. These authors begin by assuming that the electric field components, E_i', are functions of the current density components, J_j' and the stress components, $T_{k\ell}'$. E_i' is then expanded in a series about the state of zero stress and zero current. The differential increments in the series expansion are then replaced by the variables themselves yielding the basic tensor equation

$$E_i' = \rho_{ij}' J_j' + \pi_{ijk\ell}' J_j' T_{k\ell}'. \tag{23}$$

For cubic crystals the resistivity tensor ρ_{ij}' is diagonal for zero stress and has only the components $\rho_{ij}'=\rho_o\delta_{ij}$ where ρ_o is the zero-stress resistivity and δ_{ij} is the Kronecker delta. For these materials it is customary to factor out the zero-stress resistivity from the $\pi_{ijk\ell}'$. Then

$$E_i' = \rho_o \left(\delta_{ij} + \frac{\pi_{ijk\ell}'}{\rho_o} T_{k\ell}'\right) J_j', \tag{24}$$

where $(\pi_{ijk\ell}'/\rho_o)$ are the piezoresistance coefficients as defined

and employed by most authors in quoting experimental values for the coefficients. In applications, Eqn. (24) is usually shortened by using the single-subscript notation for the stress components and a double-subscript notation for the piezoresistance coefficients [11→1, 22→2, 33→3, 23→4, 13→5, 12→6][15,16]. The double-subscript π's then can be displayed as a 6x6 matrix, which for Si and for a Cartesian coordinate system directed along the cubic crystal axes is of the form

$$\begin{pmatrix} \pi_{11} & \pi_{12} & \pi_{12} & 0 & 0 & 0 \\ \pi_{12} & \pi_{11} & \pi_{12} & 0 & 0 & 0 \\ \pi_{12} & \pi_{12} & \pi_{11} & 0 & 0 & 0 \\ 0 & 0 & 0 & \pi_{44} & 0 & 0 \\ 0 & 0 & 0 & 0 & \pi_{44} & 0 \\ 0 & 0 & 0 & 0 & 0 & \pi_{44} \end{pmatrix} . \qquad (25)$$

The three constants π_{11}, π_{12}, π_{44} then completely characterize the bulk piezoresistance matrix for Si.

Equations (23) and (24) refer to an arbitrarily oriented Cartesian coordinate system, and the associated matrix of coefficients will not be of the simple form in Eqn. (25). Pfann and Thurston[16] and Thurston[17] have presented tables listing all π' coefficients for rotated (transformed) axes. In terms of the primed (rotated) coordinate system, no elements of the π' matrix are required to be zero and the matrix is, in general, asymmetric in that some π'_{ij}'s differ from the π'_{ji}'s by a factor of two.

For an arbitrarily oriented coordinate system (X',Y',Z') or (X'_1,X'_2,X'_3) in which X' (X'_1) and Y' (X'_2) are in the plane of the

$Si/A\ell_2O_3$ film and $Z'(X_3')$ is normal to the $Si/A\ell_2O_3$ film, the Eqn. (24) then becomes

$$
\begin{aligned}
E_1'/\rho_o &= J_1'(1+\pi_{11}'T_1'+\pi_{12}'T_2'+\pi_{16}'T_6'),\\
E_2'/\rho_o &= J_1'(\pi_{61}'T_1'+\pi_{62}'T_2'+\pi_{66}'T_6'),\\
E_3'/\rho_o &= J_1'(\pi_{51}'T_1'+\pi_{52}'T_2'+\pi_{56}'T_6'),\\
E_1'/\rho_o &= J_3'(\pi_{51}'T_1'+\pi_{52}'T_2'+\pi_{56}'T_6'),\\
E_2'/\rho_o &= J_3'(\pi_{41}'T_1'+\pi_{42}'T_2'+\pi_{46}'T_6'),\\
E_3'/\rho_o &= J_3'(1+\pi_{31}'T_1'+\pi_{32}'T_2'+\pi_{36}'T_6').
\end{aligned}
\qquad (26)
$$

The π_{ij}' include the resistivity ρ_o and in some cases a factor of two in the definition. In Eqns. (26) we have assumed that the stresses T_1', T_2' and T_6' are the only non-zero stress components in the Si as discussed in Section III. In the first three of Eqns. (26) it was assumed that the current flow was solely in the 1 direction (only J_1' non-zero), and in the last three of Eqns. (26) the current is solely in the 3 direction (only J_3' non-zero). These two cases are adequate to cover all experimental device configurations of interest.

The first and last of Eqns. (26) can be written in a form more directly related to the carrier mobility. These two equations deal with so-called longitudinal piezoresistance effects in that the field and current components are both in the same direction. We let ρ_1' and ρ_3' be the resistivities in the 1 and 3 coordinate directions, respectively. Then, in terms of the zero-stress resistivity ρ_o,

$$\frac{E_1'}{J_1'\rho_o} \equiv \frac{\rho_1'}{\rho_o} \equiv \frac{\rho_o+\Delta\rho_1'}{\rho_o} \quad ; \quad \frac{\Delta\rho_1'}{\rho_o} = \pi_{11}'T_1' + \pi_{12}'T_2' + \pi_{16}'T_6' \; ;$$

$$\frac{E_3'}{J_3'\rho_o} \equiv \frac{\rho_3'}{\rho_o} \quad \frac{\rho_o+\Delta\rho_3'}{\rho_0} \quad ; \quad \frac{\Delta\rho_3'}{\rho_0} = \pi_{31}'T_1' + \pi_{32}'T_2' + \pi_{36}'T_6' \; . \tag{27}$$

The Hall mobility μ in a given direction can be related to the resistivity ρ by $\mu = R_H/\rho$, where R_H = the Hall constant. Thus

$$\mu_1/\mu_o = \frac{1}{1+\Delta\rho_1'/\rho_o} \quad ; \quad \mu_3/\mu_o = \frac{1}{1+\Delta\rho_3'/\rho_o} \; , \tag{28}$$

where $\Delta\rho_1'/\rho_o$ and $\Delta\rho_3'/\rho_o$ are as defined in Eqn. (27). Our primary interest in the Hall mobility will be in mobilities for current flows J_1' in the plane of the Si film. In subsequent discussion, a mobility μ without a subscript will be taken to relate to μ_1. Eqns. (28) are fundamental and, in the linear piezoresistance model, all connections between mobilities and resistivities will assume $\mu = R_H/\rho$ and Eqns. (28).

The above discussion relates to a linear piezoresistance model in that the change in resistivity is proportional to the stress. However, since stress levels in $Si/A\ell_2O_3$ films are high and relate to strains much larger than those usually encountered in "bulk" Si piezoresistance applications, it is of interest to consider non-linear corrections to the linear model.

A non-linear theory of piezoresistance does not presently exist. The rigorous development of such a theory appears to be a formidable task and will not be attempted here. We shall simply consider corrections to the longitudinal piezoresistance

$\rho_1' \equiv E_1'/J_1'$ and $\rho_3' \equiv E_3'/J_3'$ which, while not rigorously correct, are probably an improvement on the linear model for those cases in which the predicted change in resistivity due to stress is substantial.

Schlötterer[11] has related the change in resistivity to the stress using

$$\frac{\Delta\rho}{\rho} = k_1 T + k_2 T^2 \ , \tag{29}$$

following Mason, Forst and Tornillo[18]. The latter authors employed a Si many-valley model and considered the effects of a uniaxial stress. No direct use was made of the π_{ij} coefficients. Schlötterer then assumed, based upon the work of Sanchez and Wright[19], that for practical use the relation $k_2 \simeq 0.5\ k_1^2$ was valid. For present purposes, we shall simply assume this relation is approximately correct and will not attempt to justify it.

The procedure followed by Schlötterer would, in our case of anisotropic stress, yield mobilities

$$\mu_1/\mu_o = \frac{1}{1+(\pi_{1j}' T_j')+\frac{1}{2}(\pi_{1j}' T_j')^2}$$

and

$$\mu_3/\mu_o = \frac{1}{1+(\pi_{3j}' T_j')+\frac{1}{2}(\pi_{3j}' T_j')^2} \ , \tag{30}$$

where the implied sum on j includes j=1,2 and 6 for $Si/A\ell_2O_3$ films. The primes on π and T signify that π and T are to be calculated for the arbitrary coordinate system under consideration.

It might be argued that if Eqn. (29) is approximately correct for the stress and strain levels of Ref. (19), then the larger stresses in $Si/A\ell_2O_3$ films may require the inclusion of higher order terms in the stress. We have derived a correction which is in the spirit of Eqn. (29) but which includes higher order terms.

We consider Eqn. (23) for j=i. Differentiating with respect to $T'_{k\ell}$ we obtain

$$\delta(E'_i/J'_i) = \rho'_{ii} \left(\frac{\pi'_{iik\ell}}{\rho'_{ii}} \right) (\delta T'_{k\ell}). \tag{31}$$

Schlötterer[11] presents a graph of π_{ij} coefficients for a range of carrier concentrations. The experimental π's are approximately constant for moderate changes in carrier concentration. This suggests to us that the terms $(\pi'_{iik\ell}/\rho'_{ii})$ in Eqn. (31) are approximately constant for moderate changes in resistivity ρ'_{ii}. We shall assume this to be the case. Noting that $(E'_i/J'_i) \equiv \rho'_{ii} = \rho'_i$, Eqn. (31) integrates to yield

$$\rho'_i = \rho_o \quad e^{+(\pi'_{ij}T'_j)} \tag{32}$$

in the contracted subscript notation. Here $\rho'_i(T'_j=0) = \rho_o$ is the zero-stress (scalar) resistivity. The longitudinal mobilities for this model are then

$$\mu_1/\mu_o = \frac{1}{e^{+(\pi'_{1j}T'_j)}} \; ; \; \mu_3/\mu_o = \frac{1}{e^{+(\pi'_{3j}T'_j)}} . \tag{33}$$

Eqns. (28), (30) and (33) thus represent mobilities based on linear (1st order), second, and exponential order stress models,

respectively, and are all mutually consistent to within their respective orders.

Numerical data for comparison of mobilities in the linear and non-linear models are given in Table III. The linear mobility is taken as the independent variable and the non-linear mobilities are then calculated from Eqns. (28), (30) and (33).

In this paper, the linear model will be used in all analytic expressions and formulae presented for the various orientations of p- and n-type Si/Al_2O_3 films studied. In most cases where the resulting linear and non-linear numerical mobilities differ significantly, both the linear and exponential order mobilities will be given.

A more mathematically rigorous non-linear model than in Eqns. (31) and (32) has also been investigated. This model is, in principle, applicable to the transverse as well as the longitudinal piezoresistances. The result is a complicated matrix analog of the scalar Eqn. (32) and numerical data cannot be obtained in closed form. It thus appears to be without profit to further pursue this approach at this time.

In concluding the discussion of non-linear piezoresistance effects, the position taken will be re-emphasized. Neither of the correction terms employed in Table III is considered to be rigorously correct. Nonetheless, in those cases where linear and non-linear mobilities differ markedly, it is felt that the non-linear mobility (in particular the exponential order mobility) is much more accurate than the linear mobility and must be employed.

A prime was used in all piezoresistance formulae presented thus far. The prime signifies that the π's and T's are referenced to an arbitrary fixed coordinate system. We now wish to become specific to the case of $Si/A\ell_2O_3$ films. For a given $Si/A\ell_2O_3$ film growth, we are interested in the anisotropy of piezoresistance and mobility as a function of orientation or direction in the plane of the film.

Thus, let $X'Y'Z'$ represent reference axes with X' and Y' in the plane of the film and Z' normal to the plane. The coordinate transformation relating this set of reference axes to the Si crystal axes will be denoted by (ℓmn) as in Eqns. (3) or (8). Now let (α) be a matrix representing a rotation about the Z' direction. Then

$$(\alpha) = \begin{pmatrix} \cos\theta & \sin\theta & 0 \\ -\sin\theta & \cos\theta & 0 \\ 0 & 0 & 1 \end{pmatrix} , \tag{34}$$

where the sense of the rotation is that a positive angle θ rotates the X' axis toward the Y' axis. Following Eqn. (8), the $(\ell mn)'$ type matrix explicitly involving the angle θ and referenced to the $X'Y'Z'$ axes is

$$(\ell mn)' = (\alpha)\ (\ell mn). \tag{35}$$

This rotation could also be applied to the $A\ell_2O_3$ substrate coordinate system,but for present purposes this is unnecessary.

Let us return to Eqns. (26). Now the prime in the equations will be interpreted to refer to a coordinate system at an angle θ from the reference coordinate system with X and Y in the Si plane and Z normal to the Si film plane. The π coefficients are then obtained using $(\ell mn)'$ in Eqn. (35) and the table in Ref. (15). The π coefficients will then be explicit functions of θ the angle of rotation. The stresses T_1', T_2' and T_i' are similarly interpreted and are given by

$$
\begin{aligned}
T_1' &= \left(\frac{T_1+T_2}{2}\right) + \left(\frac{T_1-T_2}{2}\right)\cos 2\theta + T_6 \sin 2\theta, \\
T_2' &= \left(\frac{T_1+T_2}{2}\right) - \left(\frac{T_1-T_2}{2}\right)\cos 2\theta - T_6 \sin 2\theta, \\
T_6' &= -\left(\frac{T_1-T_2}{2}\right)\sin 2\theta + T_6 \cos 2\theta,
\end{aligned}
\tag{36}
$$

where now T_1',T_2' and T_6' are the stresses in the film at an angle θ from the reference and T_1,T_2,T_6 are the reference stresses at θ=0.

V. APPLICATION TO (001), (221), and (111)Si FILM GROWTH

In this section the calculation of mobility anisotropy for Si film growths of three different orientations, (001), (221), and (111), will be discussed. Measured experimental anisotropies and calculated theoretical results for (001)Si[1] and for (221)Si[2] have been previously reported by the author. The purpose of the present section if to present a more detailed theoretical description and provide information not reported in the earlier accounts.

A. (001)Si/(01$\bar{1}$2)$A\ell_2O_3$ (Mode I Epitaxy)

The case of (001)Si//(01$\bar{1}$2)$A\ell_2O_3$ is an example of Mode I epitaxy as defined in Section II and in Table II. For calculation of the piezoresistance and mobility anisotropy for this orientation we shall adopt reference coordinate systems given as (X_f', Y_f', Z_f') and (X_s', Y_s', Z_s'), respectively, in Table II. The (LMN) matrix relating this coordinate system in the $A\ell_2O_3$ substrate to the original Cartesian crystal axes is then given by (Eqn. (3))

$$(LMN) = \begin{pmatrix} 1 & 0 & 0 \\ 0 & \frac{a}{c\eta} - \frac{1}{\eta\sqrt{3}} & \\ 0 & \frac{1}{\eta\sqrt{3}} & \frac{a}{c} \end{pmatrix} = \begin{pmatrix} 1 & 0 & 0 \\ 0 & +.535703144 & -.8444063841 \\ 0 & +.8444063841 & +.535703144 \end{pmatrix}, \quad (37)$$

where η is a normalization constant = $(1/3+(a/c)^2)^{\frac{1}{2}}$ and a (c/a) ratio of 2.730159 has been assumed for $A\ell_2O_3$. The (ℓmn) matrix relating to our reference axes in Si and the (ℓmn)$'$ matrix incorporating the rotation about the Z_f' axis are both trivial and are given below.

$$(\ell mn) = \begin{pmatrix} 1 & 0 & 0 \\ 0 & 1 & 0 \\ 0 & 0 & 1 \end{pmatrix} \quad ; \quad (\ell mn)' = \begin{pmatrix} \cos\theta & \sin\theta & 0 \\ -\sin\theta & \cos\theta & 0 \\ 0 & 0 & 1 \end{pmatrix} . \tag{38}$$

Employing the $(\ell mn)'$ matrix in Eqn. (38), the π' transformation table in Ref. (15), and Eqns. (36) we find the piezoresistance equations (Eqns. (26)) become

$$\left(\frac{E_1'}{\rho_o J_1'} - 1\right) = \frac{\Delta\rho_1'}{\rho_o} = \left(\frac{T_1+T_2}{2}\right)(\pi_{11}+\pi_{12}) + \left(\frac{T_1-T_2}{2}\right)(\pi_{11}-\pi_{12})\cos 2\theta + T_6\pi_{44}\sin 2\theta , \tag{39}$$

$$\left(\frac{E_2'}{\rho_o J_1'}\right) = -\left(\frac{T_1-T_2}{2}\right)(\pi_{11}-\pi_{12})\sin 2\theta + T_6\pi_{44}\cos 2\theta , \tag{40}$$

$$\left(\frac{E_3'}{\rho_o J_3'} - 1\right) = \frac{\Delta\rho_3'}{\rho_o} = \left(\frac{T_1+T_2}{2}\right)2\pi_{12} . \tag{41}$$

For (001)Si, $(E_3'/\rho_o J_1') = (E_1'/\rho_o J_3') = (E_2'/\rho_o J_3') = 0$. Eqns. (39) and (41) reduce to Schlötterer's[11] Eqns.(5a) and (5c) in the limit where $T_1=T_2$ and $T_6=0$. In the above equations π_{11}, π_{12}, π_{44} are the basic piezoresistance constants shown in Eqn. (25) and referenced to the Si crystal axes.

We next solve for the stresses T_1, T_2 and T_6 from Eqns. (22). Here the primes on the C_{ij}'s and the ε_1's relate to $\theta=0$ and hence to the (ℓmn) matrix in Eqn. (38) and to the (LMN) matrix in Eqn. (37), respectively. In accordance with our notation, the primes on the stresses are to be suppressed. We obtain

$$
\begin{aligned}
T_1 &= C_{11}\varepsilon_1' + C_{12}\varepsilon_2' + C_{12}\varepsilon_3', \\
T_2 &= C_{12}\varepsilon_1' + C_{11}\varepsilon_2' + C_{12}\varepsilon_3', \\
T_3 &= C_{12}\varepsilon_1' + C_{12}\varepsilon_2' + C_{11}\varepsilon_3', \\
T_4 &= C_{44}\varepsilon_4', \\
T_5 &= C_{44}\varepsilon_5', \\
T_6 &= C_{44}\varepsilon_6',
\end{aligned}
\tag{42}
$$

where ε_1', ε_2', and ε_6' are applied thermal strains and ε_3', ε_4', and ε_5' are Poisson reaction strains.

In accordance with our stress model, $T_3=T_4=T_5=0$. We then find that for this orientation of film and substrate, the reaction strains ε_4' and ε_5' are zero. Solving for T_1, T_2, T_6, we obtain the implicit relations

$$
\begin{aligned}
\frac{T_1+T_2}{2} &= \frac{C_{11}^2+C_{11}C_{12}-2C_{12}^2}{2C_{11}} [(2-N_1^2-N_2^2)\varepsilon_1 + (N_1^2+N_2^2)\varepsilon_3], \\
\frac{T_1-T_2}{2} &= -\frac{(C_{11}-C_{12})}{2} (N_1^2-N_2^2) (\varepsilon_1-\varepsilon_3), \\
T_6 &= -2C_{44} N_1N_2 (\varepsilon_1-\varepsilon_3),
\end{aligned}
\tag{43}
$$

where N_1 and N_2 are defined in Eqns. (3) and (20) and given numerically in Eqn. (37). The crystallographic axis strains ε_1 and ε_3 have been given in Section III and are

$$
\begin{aligned}
\varepsilon_1 &= (\alpha_s-\alpha_1)\Delta T, \\
\varepsilon_3 &= (\alpha_s-\alpha_2)\Delta T,
\end{aligned}
\tag{44}
$$

where α_s is the thermal expansion coefficient for Si and α_1, α_2 are the thermal expansion coefficients for Al_2O_3 in directions perpendicular and parallel, respectively, to the c-axis.

The stresses in Eqn. (43) can now be evaluated. For elastic constant data for Si we use that given by Hearmon[20]. For the Si thermal expansion, an average value of $\alpha_s = 3.9 \times 10^{-6}$/deg C[11] was employed. For our primary data on Al_2O_3 thermal expansion we use that of Austin[21] with $\alpha_1 = 8.31 \times 10^{-6}$/deg C and $\alpha_2 = 9.03 \times 10^{-6}$/deg C Thus $(\alpha_1 - \alpha_2) = -0.72 \times 10^{-6}$/deg C for Al_2O_3. Recent measurements[22] at this laboratory using a differential technique have given a difference in thermal expansion coefficients $\alpha_1 - \alpha_2$ of $(-1.08 \pm 0.12) \times 10^{-6}$/deg C for the Al_2O_3 substrate. Calculations have been performed using both sets of expansion data for Al_2O_3 as a means of determining the sensitivity of the calculated results to the expansion data[23]. The results are given below for $\Delta T = 1100$C deg.

Case 1; $(\alpha_1 - \alpha_2) = -0.72 \times 10^{-6}$/deg C[21]

$\frac{1}{2}(T_1 + T_2) = -0.9206 \times 10^{10}$ dyn/cm^2

$\frac{1}{2}(T_1 - T_2) = +0.2852 \times 10^{9}$ dyn/cm^2

$T_6 = 0.0$

(45)

Case 2; $(\alpha_1 - \alpha_2) = -1.08 \times 10^{-6}$/deg C[22]

$\frac{1}{2}(T_1 + T_2) = -0.9105 \times 10^{10}$ dyn/cm^2

$\frac{1}{2}(T_1 - T_2) = +0.4278 \times 10^{9}$ dyn/cm^2

$T_6 = 0.0$

Substitution of these values for the stresses and values of piezoresistance coefficients for Si from Smith[24,25] yields the results shown in Table IV.

Let us first consider the p-type Si results of Table IV. For this (001)Si orientation the p-type piezoresistance effects ($\Delta\rho_1'/\rho_o$, $E_2'/\rho_o J_1'$, and $\Delta\rho_3'/\rho_o$) are all quite small and would yield variations in mobility much smaller than the experimental scatter in data normally present in such measurements. For all practical purposes then, piezoresistance in p-type (001)Si films can apparently be ignored. On the other hand, we shall find that p-type piezoresistance effects for some other Si orientations are substantially larger than the n-type piezoresistance effects.

Next consider the n-type Si longitudinal piezoresistance data $\Delta\rho_1'/\rho_o$ of Table IV. Since the mobility μ can be related to the resistivity ρ_1 by $\mu=R_H/\rho_1$, where R_H = the Hall constant, the theoretical mobility can be written

$$\begin{aligned} &\underline{\text{Case 1}} \\ &\mu/\mu_o = [1+\Delta\rho_1'/\rho_o]^{-1} = [1.441924-.044488\ \cos 2\theta]^{-1}, \\ &\underline{\text{Case 2}} \\ &\mu/\mu_o = [1+\Delta\rho_1'/\rho_o]^{-1} = [1.437032-.066732\ \cos 2\theta[^{-1}, \end{aligned} \tag{46}$$

where μ_o is the zero-stress mobility. From Eqn. (46) we note that the mobility will be a maximum along the [100]Si direction and will be a minimum 90 deg away along the [010]Si direction.

The amount of anisotropy -- the parameter which can be most conveniently and definitively extracted from experimental data -- can be described conveniently by a parameter A which we define as

$A = (\mu_{max}-\mu_{min})/\mu_A$, where $\mu_A = 1/2(\mu_{max}+\mu_{min})$ is an approximate average mobility in the plane[26]. In terms of these parameters we find A = 6.17% and $\mu_A = 0.694\mu_o$ for Case 1 and A = 9.29% and $\mu_A = 0.697\mu_o$ for Case 2 values of thermal expansion data. We thus find an anisotropy in mobility of from 6.2% to 9.3% superimposed on a substantial ≈30% overall theoretical reduction in mobility for n-type (001)Si.

The theoretically predicted transverse piezoresistance effect, corresponding to an electric field E_2' in the plane of the film and orthogonal to the current J_1' direction, is also given in Table IV. This effect is characterized by the magnitude of the coefficient of the sin2θ term which is +0.044488 and +0.066732, respectively, for Case 1 and Case 2.

The longitudinal piezoresistance effect $\Delta\rho_1'/\rho_o$ and the transverse effect $E_2'/\rho_o J_1'$ have both been measured experimentally and reported in Ref. (1). The values of the anisotropy parameter A determined experimentally ranged from 7.6% to 11.7%, with an average value of 9.5%. The measured transverse-effect data, due to the smallness of the voltage being measured, exhibited more scatter than did the longitudinal effect. A least-squares fit to the data yielded a sin2θ coefficient of 0.08. The theoretically predicted longitudinal and transverse piezoresistance effects for Case 2 thermal expansion data are thus in reasonable agreement with experiment. Thus, the conclusion in Ref. (1) was that the mobility anisotropy and transverse effect could be substantially accounted for in terms of substrate-induced stresses without recourse to other phenomena. For a detailed discussion the reader is referred to Ref. (1).

B. (221)/Si/$(11\bar{2}2)A\ell_2O_3$ (Mode II Epitaxy)

The case of (221)Si/$(11\bar{2}2)A\ell_2O_3$ is an "off-orientation" example of Mode II epitaxy as discussed in Section II. In calculating the piezoresistance effects for this film orientation, we shall adopt reference coordinate systems given as (X_f', Y_f', Z_f') and (X_s', Y_s', Z_s'), respectively, in Table II under the (221)Si/$(11\bar{2}2)A\ell_2O_3$ heading.

The parallel relations in Table II lead to the following (LMN) matrix relative to our reference axes:

$$(LMN) = \begin{pmatrix} \frac{\sqrt{3}}{2} & -1/2 & 0 \\ \frac{(a/c)}{2\eta} & \frac{\sqrt{3}(a/c)}{2\eta} & \frac{-1}{\eta} \\ \frac{1}{2\eta} & \frac{\sqrt{3}}{2\eta} & \frac{(a/c)}{\eta} \end{pmatrix}; \quad \begin{matrix} N_1 = 0.0 \\ N_2 = -0.93899, \end{matrix} \qquad (47)$$

where η is a normalization constant = $(1+(a/c)^2)^{\frac{1}{2}}$ and (c/a)=2.730159 was assumed.

The $(\ell mn)'$ matrix incorporating the rotation about the Z_f' axis is given by

$$(\ell mn)' = \frac{1}{3\sqrt{2}} \begin{pmatrix} +3\cos\theta+\sin\theta & -3\cos\theta+\sin\theta & -4\sin\theta \\ -3\sin\theta+\cos\theta & +3\sin\theta+\cos\theta & -4\cos\theta \\ 2\sqrt{2} & 2\sqrt{2} & \sqrt{2} \end{pmatrix}, \qquad (48)$$

where θ is measured from the $[1\bar{1}0]$Si direction toward the $[11\bar{4}]$Si direction. Using this $(\ell mn)'$ matrix and the transformation properties of the π's, the (221)Si//$(11\bar{2}2)A\ell_2O_3$ piezoresistance equations become

$$\left(\frac{E_1'}{\rho_o J_1'} - 1\right) = \frac{\Delta\rho_1'}{\rho_o} = \left(\frac{T_1+T_2}{2}\right)\left[(\pi_{11}+\pi_{12}) - (\pi_{11}-\pi_{12}-\pi_{44})\frac{4}{27}(2+\cos 2\theta)\right]$$

$$+\left(\frac{T_1-T_2}{2}\right)\left[(\pi_{11}-\pi_{12})\cos 2\theta-(\pi_{11}-\pi_{12}-\pi_{44})\frac{1}{27}(4+11\cos 2\theta)\right]$$

$$+ T_6\left[(\pi_{11}-\pi_{12})\sin 2\theta-(\pi_{11}-\pi_{12}-\pi_{44})\frac{8}{9}\sin 2\theta\right],$$

$$\left(\frac{E_2'}{\rho_o J_1'}\right) = \left(\frac{T_1+T_2}{2}\right)(\pi_{11}-\pi_{12}-\pi_{44})\frac{4}{27}\sin 2\theta$$

$$-\left(\frac{T_1-T_2}{2}\right)\left[\pi_{44}\sin 2\theta +(\pi_{11}-\pi_{12}-\pi_{44})\frac{16}{27}\sin 2\theta\right]$$

$$+ T_6\left[\pi_{44}\cos 2\theta + (\pi_{11}-\pi_{12}-\pi_{44})\frac{1}{9}\cos 2\theta\right],$$

$$\left(\frac{E_3'}{\rho_o J_1'}\right) = -\left(\frac{T_1+T_2}{2}\right)(\pi_{11}-\pi_{12}-\pi_{44})\frac{2\sqrt{2}}{27}\sin\theta \qquad (49)$$

$$+\left(\frac{T_1-T_2}{2}\right)(\pi_{11}-\pi_{12}-\pi_{44})\frac{8\sqrt{2}}{27}\sin\theta$$

$$+ T_6(\pi_{11}-\pi_{12}-\pi_{44})\frac{2\sqrt{2}}{9}\cos\theta,$$

$$\frac{E_1'}{\rho_o J_1'} = \frac{E_3'}{\rho_o J_1'}$$

$$\frac{E_2'}{\rho_o J_3'} = -\left(\frac{T_1+T_2}{2}\right)(\pi_{11}-\pi_{12}-\pi_{44})\frac{2\sqrt{2}}{27}\cos\theta$$

$$+\left(\frac{T_1-T_2}{2}\right)(\pi_{11}-\pi_{12}-\pi_{44})\frac{8\sqrt{2}}{27}\cos\theta$$

$$- T_6(\pi_{11}-\pi_{12}-\pi_{44})\frac{2\sqrt{2}}{9}\sin\theta,$$

and

$$\left(\frac{E_3'}{\rho_o J_3} - 1\right) = \frac{\Delta\rho_3'}{\rho_o} = \left(\frac{T_1+T_2}{2}\right)\left[2\pi_{12} + (\pi_{11}-\pi_{12}-\pi_{44})\frac{16}{27}\right]$$

$$+ \left(\frac{T_1-T_2}{2}\right)\left[(\pi_{11}-\pi_{12}-\pi_{44})\frac{8}{27}\right] .$$

We next solve for the stresses T_1, T_2 and T_6 from Eqns. (22) and for this film/substrate orientation obtain

$$
\begin{aligned}
T_1 &= C'_{11}\varepsilon'_1 + C'_{12}\varepsilon'_2 + C'_{13}\varepsilon'_3 + C'_{14}\varepsilon'_4, \\
T'_2 &= C'_{12}\varepsilon'_1 + C'_{22}\varepsilon'_2 + C'_{23}\varepsilon'_3 + C'_{24}\varepsilon'_4, \\
T'_3 &= C'_{13}\varepsilon'_1 + C'_{23}\varepsilon'_2 + C'_{33}\varepsilon'_3 + C'_{34}\varepsilon'_4, \\
T'_4 &= C'_{14}\varepsilon'_1 + C'_{24}\varepsilon'_2 + C'_{34}\varepsilon'_3 + C'_{44}\varepsilon'_4, \\
T'_5 &= C'_{55}\varepsilon'_5 + C'_{56}\varepsilon'_6, \\
T'_6 &= C'_{56}\varepsilon'_5 + C'_{66}\varepsilon'_6,
\end{aligned}
\tag{50}
$$

where the primes on the C_{ij}'s refer to "rotated" elastic coefficients using (ℓmn) of Eqn. (48) with the angle θ=0 and the transformation table of Ref. (14). This system of equations is sufficiently complicated to render an analytic solution of Eqns. (50) in terms of the applied strains ε'_1, ε'_2 and ε'_6 impractical. We have therefore simply solved the equations numerically, using the elastic constants for Si.

Using Eqns. (21) and the (LMN) matrix in Eqn. (47) we obtain $\varepsilon'_1 = (\alpha_s-\alpha_1)\Delta T$, $\varepsilon'_2=(\alpha_s-\alpha_1)\Delta T + 0.8817095\ (\alpha_1-\alpha_2)\Delta T$, and $\varepsilon'_6=0$. Again setting $T_3=T_4=T_5=0$, and solving for T_1 and T_2, we find the following implicit relations:

$$
\begin{aligned}
\frac{T_1+T_2}{2} &= [22.338504(\alpha_s-\alpha_1)\Delta T + 9.2261599(\alpha_1-\alpha_2)\Delta T]\times 10^{11}\ \mathrm{dyn/cm^2}; \\
\frac{T_1-T_2}{2} &= [1.4106208(\alpha_s-\alpha_1)\Delta T - 4.64325004(\alpha_1-\alpha_2)\Delta T]\times 10^{11}\ \mathrm{dyn/cm^2}; \\
T_6 &= 0.
\end{aligned}
\tag{51}
$$

We note in Eqn. (51) that the thermal stresses would be anisotropic even in the limit $\alpha_1=\alpha_2$, in which the thermal expansion is isotropic; this is in contrast to the (001)Si case in which the stress anisotropy depends solely and directly on the thermal expansion anisotropy.

The stress equations evaluated for Case 1 and Case 2, our two sets of thermal expansion data, and for T=1100C deg yield

Case 1

$$\frac{1}{2}(T_1+T_2) = -1.156712\times10^{10}\,\mathrm{dyn/cm^2},$$

$$\frac{1}{2}(T_1-T_2) = -0.3165467\times10^{9}\,\mathrm{dyn/cm^2},$$

$$T_6 = 0.0 \qquad (52)$$

Case 2

$$\frac{1}{2}(T_1+T_2) = -1.149017\times10^{10}\,\mathrm{dyn/cm^2},$$

$$\frac{1}{2}(T_1-T_2) = -0.1047437\times10^{9}\,\mathrm{dyn/cm^2},$$

$$T_6 = 0.0.$$

The average stress $(T_1+T_2)/2$ is approximately the same in the two cases. However, $(T_1-T_2)/2$ decreases substantially for the larger $(\alpha_1-\alpha_2)$ case and reflects competing origins for the stress anisotropy, as is apparent from Eqns. (51).

Substitution of the above stresses yields the data for $\Delta\rho_1'/\rho_o$, $E_2'/\rho_o J_1'$ and $E_3'/\rho_o J_1'$ shown in Table V. The remaining

piezoresistance effects, $E_2'/\rho_o J_3'$ and $\Delta\rho_3'/\rho_o$, are also non-zero for this (221)Si orientation and can, if desired, be evaluated using the information given.

One general characteristic of the data of Table V compared to the data for (001)Si/(01$\bar{1}$2)$A\ell_2O_3$ should be noted. For (001)Si, the anisotropy in mobility and the transverse effect $E_2'/\rho_o J_1'$ both depend directly on the anisotropy in $A\ell_2O_3$ thermal expansion and are thus relatively different for Case 1 and Case 2 expansion data. However, for (221)Si an important contribution to the piezoresistance effects is independent of the anisotropy in thermal expansion. The data in Table V thus show little relative change between Case 1 and Case 2 expansion data.

We next consider the transverse effect $E_3'/\rho_o J_1'$ data in Table V. This effect depends principally upon the term $(\pi_{11}-\pi_{12}-\pi_{44})$, which is numerically similar for n- and p-Si. Thus all $E_3'/\rho_o J_1'$ data in Table V are substantially identical. This effect involves the generation of a field E_3', normal to the Si film plane, induced by the current J_1' in the plane of the film. Whether this field is of practical significance is not clear and no experimental studies have been performed. In principle, if the zero-stress resistivity and mobility are functions of z-coordinate position (depth) into the film -- as is always the case to some degree in thin hetero-epitaxial films -- then the field generated could be non-uniform in the z-direction and act to produce a modified charge carrier distribution in the film.

We next consider the transverse effect $E_2'/\rho_o J_1'$. Again, all data in Table V are similar for the reasons given above. For

n-type Si the coefficient of the $\sin 2\theta$ term is +0.21227 for Case 1 and +0.2314387 for Case 2. These results are in good agreement with those of Ref. (2) in which a least-squares fit to experimental data yields a coefficient of +0.2.

We next consider the longitudinal piezoresistance $\Delta\rho_1'/\rho_o$ and the associated mobility. Using $\mu = R_H/\rho$, where R_H is the Hall constant, the mobility $\mu/\mu_o = 1/(1+\Delta\rho_1'/\rho_o)$. The characterizations of the mobility in terms of μ_{max}, μ_{min}, μ_A and A are given in Table V. Mobility data derived from the exponential order non-linear model are also shown in Table V and denoted by μ^e_{max}, μ^e_{min}, μ^e_A and A^e. This notation will be used also in subsequent discussion and employs the superscript e to denote the use of the exponential order non-linear mobility formulae of Eqn. (33).

The general conclusion of the theory is that for p-type (221)Si a substantial mobility enhancement should result from thermal stresses, and mobility anisotropies approaching 50% should be obtained. However, no experimental data is available and comparison of theory with experiment cannot be made.

For n-type (221)Si a mobility maximum occurs along the $[1\bar{1}0]$Si direction and a mobility minimum occurs 90 deg away along the $[11\bar{4}]$Si direction. The theory predicts that at an angle of ~36.6 deg from the $[1\bar{1}0]$Si direction the effect of thermal stress on the mobility is zero, so that $\mu(36.6 \text{ deg}) = \mu_o$, the unstressed mobility. The difference between the bulk mobility and the value of mobility measured at this angle thus represents the mobility degradation due to causes other than thermally induced stress.

Experimental data for n-type (221)Si mobility measurements are given in Ref. (2) and indicate an average value of μ_o, the unstressed mobility, of 600 cm^2/V-sec and an average anisotropy of A=39%. The fact that μ_o is so much smaller than the bulk mobility[27] strongly suggests that thermally induced stress is not the dominant mechanism in lowering the mobility in epitaxial films. The average experimental anisotropy of 39% is in good agreement with that predicted theoretically and lends confidence to the theoretical model employed.

The enhanced mobility predicted for some current direction suggests that the (221) plane of n-type $Si/A\ell_2O_3$ may yield superior electron mobilities. In comparison with (001)Si and (111)Si grown at this laboratory, the (221) plane has indeed yielded higher mobilities[2].

C. (111)$Si/A\ell_2O_3$ (Mode II, III, IV Epitaxy)

There are at least three substrate orientations and different modes of epitaxy yielding (111)Si growth. In terms of our model and piezoresistance calculations, these different modes differ only in the substrate-induced thermal strains and can therefore be treated all at the same time.

Following the procedure illustrated in the (001)Si and (221)Si applications, the $(\ell mn)'$ matrix for (111)Si is

$$(\ell mn)' = \frac{1}{\sqrt{6}} \begin{pmatrix} \sqrt{3}\cos\theta + \sin\theta & -\sqrt{3}\cos\theta + \sin\theta & -2\sin\theta \\ \cos\theta - \sqrt{3}\sin\theta & \cos\theta + \sqrt{3}\sin\theta & -2\cos\theta \\ \sqrt{2} & \sqrt{2} & \sqrt{2} \end{pmatrix}, \qquad (53)$$

where the angle θ is measured from the $[1\bar{1}0]$Si direction toward the $[11\bar{2}]$Si direction. The piezoresistance equations, for (111)Si and explicitly involving the angle θ, become

$$\Delta\rho_1'/\rho_o = \left(\frac{T_1+T_2}{2}\right)\frac{(2\pi_{11}+4\pi_{12}+\pi_{44})}{3} + \left(\frac{T_1-T_2}{2}\right)\frac{(\pi_{11}-\pi_{12}+2\pi_{44})}{3}\cos 2\theta$$
$$+T_6\frac{(\pi_{11}-\pi_{12}+2\pi_{44})}{3}\sin 2\theta,$$

$$E_2'/\rho_o J_1' = \left[-\frac{(T_1-T_2)}{2}\sin 2\theta + T_6\cos 2\theta\right]\left(\frac{\pi_{11}-\pi_{12}+2\pi_{44}}{3}\right),$$

$$E_3'/\rho_o J_1' = \left[\left(\frac{T_1-T_2}{2}\right)\sin\theta + T_6\cos\theta\right]\frac{\sqrt{2}}{3}(\pi_{11}-\pi_{12}-\pi_{44}), \qquad (54)$$

$$E_1'/\rho_o J_3' = E_3'/\rho_o J_1',$$

$$E_2'/\rho_o J_3' = \left[\left(\frac{T_1-T_2}{2}\right)\cos\theta - T_6\sin\theta\right]\frac{\sqrt{2}}{3}(\pi_{11}-\pi_{12}-\pi_{44}),$$

$$\Delta\rho_3'/\rho_o = \left(\frac{T_1+T_2}{2}\right)\frac{\sqrt{2}}{3}(\pi_{11}+2\pi_{12}-\pi_{44}) \quad (28).$$

The stress equations (Eqn. (22)) are then solved next, subject again to the boundary condition $T_3=T_4=T_5=0$. The form of the elastic constant matrix is similar to that for the (221)Si case but numerically simpler. The reaction strains ε_3' and ε_4' are non-zero. ε_5' is non-zero unless ε_6' is zero, as will be seen to be the case for some substrate orientations.

The results for the stresses T_1, T_2 and T_6, given in terms of N_1 and N_2 relevant to the particular substrate orientation, are

$$\left(\frac{T_1+T_2}{2}\right) = \frac{3C_{44}[C_{11}+2C_{12}]}{C_{11}+2C_{12}+4C_{44}} \left[(2-N_1^2-N_2^2)\ (\alpha_s-\alpha)\Delta T+(N_1^2+N_2^2)\ (\alpha_s-\alpha_2)\Delta T\right] ,$$

$$\left(\frac{T_1-T_2}{2}\right) = \frac{3}{2}\ \frac{C_{44}(C_{11}-C_{12})}{C_{11}-C_{12}+C_{44}}\ (N_1^2-N_2^2)\ (\alpha_1-\alpha_2)\Delta T , \qquad (55)$$

$$T_6 = 3\ \frac{C_{44}(C_{11}-C_{12})}{C_{11}-C_{12}+C_{44}}\ N_1N_2\ (\alpha_1-\alpha_2)\Delta T .$$

Data for (111)Si Mode II, III, IV epitaxy are given in Table VI. The values of the substrate transformation direction cosines N_1 and N_2 are shown, and the resulting stresses calculated for Case 1 and Case 2 expansion data are also given.

In Table VI only the longitudinal piezoresistance effect $\Delta\rho_1'/\rho_o$ has been considered and the mobility derived from this is shown. Because the anisotropy formulae all involve functions of cos2θ and sin2θ there will be four mobility extrema, with two maxima and two minima. Adjacent maxima and minima are separated by 90 deg. For n-type Si the mobility maxima for Modes II and IV occur at θ=0 which is along the $[1\bar{1}00]$ and $[1\bar{2}10]A\ell_2O_3$ directions, respectively. For Mode III, a maximum mobility occurs at θ=38.242 deg, which is also along the $[1\bar{1}00]A\ell_2O_3$ direction.

The $[1\bar{1}00]$, $[1\bar{2}10]$ and $[1\bar{1}00]$ directions for Modes II, III, IV, respectively, all are perpendicular to the C-axis or [0001] direction. These directions thus pertain to directions yielding the minimum $A\ell_2O_3$ thermal expansion lying within the plane of the film. Clearly the mobilities in these directions should represent relative extrema. Whether a given extremum direction yields a maximum or minimum mobility depends upon the sign of the relevant piezoresistance coefficients. Thus, the mobility maxima and

minima locations in the plane are interchanged for p-type Si as compared with n-type Si.

The effects of stress on mobility for n-type (111)Si are small, as indicated in Table VI. The average mobilities are close to the unstressed mobility, and the anisotropies range from a low of 2.46% (Case 1, Mode IV) to a high of 9.63% (Case 2, Mode III). The Case 2, Mode III, anisotropy is, however, high enough that it should be considered in employing the mobility as a means of evaluating the effects of change in growth parameters.

The effects of thermal stress on p-type (111)Si are much more significant than for n-type (111)Si. A substantial overall mobility enhancement approaching a factor of two is predicted. Based on the (001)Si and (221)Si data, Case 2 thermal expansion data would be most applicable. For this case, the anisotropy factors A range from 6% up to 15% and thus could be of experimental significance in measurements of thin film mobilities.

VI. APPLICATION TO AN OFF-PLANE (111)Si ORIENTATION

In the previous section the piezoresistance and mobility anisotropy were calculated for Mode III epitaxy with a $(11\bar{2}0)Al_2O_3$ substrate orientation. An examination of Fig. 4 of Ref. (5), showing a stereographic projection illustrating Si/Al_2O_3 epitaxial relations, indicates that a $(11\bar{2}0)Al_2O_3$ substrate orientation is either on or close to the boundary between Mode II and Mode III epitaxy. Therefore, in order to insure good quality Si film growths of only one orientation the Al_2O_3 substrate is often intentionally cut a few degrees off the $(11\bar{2}0)$ orientation[29]. In this section we shall apply the theory developed in this paper to a substrate orientation which is ≈5 deg off the $(11\bar{2}0)$ plane. This application illustrates some of the formalism developed in Section II and also provides information on changes in mobility to be expected for slight off-plane Si/Al_2O_3 film growths.

The question of equivalent orientations and internal mathematical consistency was briefly discussed in Section II. This problem arises naturally in the characterization of some off-plane $\approx(11\bar{2}0)Al_2O_3$ substrates used in this laboratory to obtain good quality ≈(111)Si film growths.

The determinations of the substrate surface orientation and of the film/substrate parallel relations both involve the identification and labeling of certain principal x-ray reflections from the Si film (e.g., {311}) and from the Al_2O_3 substrate (e.g., $\{11\bar{2}0\}$). The ambiguity in labeling these reflections--three choices each for Si and Al_2O_3--leads to different but equivalent coordinate systems and characterizations of substrate surface and parallel relations.

The question of mathematical consistency comes in when substrate surface orientation characterization and determination of the parallel relations are not made with an identical labeling of x-ray reflections. In this case, care must be taken to insure that the pole diagrams selected to characterize the film and substrate surfaces are consistent with the parallel relations assumed to hold for the film/substrate composite.

Pole diagrams for one substrate orientation of interest are shown in Fig. 1. Figures 1a, 1b, 1c are equivalent in terms of describing the film and substrate surfaces, but as shown relate to different parallel relations. The orientation shown as Fig. 1a applies to the parallel relations previously adopted in Section II and will be employed in the subsequent calculations. The substrate orientation indicated in Fig. 1a was cut +5 deg from the $(11\bar{2}0)$ plane toward the $(01\bar{1}0)$ plane and along the zone indicated. The axis of rotation for the cut is the [0001] direction. For this mode of epitaxy, the (111)Si plane is || to the $(11\bar{2}0)Al_2O_3$ plane. However, the relevant crystallographic zones in Al_2O_3 and Si are not exactly parallel so that the Si axis of rotation is only approximately the $[0\bar{1}1]$ direction. The pole diagram shown for Si is thus only approximate and will not be used to generate the (ℓmn) matrix for Si required to calculate piezoresistance effects.

The rotation in Al_2O_3 of Fig. 1a is about the hexagonal c-axis which is the Cartesian z-axis. If (β) is the rotation matrix acting upon a column vector, and which, for θ=+30 deg, rotates the Cartesian vector related to $[11\bar{2}0]$ into the Cartesian

vector related to $[01\bar{1}0]$, then the $(LMN)'$ matrix for this off-plane substrate is given by $(LMN)' = (LMN)\,(\tilde{\beta})$, where $(\tilde{\beta})$ is the transpose of (β) and (LMN) relates to the "on-plane" $(11\bar{2}0)$ case. Since the rotation is about the z-axis, the direction cosines N_1 and N_2 which define the thermal strains are constant and independent of the angle of rotation .

From Section II, the $(\ell mn)'$ matrix associated with the off-plane Si film is given by $(\ell mn)' = (LMN)'(SF) = (LMN)(\tilde{\beta})(SF)$, where (SF) is taken from Table II. For $(\ell mn)'$ we obtain (θ=+5 deg)

$$(\ell mn)' = \begin{pmatrix} 1/\sqrt{2} & 0 & 0 \\ 0 & 1/\sqrt{6} & 0 \\ 0 & 0 & 1/\sqrt{3} \end{pmatrix} \begin{pmatrix} +1.052475 & -0.9428301 & +0.0580268 \\ +1.0716329 & +1.078041 & -1.920788 \\ +0.8742111 & +1.04188 & +1.0724898 \end{pmatrix}, \qquad (56)$$

where the normalization factors used were chosen to facilitate comparison with the on-plane simple $(111)Si/(11\bar{2}0)Al_2O_3$ case. From the third row of Eqn. (56) we see that the Si film surface lies approximately along the zone between the (111) and (011)Si planes.

The above discussion relates to an off-plane substrate orientation which is +5 deg away from the $(11\bar{2}0)$ plane. Calculations have also been performed for a -5 deg rotation yielding an off-plane substrate surface which lies between the $(11\bar{2}0)$ and $(10\bar{1}0)$ planes. Although perhaps of less experimental interest, this latter -5 deg rotation data coupled with the on-plane data and the +5 deg rotation data provide insight into the sensitivity of piezoresistance and mobility to small changes in substrate orientation for this mode of (111)Si epitaxy.

The formulas for the longitudinal piezoresistance for $\theta = \pm 5$ deg are rather lengthy and will not be given. We note only that there are contributions to the anisotropy in piezoresistance which do not vanish in the limit, $T_1 = T_2$, of stress isotropy. This result is similar to that found for the (221)Si films, as one would expect.

The stresses T_1, T_2 and T_6 are numerically different for these various orientations, even though the direction cosines N_1 and N_2 determining the thermal strains are independent of rotation angle, since the Si elastic constant matrix is itself different for the different orientations. Numerical results for the $(11\bar{2}0)+5$ deg, $(11\bar{2}0)$, and $(11\bar{2}0)-5$ deg orientations are shown in Table VI. The average stress (T_1+T_2) is nearly constant. However $(T_1-T_2)/2$ and T_6 vary appreciably.

Numerical data for the mobilities derived from the longitudinal piezoresistance $\Delta\rho_1'/\mu_o$ are given in Table VII. Values for μ_{max}/μ_o, μ_{min}/μ_o, $\theta_{\mu_{max}}$ --the angle from the reference axis at which the mobility is a maximum--and the anisotropy factor A are given for both linear and exponential models. Since the formulae evaluated involve $\cos 2\theta$ and $\sin 2\theta$ terms, adjacent maxima and minima are separated by 90 deg and equivalent maxima and minima are separated by 180 deg. Exact comparisons of the angles $\theta_{\mu_{max}}$ are somewhat (less than ± 5 deg) ambiguous since the reference axis is different in each case.

The results for both n and p-type Si are different in the various cases and reflect competing phenomena in establishing the total anisotropy. As expected, the effects of stress on n-type

Si Hall mobilities are much less than for p-type Si. The maximum mobility μ_{max} varies by +7.5% and the anisotropy A^e changes by ≈15% for p-type Si and a +5 deg change in substrate orientation. Thus the mobility, based on thermal expansion stresses, would be expected to be a sensitive function of substrate orientation.

The dependence of p-type Si mobilities on orientation suggests that proper selection of substrate orientation can lead to enhanced mobilities. Of course, physical phenomena other than thermal stress, may also play an important role and have to be considered in selection of optimum substrate and film orientations.

VII. APPLICATION TO THE GENERAL (XX1) Si ORIENTATION

The applications of the thermal stress-piezoresistance model have thus far been limited primarily to film and substrate orientations which are of current experimental interest. In this section we shall apply the model in a predictive sense to general Si film orientations of the form (xx1) to determine the effect of thermal stress on the mobility for other Si orientations which have not been researched experimentally.

Workers in the field of Si epitaxy have long recognized that Si film quality depends upon a number of physical phenomena. The use of thermal stress model mobility data to determine Si orientations of possible experimental interest thus focuses attention on only one part of the epitaxy problem. Nonetheless, the effect of thermal expansion stress on Si film mobilities is substantial and the use of the thermal stress model to predict Si film orientations of potential experimental interest is an important and useful new theoretical tool.

Extensive computer calculations for the (xx1)Si film orientation have been performed. By varying x from zero to infinity, several Si film orientations of the form (xx1) lying along the zone(s) defined by (001)Si, (111)Si, and (110)Si were treated and numerical data obtained. Since Si film quality is usually highest for (001) and (111) types of growth, this general treatment is expected to encompass the orientations of major interest.

In the theoretical treatment, the four modes of $Si/A\ell_2O_3$ epitaxy and the mode of $Si/MgA\ell_2O_4$ epitaxy defined in Section II

are all included. The procedure is to assume for purposes of the calculation that each given mode exists for all Si orientations lying between (001)Si and (110)Si. In reality this is not true and boundaries between the various modes must be considered. In general, in proceeding away from the "natural" plane for a given mode--say (001)Si//(01$\bar{1}$2)$A\ell_2O_3$ (Mode I)--the quality of the film deteriorates and the Si film may become multimoded or defected. An adequate number of growth parameter studies have,however, not been directed specifically toward this question. Thus, the exact relationship between film quality and the number of degrees off of the orientation of a pure mode is not known in detail, although some general information has been established by earlier workers[6]. The (221)Si//(11$\bar{2}$2)$A\ell_2O_3$ is an example of an orientation that is ≈16 deg off the "natural" (111)Si//(11$\bar{2}$4)$A\ell_2O_3$ plane and yet yields good quality films[2].

The reference axes for all of the (xx1)Si plane calculations are assumed to be $X_f'=[1\bar{1}0]$, $Y_f'=[1,1,\bar{2}x]$ and $Z_f'=[xx1]$. The (ℓmn) matrix for this choice of axes is then

$$(\ell mn) = \frac{1}{\sqrt{2}b}\begin{pmatrix} b & -b & 0 \\ 1 & 1 & -2x \\ \sqrt{2} & \sqrt{2} & \sqrt{2} \end{pmatrix}, \qquad (57)$$

where $b=(1+2x^2)^{\frac{1}{2}}$. The substrate surface orientations associated with the (xx1)Si plane can be obtained from the row vector (L_3,M_3,N_3) in the (LMN) matrix by using Eqn. (6) and the (SF) transformation matrices given in Section II. The ability to mathematically treat general $Si/A\ell_2O_3$ orientations of the above and other arbitrary forms is, of course, the main reason a general mathematical

description of Si epitaxy was sought, developed, and presented in Section II.

The mobility has been determined from evaluation of the longitudinal piezoresistance $\Delta\rho_1'/\rho_o$ for four modes of $Si/A\ell_2O_3$ epitaxy and one mode of $Si/MgA\ell_2O_4$ epitaxy. Calculations were performed for twelve values of x in (xx1)Si ranging from (001)Si) through (110)**Si**, and both n and p-type Si were treated. For the $Si/A\ell_2O_3$ modes, Case 2 thermal expansion data ($\alpha_1-\alpha_2=-1.08\times10^{-6}$/deg C) was employed. For the case of $MgA\ell_2O_4$ an average (isotropic) expansion coefficient of 8.1×10^{-6}/deg C was employed[10]. A temperature difference of $\Delta T=1100$C deg was assumed for both cases.

The numerical data obtained are given in Tables IX-XIII. In the tables, the first column lists the value of x in (xx1)Si. The second column shows the number of degrees the subject plane is from the (001)Si plane and toward the (110)Si plane. The remaining columns list the maximum mobility ratio μ_{max}/μ_o, the minimum mobility ratio μ_{min}/μ_o, and the anisotropy parameter A. For p-type Si, mobilities calculated from the linear and exponential models differ markedly. Three additional columns have therefore been added to Tables IX-XIII for μ^e_{max}/μ_o, μ^e_{min}/μ_o and A^e data based upon the exponential non-linear correction term. However, in applications and discussion, only the non-linear data will be employed.

Before discussing the numerical data, it may be useful to again comment briefly on the various origins of the anisotropy in mobility. Basically it is the anisotropy (in the plane of the Si film) of the piezoresistance coefficients, of the elastic constants and of the substrate-induced thermal strain that leads to anisotropies in carrier mobilities.

With respect to the Si film, the carrier mobility anisotropy originating in the Si piezoresistance coefficients and in the elastic constants can be considered as intrinsic to the Si and the mobility anisotropy originating in substrate thermal expansion anisotropy as extrinsic to the Si. In general, the calculated mobility anisotropy will represent an admixture of intrinsic and extrinsic effects and no useful subdivision is possible.

For $Si/MgAl_2O_4$ (Mode V) the substrate thermal expansion is isotropic and thus extrinsic mobility anisotropy is zero. The Si piezoresistance coefficients and elastic constants are isotropic for the cases of (001)Si and (111)Si. Thus the intrinsic mobility anisotropy is also zero for these two orientations.

For the Si/Al_2O_3 modes of epitaxy, the calculated anisotropy for (001)Si and (111)Si is extrinsic and smaller than the intrinsic anisotropy for most other orientations. Thus the anisotropy parameter A as a function of orientation would be expected to exhibit local minima for the (001)Si and (111)Si orientations. The data of Tables IX-XIII illustrate this point with local minima in A occurring at or near these two orientations.

The thermal stress mobility data in Tables IX-XIII are extensive enough to permit a systematic investigation of theoretical mobility as a function of orientation in the defined zone. We first discuss those characteristics which are qualitatively similar for n- and p-type Si films.

The maximum mobility data, μ_{max}/μ_o or μ^e_{max}/μ_o, show that both n- and p-type mobilities are minimum for (001)Si and increase as one proceeds across the defined zone toward (110)Si. A local minimum in the maximum mobility is evident near (111)Si. The

theoretical maximum mobilities for the (001), (111), and (221)Si orientations thus can be ranked with $\mu_{max}(001)<\mu_{max}(111)<\mu_{max}(221)$. Films grown in this laboratory appear, on the average, to confirm this prediction[1,2].

The minimum mobilities, μ_{min}/μ_o or μ^e_{min}/μ_o, are also qualitatively similar for n- and p-type films and exhibit minima for (001) and (110)Si and maxima near (111)Si. The fact that the maxima in μ_{min}/μ_o or μ^e_{min}/μ_o and the minima in μ_{max}/μ_o or μ^e_{max}/μ_o mobilities are near (111)Si is, of course, due to the minima in the anisotropy parameters A or A^e which occur near (111)Si.

Although the n- and p-type mobility data do exhibit qualitative similarities, there are marked quantitative differences. Let us consider the n-type Si mobility first. The maximum mobility μ_{max} ranges from a≈30% reduction in mobility near (001)Si up to a ≈25% enhancement in mobility near (110)Si, as compared with the zero-stress value μ_o. The minimum mobility μ_{min} is always less than μ_o by amounts ranging from ≈30-40% near (001) and (110)Si down to perhaps 5% near (111)Si.

For p-type Si films, the effect of stress is always to increase the mobility, and both μ^e_{max} and μ^e_{min} are greater than μ_o across the entire zone. The stress enhancement of the maximum mobility is minimal for (001)Si and increases rapidly in going across the zone. Values of the maximum mobility ratio μ^e_{max}/μ_o are in the range 1.06-1.09 for (001)Si, 1.80-1.96 for (111)Si, 2.10-2.27 for (221)Si and 2.32-2.44 for (110)Si. Thus, as compared to (001)Si, substantially larger theoretical mobilities can be achieved by choice of film/substrate orientations lying within the zone..

The anisotropy parameter A^e for p-type Si films is also a strong function of orientation and is in the range 0-5% for (001)Si, 6-16% for (111)Si, 45-55% for (221)Si, and 74-80% for (110)Si. The predicted anisotropy along most of the zone is large enough that orientation direction within the plane of the film should be taken into account in experimental mobility measurements to evaluate the effect of changes in film growth parameters. The general characteristics of both n- and p-type Si are illustrated in Figs. (2) and (3) where the shaded regions indicate the range of mobilities associated with Modes I-IV.

The theoretical mobility data presented in Tables IX-XIII and Figs. 2 and 3 are the results of a "model" and the assumptions of this model must be borne in mind in employing this data to estimate experimental mobilities.

The first point concerns the assumptions underlying the (001)-(110)Si "continuous-zone" calculation. Mathematically we have assumed that all modes of epitaxy hold across the entire zone. Realistically, however less significance should be attached to mobility data for points in the zone which are far removed from zonal regions in which the modal relations have been shown experimentally to hold and good quality films obtained.

The basic assumptions of the thermal stress-piezoresistance model already have been discussed. For the case of n-type Si, comparisons between theory and experiment for the mobility anisotropy and the transverse field effect have been made for (001) and (221)Si orientations. Substantial agreement was obtained, thus lending confidence to the thermal stress model[1,2]. This suggests that the continuous-zone theoretical predictions for n-type Si should

be useful for zonal points in the vicinity of the (001) and (221) orientations for the appropriate modes of epitaxy.

For p-type Si, no mobility anisotropy measurements have as yet been performed and compared with the stress model calculations. Nonetheless, we believe the calculated effects of stress on p-type mobilities are relevant and significant and that the zonal calculations are useful in a predictive sense to indicate new orientations worthy of experimental study.

VIII. DISCUSSION AND CONCLUSIONS

The principal objective of the present investigation has been the theoretical determination of the effects of thermal-expansion-induced stress on the carrier mobility in n- and p-type $Si/A\ell_2O_3$ films.

A mathematical description of heteroepitaxial relations was developed in Section II, and while original, is mathematically straightforward. The main utility of the formalism is in mathematically treating "off-orientation" $Si/A\ell_2O_3$ films.

A model for calculating thermal-expansion-induced anisotropic stresses was developed in Section III. Within the framework of a thin-film-thick-substrate approach, the model rigorously includes and treats the anisotropy in thermal expansion coefficients and the anisotropy in the Si stresses.

A few points concerning the thermal stresses calculated for the $Si/A\ell_2O_3$ orientations treated in the paper should be mentioned. The average stress, $(T_1+T_2)/2$, ranged from $\sim -0.83\times10^{10}$ dyn/cm^2 up to $\sim -1.20\times10^{10}$ dyn/cm^2, depending upon mode of epitaxy and orientation within the mode. These values are consistent with available experimental estimates[4,5].

The second point concerns the existence of shear stresses in the Si films. Apparently it is generally assumed in the literature and by workers in the field that there are no shear stresses in thin $Si/A\ell_2O_3$ films[30]. On the other hand, a non-zero shear stress T_6 in the plane of the film arises naturally in our anisotropic stress model and will be discussed briefly.

In the thin-film-thick-substrate model, the Si film stress is characterized by T_1, T_2 and T_6 evaluated for some choice of reference axes with x and y in the plane of the film. It turns out that the existence of the shear stress T_6 is a consequence of the stress anisotropy and will be present unless $T_1=T_2$. The argument is as follows. Let the stress terms $(T_1-T_2)/2$ and T_6 be defined for the reference axes. Then rotate the coordinate system by 45 deg. From Eqn. (36), $(T_1'-T_2')/2=T_6$ and $T_6'=-(T_1-T_2)/2$ and the two stress terms have interchanged. Thus, $(T_1-T_2)/2$ and T_6 are physically equivalent and hence it is only for the isotropic case, $T_1=T_2$, that there is physically no shear stress.

For the calculations performed, the values of $(T_1-T_2)/2$ and T_6 ranged from zero up to ≈10% of the average stress. Values equal to 5-7% of the average stress were more typical for most orientations and modes of epitaxy. The relative magnitudes of both $(T_1-T_2)/2$ and T_6 are strong functions of the mode and of the film orientations and vary appreciably.

The basic piezoresistance effect was discussed in Section IV and formulae employed in the paper were presented. The major emphasis was upon the linear piezoresistance model. However, a non-linear correction proceedure was also developed which attempts to account for higher order stress effects. The resulting non-linear model was employed extensively for p-type Si data for which the linear model is believed to overestimate the effects of stress on the resistivity.

For both the linear and non-linear models, it was further assumed that the thin Si film is thick enough that bulk piezo-resistance coefficients and bulk coefficient transformation proper-

ties are applicable. Thus any device situation in which surface conduction is important could lie outside the framework of the model, per se, and would have to be examined on an individual basis.

The Si piezoresistance coefficients π_{ij} are functions of the carrier concentration. Assuming that this relationship is approximately the same in $Si/A\ell_2O_3$ and in Si films of the same carrier concentration, coefficient data such as that summarized in Ref. (11) indicate the numerical calculations of the present paper are applicable for concentrations up to $\approx 10^{17}/cm^{-3}$. For higher concentrations different and, with the exception of π_{44}, generally smaller coefficients would be applicable.

Application of the thermal-stress-piezoresistance model to the discrete (001), (221) and (111)Si orientations was made in Section V. In general, the longitudinal effect $\Delta\rho_1'/\rho_o$ leads to a mobility variation of the form $(\mu/\mu_o)=[a-b\cos 2\theta]^{-1}$, while the transverse effect leads to a field variation of the form $E_2'/\rho_o J_1'=b\sin 2\theta$ The zero-stress mobility, μ_o, and resistivity, ρ_o, are not known and cannot be determined directly from experimental data. They are thus essentially derived parameters and would be expected to be a function of growth conditions and to vary slightly from sample to sample.

The anisotropy parameter A and the angular orientations in the Si plane yielding mobility maxima and minima are independent of μ_o and thus permit direct comparisons between theory and experiment. These parameters, rather than the mobility, per se, should therefore be emphasized. Similarly, the orientations of maxima and minima in the transverse field are basic in directly correlating the transverse field data.

Comparison between theory and experiment for the anisotropy A and the location of the various maxima and minima for (001)Si[1] and (221)Si[2] gave good agreement

and argues that the mobility anisotropy can be explained without recourse to other effects or physical phenomena. However, the agreement obtained cannot entirely rule out other phenomena. In this vein, the occurrence of $\cos 2\theta$ and $\sin 2\theta$ terms in the piezoresistance effects is not specific to any one physical phenomenon but instead is simply a symmetry requirement.

Measurements of mobility anisotropy and transverse field have also been carried out in these laboratories for a number of n-type (111)Si/$(11\bar{2}0)A\ell_2O_3$ and (111)Si/$(10\bar{1}4)A\ell_2O_3$ films. The mobility anisotropy factor A, averaged over a number of samples, was ≈30% for (111)Si/$(10\bar{1}4)A\ell_2O_3$ and ≈16% for (111)Si/$(11\bar{2}0)A\ell_2O_3$. These anisotropy factors are substantially greater than those predicted from the thermal stress model and indicate, in contrast to the (001)Si and (221)Si cases, that other phenomena are required in explanation.

Application of the thermal stress-piezoresistance model to off-plane ~(111)Si orientations was made in Section VI. Calculations were performed for substrate orientations lying ±5 deg from the $(11\bar{2}0)$ plane in a general (non-symmetry) direction. The numerical results indicate that changes in substrate orientation of this order can produce noticeable changes in anisotropy and substantial changes in the location of mobility maxima and minima.

In Section VII application of the model was made to general Si orientations of the form (xxl). The model was employed in a predictive sense to determine the effect of thermal stress on the

mobility for other Si orientations which have not yet been researched experimentally. In these calculations, twelve Si orientations lying along the zone(s) defined by (001)Si, (111)Si, (221)Si and (110)Si were treated and numerical data obtained for the four common modes of $Si/A\ell_2O_3$ epitaxy and for one mode of $Si/MgA\ell_2O_4$ epitaxy.

The mobility data are rather similar numerically for the various modes and indicate only a weak dependence upon the particular mode of epitaxy. The n- and p-type maximum mobility data, μ_{max}/μ_o or μ^e_{max}/μ_o, are qualitatively similar in that the mobility is a minimum for (001)Si and increases as one proceeds across the defined zone toward (110)Si. Both n- and p-type maximum mobilities exhibit a slight local minimum in the vicinity of (111)Si.

For n-type Si, the effect of thermal stress on the maximum mobility ranges from a≈30% reduction in mobility for (001)Si up to a ≈25% enhancement in mobility near (110)Si. The ratio of (110)Si to (001)Si mobilities μ_{max}/μ_o is ≈1.7-1.9 which represents a substantial and significant increase in theoretical mobilities. Measurements[1,2,3] in these laboratories tend to support this general characteristic in that n-type (221)Si films have yielded higher mobilities than $(111)Si/(11\bar{2}0)A\ell_2O_3$ films, which in turn have yielded higher mobilities than (001)Si films.

For p-type Si, the effect of thermal stress is always to produce an enhancement in both maximum and minimum mobilities, μ^e_{max}/μ_o and μ^e_{min}/μ_o. The maximum mobility μ^e_{max}/μ_o is ≈1.07 for (001)Si and increases, as one proceeds across the defined zone, to ≈2.4 for (110)Si. These results indicate that the thermal stress effect on mobility has a strong orientation dependence and

that substantially larger mobilities may be achieved by choice of film/substrate orientation.

Collectively, the theoretical thermal stress mobility data for n- and p-type $Si/A\ell_2O_3$ suggest that it would be worthwhile to experimentally explore Mode I epitaxial film growths in the range of ~0-25 deg from (001)Si and Modes II, III and IV epitaxial film growths in the range $\pm$25 deg from (111)Si.

Summarizing, the effect of substrate-induced thermal expansion stress on mobility in $Si/A\ell_2O_3$ films has been theoretically determined within the framework of a thin-film-thick-substrate piezoresistance model which incorporates the anisotropy in substrate thermal expansion and in Si film stresses.

It is well known that $Si/A\ell_2O_3$ film growth quality dependsupon a number of factors including intrinsic stress, dislocation generation and impurity or heavy metal complexes, in addition to the thermal stress effect treated in this paper. All of these phenomena could produce effects on mobility which are dependent upon crystallographic orientation. Although a formidable task, additional theoretical and experimental work directed toward understanding these phenomena should be attempted.

The present study of thermal stress effects represents the first systematic investigation of mobility as a function of orientation. We believe the model is a useful theoretical tool, and, in conjunction with experimental investigations and additional selected orientation growth studies, can lead to a better understanding and to means of optimizing $Si/A\ell_2O_3$ films for some applications.

ACKNOWLEDGMENTS

The impetus for the theoretical investigation reported here was provided by experimental studies of mobility anisotropy in Si/Al_2O_3 films. Comparisons of theory and experiment have been invaluable in establishing the validity of the theoretical model. The author is grateful to A. C. Thorsen for helpful discussions of mobility anisotropy in Si/Al_2O_3 films and for providing detailed experimental data, to J. P. Wendt for carrying out the electrical measurements, to H. M. Manasevit, F. M. Erdmann and R. Harada for supplying the samples used in the experimental study. The author also acknowledges Lavada A. Moudy for many helpful discussions regarding the orientation and parallel relationships in the Si/Al_2O_3 system, and R. P. Ruth for a critical review of the manuscript.

REFERENCES

1) A. J. Hughes and A. C. Thorsen, J. Appl. Phys. 44, 2304 (1973).

2) A. C. Thorsen and A. J. Hughes, Appl. Phys. Lett. 21, 579 (1972).

3) A. J. Hughes (unpublished)

4) D. J. Dumin, J. Appl. Phys. 36, 2700 (1965).

5) C. Y. Ang and H. M. Manasevit, Solid St. Electron. 8, 994 (1965).

6) H. M. Manasevit, R. L. Nolder and L. A. Moudy, Met. Soc. of AIME 242, 465 (1966). Two typographical errors in this reference have been corrected in our Table I.

7) Lavada A. Moudy (private communication).

8) R. W. Hoffman, The Mechanical Properties of Thin Films; in "The Use of Thin Films in Physical Investigations," ed. J. C. Anderson. Academic Press, pp. 261-280 (1966).

9) K. L. Chopra, "Thin Film Phenomena," McGraw-Hill, pp. 266-327 (1969).

10) Diana M. Jefkins, J. of Phys. D, Appl. Phys. 3, 770 (1970).

11) H. Schlötterer, Solid State Electron. 11, 947 (1968).

12) J. F. Nye, "Physical Properties of Crystals," (Oxford University Press, London, 1957) Chap. 6.

13) Reference 12, Chapter 8.

14) J. J. Wortman and R. A. Evans, J. Appl. Phys. 36, 153 (1965).

15) W. P. Mason and R. N. Thurston, J. Acoust. Soc. Amer 29, 1096 (1957).

16) W. G. Pfann and R. N. Thurston, J. Appl. Phys. 32, 2008 (1961).

17) R. N. Thurston in Physical Acoustics, edited by W. P. Mason (Academic Press, New York, 1964) Vol. I-Part B, p. 215.

18) W. P. Mason, J. J. Forst, and L. M. Tornello, Instrument Soc. of Amer., Conf. Preprint 15-NY60 (1960).

19) J. C. Sanchez and W. V. Wright, Instrument Soc. of Amer., Conf. Preprint 37-SL61 (1961).

20) R.F.S. Hearmon, "Landolt-Bornstein Numerical Data and Functional Relationships in Science and Technology, New Series," edited by K. H. Hellwege (Springer-Verlag, New York, 1969), Vol. III/2, p. 3. The values of elastic constants employed in the text were $C_{11}=16.5\times10^{11}$, $C_{12}=6.4\times10^{11}$, and $C_{44}=7.93\times10^{11}$ dyn/cm^2.

21) J. B. Austin, J. Am. Ceram. Soc. 14, 795 (1931).

22) S. B. Austerman (private communication).

23) In using the differential data, we have assumed that $(\alpha_1+\alpha_2)/2=8.67\times10^{-6}$/deg C which is the average value determined by Austin[21].

24) C. S. Smith, Phys. Rev. 94, 42 (1954).

25) The values of piezoresistance coefficients employed in the text for n-type Si were $\pi_{11}=-102\times10^{-12}$, $\pi_{12}=+54\times10^{-12}$, and $\pi_{44}=-14\times10^{-12}$ cm^2/dyn and for p-type Si were $\pi_{11}=+7.13\times10^{-12}$, $\pi_{12}=-.567\times10^{-12}$, and $\pi_{44}=+138\times10^{-12}$ cm^2/dyne. The assumption implicit here is that the bulk piezoresistance coefficients can be employed for these ~2μ-thick Si films. This is reasonable for this application but may be incorrect for narrow channel FET devices in which carrier quantization and altered piezoresistance coefficients would both have to be considered.

26) For a mobility variation of the form $\mu/\mu_o=(a+b\cos2\theta)^{-1}$, the true rotational average value is $\mu/\mu_o=(a^2-b^2)^{-\frac{1}{2}}$, compared with $\mu_A/\mu_o=a/(a^2-b^2)$. For the numerical parameters of Eqn. (46),

FIGURE CAPTIONS

Fig. 1 Three equivalent pole diagrams characterizing an off-orientation ≈(111)Si film growth. The parallel relations associated with these three pole diagrams are:

A) $[1\bar{1}0]Si//[2\bar{2}01]A\ell_2O_3$ and $(111)Si//(11\bar{2}0)A\ell_2O_3$;

B) $[\bar{1}01]Si//[2\bar{2}01]A\ell_2O_3$ and $(111)Si//(11\bar{2}0)A\ell_2O_3$;

C) $[1\bar{1}0]Si//[\bar{2}021]A\ell_2O_3$ and $(111)Si//(1\bar{2}10)A\ell_2O_3$.

Although all three diagrams are equivalent, only that of Fig. 1A is consistent mathematically with the parallel relations assumed in Section II and has been employed in the calculations.

Fig. 2 The mobility ratio (μ/μ_o) for n-type Si is plotted versus orientation in the (xxl)Si zone. The shaded regions indicate the collective range in mobility for the four modes of $Si/A\ell_2O_3$ epitaxy. (Data for the individual modes is given in the tables.)

Fig. 3 The mobility ratio (μ^e/μ_o) based upon the exponential non-linear correction factor for p-type Si is plotted versus orientation in the (xxl)Si zone. The shaded regions indicate the collective range in mobility for the four modes of $Si/A\ell_2O_3$ epitaxy. (Data for the individual modes is given in the tables.)

Preceding page blank

Table I. General Silicon-Sapphire Orientation Relationships

Mode	Orientation Planes Silicon//Sapphire	Orientation Direction Silicon//Sapphire
I	(001)//(01$\bar{1}$2)	[100]//[2$\bar{1}\bar{1}$0]
II	(111)//(11$\bar{2}$4) (110)//(11$\bar{2}$0)	[1$\bar{1}$0]//[1$\bar{1}$00]
II	(221)//(11$\bar{2}$2)	[1$\bar{1}$0]//[1$\bar{1}$00]
III	(111)//(11$\bar{2}$0) (11$\bar{2}$)//(1$\bar{1}$0$\bar{4}$)	[1$\bar{1}$0]//[2$\bar{2}$01]
IV	(111)//(10$\bar{1}$4)	[1$\bar{1}$0]//[1$\bar{2}$10] [11$\bar{2}$]//[20$\bar{2}\bar{1}$]

TABLE II. Parallel Directions and Transformation Matrices for Modes I, II, III, IV and V

Mode I $(001)Si||(01\bar{1}2)A\ell_2O_3$

$X_f'||[100]$; $X_s'||[2,\bar{1},\bar{1},0]_4$ and $||[1,0,0]_c$

$Y_f'||[010]$; $Y_s'||[0,1,\bar{1},\bar{1}]_4$ and $||[0, \sqrt{3}r(c/a)]_c$

$Z_f' \perp (001)$; $Z_s' \perp (01\bar{1}2)_4$ and $||[0,1/\sqrt{3}, (a/c)]_c$

$$(SF) = \begin{pmatrix} 1 & 0 & 0 \\ 0 & +.5357031437 & +.8444063836 \\ 0 & -.8444063836 & +.5357031437 \end{pmatrix}$$

Mode II $(111)Si||(11\bar{2}4)A\ell_2O_3$

$X_f'||[1\bar{1}0]$; $X_s'||[1\bar{1}00]_4$ and $||[\sqrt{3}, -1, 0]_c$

$Y_f'||[11\bar{2}]$; $Y_s'||[22\bar{4}\bar{3}]_4$ and $||[1,\sqrt{3}, -(c/a)]_c$

$Z_f' \perp [111]$; $Z_s' \perp (11\bar{2}4)_4$ and $||[1,\sqrt{3}, 4(a/c)]_c$

$$(SF) = \begin{pmatrix} +.9658761431 & -.2588687289 & -.0083820038 \\ +.2587329909 & +.9658397723 & -.0145180564 \\ +.0118539434 & +.0118539434 & +.9998594737 \end{pmatrix}$$

Mode III $(221)Si||(11\bar{2}2)A\ell_2O_3$

$X_f'||[1\bar{1}0]$; $X_s'||[1\bar{1}00]_4$ and $||[\sqrt{3}, -1, 0]_c$

$Y_f'||[11\bar{4}]$; $Y_s'||[11\bar{2}\bar{3}]_4$ and $||[1,\sqrt{3}, -2(c/a)]_c$

$Z_f' \perp [221]$; $Z_s' \perp (11\bar{2}2)_4$ and $||[1,\sqrt{3}, 2(a/c)]_c$

For (SF), use $(111)Si||(11\bar{2}4)A\ell_2O_3$ case and see text for explanation

Mode III $(111)Si||(11\bar{2}0)Al_2O_3$

$X_f' || [1\bar{1}0]$; $X_s' || [2\bar{2}01]_4$ and $||[3, -\sqrt{3}, (c/a)]_c$

$Y_f' || [11\bar{2}]$; $Y_s' \perp (1\bar{1}0\bar{4})_4$ and $||[1, -1\sqrt{3}, -4(a/c)]_c$

$Z_f' \perp (111)$; $Z_s' \perp (11\bar{2}0)_4$ and $||[1, \sqrt{3}, 0]_c$

$$(SF) = \begin{pmatrix} +.9884773163 & +.0265674379 & -.1490193506 \\ +.0959690224 & +.6513279493 & +.752703029 \\ +.1170578591 & -.7583311113 & +.6412732518 \end{pmatrix}$$

Mode IV $(111)Si||(10\bar{1}4)Al_2O_3$

$X_f' || [1\bar{1}0]$; $X_s' || [1\bar{2}10]_4$ and $||[1, -\sqrt{3}, 0]_c$

$Y_f' || [11\bar{2}]$; $Y_s' || [20\bar{2}\bar{1}]_4$ and $||[3, \sqrt{3}, -(c/a)]_c$

$Z_f' \perp (111)$; $Z_s' \perp (10\bar{1}4)_4$ and $||[1, 1/\sqrt{3}, 4(a/c)]_c$

$$(SF) = \begin{pmatrix} +.9407295926 & +.2336228112 & -.2458621884 \\ -.2733660978 & +.9513787742 & -.1419486008 \\ +.2007456359 & +.2007456359 & +.9588547228 \end{pmatrix}$$

Mode V $(111)Si||(111)MgAl_2O_4$

$X_f' || [1\bar{1}0]$; $X_s' || [1\bar{1}0]$

$Y_f' || [11\bar{2}]$; $Y_s' || [11\bar{2}]$

$Z_f' \perp (111)$; $Z_s' \perp (111)$

$$(SF) = \begin{pmatrix} 1 & 0 & 0 \\ 0 & 1 & 0 \\ 0 & 0 & 1 \end{pmatrix}$$

Table III. Comparison of Linear and Non-Linear Mobilities

(μ/μ_o) Linear	(μ/μ_o) Second Order	(μ/μ_o) Exponential Order
0.70	0.658	0.651
0.80	0.780	0.779
0.90	0.895	0.895
1.00	1.000	1.000
1.10	1.095	1.095
1.20	1.180	1.181
1.30	1.256	1.259
1.40	1.324	1.331
1.50	1.385	1.396
1.75	1.508	1.535
2.00	1.600	1.649
2.50	1.724	1.822
3.00	1.800	1.948
4.00	1.882	2.117
5.00	1.923	2.225
6.00	1.946	2.301
8.00	1.969	2.399
∞	2.000	2.718

TABLE IV

$(001)Si//(01\bar{1}2)Al_2O_3$

Case 1 N-type Si

$\Delta\rho_1'/\rho_o = +.441924 - .044488 \cos 2\theta$

$E_2'/\rho_o J_1' = +.044488 \sin 2\theta$

$\Delta\rho_3'/\rho_o = -.994329$

Case 1 P-type Si

$\Delta\rho_1'/\rho_o = -.060424 + .002186 \cos 2\theta$

$E_2'/\rho_o J_1' = -.002186 \sin 2\theta$

$\Delta\rho_3'/\rho_o = +.010440$

Case 2 N-type Si

$\Delta\rho_1'/\rho_o = +.437032 - .066732 \cos 2\theta$

$E_2'/\rho_o J_1' = +.066732 \sin 2\theta$

$\Delta\rho_3'/\rho_o = -.983323$

Case 2 P-type Si

$\Delta\rho_1'/\rho_o = -.059755 + .00328 \cos 2\theta$

$E_2'/\rho_o J_1' = -.00328 \sin 2\theta$

$\Delta\rho_3'/\rho_c = +.010325$

TABLE V

$(221)Si||(11\bar{2}2)Al_2O_3$

Case 1 n-type Si

$E_3'/\rho_o J_1' = -.1532308 \sin\theta$

$E_2'/\rho_o J_1' = +.2122694 \sin 2\theta$

$\Delta\rho_1'/\rho_o = +.0618867 - .2122694 \cos 2\theta$

$\mu_{max} = 1.1770\mu_o$; $\mu_{min} = 0.78483\mu_o$; $\mu^e_{max} = 1.1623\mu_o$; $\mu^e_{min} = 0.76021\mu_o$

$\mu_A = 0.98092\mu_o$; A = 39.98% ; $\mu^e_A = 0.96125\mu_o$; A^e = 41.83%

Case 2 n-type Si

$E_3'/\rho_o J_1' = -.1646888 \sin\theta$

$E_2'/\rho_o J_1' = +.2314387 \sin 2\theta$

$\Delta\rho_1'/\rho_o = +.0658864 - .2312447 \cos 2\theta$

$\mu_{max} = 1.1981\mu_o$; $\mu_{min} = 0.77093\mu_o$; $\mu^e_{max} = 1.1798\mu_o$; $\mu^e_{min} = 0.74294\mu_o$

$\mu_A = 0.98452_o$; A = 43.39% ; $\mu^e_A = 0.96137\mu_o$; A^e = 45.44%

Case 1 p-type Si

$E_3'/\rho_o J_1' = -.1406087 \sin\theta$

$E_2'/\rho_o J_1' = +.2425342 \sin 2\theta$

$\Delta\rho_1'/\rho_o = -.5286124 - .2425342 \cos 2\theta$

$\mu_{max} = 4.3696\mu_o$; $\mu_{min} = 1.4007\mu_o$; $\mu^e_{max} = 2.1622\mu_o$; $\mu^e_{min} = 1.3312\mu_o$

$\mu_A = 2.8849\mu_o$; A = 102.9% ; $\mu^e_A = 1.7467\mu_o$; A^e = 47.57%

Case 2 p-type Si

$E_3'/\rho_o J_1' = -.15112285 \sin\theta$

$E_2'/\rho_o J_1' = +.2281746 \sin 2\theta$

$\Delta\rho_1'/\rho_o = -.5210478 - .228174 \cos 2\theta$

$\mu_{max} = 3.9876\mu_o$; $\mu_{min} = 1.4142\mu_o$; $\mu^e_{max} = 2.1153\mu_o$; $\mu^e_{min} = 1.3403\mu_o$

$\mu_A = 2.7009\mu_o$; A = 95.28% ; $\mu^e_A = 1.7278\mu_o$; A^e = 44.85%

TABLE VI

$(111)Si/A\ell_2O_3$

	Mode II	Mode III	Mode IV
N_1	0.0	+0.618993	0.0
N_2	-0.80673	-0.785396	-0.618993
Case 1			
$(T_1+T_2)/2$	-1.1671×10^{10}	-1.1987×10^{10}	-1.1429×10^{10}
$(T_1-T_2)/2$	$+0.34343\times10^{9}$	$+0.12333\times10^{9}$	$+0.20220\times10^{9}$
T_6	0.0	$+0.51312\times10^{9}$	0.0
Case 2			
$(T_1+T_2)/2$	-1.1513×10^{10}	-1.1987×10^{10}	-1.1150×10^{10}
$(T_1-T_2)/2$	$+0.51515\times10^{9}$	$+0.18499\times10^{9}$	$+0.30330\times10^{9}$
T_6	0.0	$+0.76968\times10^{9}$	0.0
n-type Si Case 1			
μ_{max}/μ_o	1.013	1.025	1.005
μ_{min}/μ_o	0.972	0.961	0.9804
A (%)	4.18	6.42	2.46
n-type Si Case 2			
μ_{max}/μ_o	1.024	1.042	1.011
μ_{min}/μ_o	0.962	0.946	0.974
A (%)	6.27	9.63	3.69

p-type Si Case 1						
μ_{max}/μ_o; μ^e_{max}/μ_o	2.604	1.851	2.851	1.914	2.442	1.805
μ_{min}/μ_o; μ^e_{min}/μ_o	2.227	1.735	2.219	1.732	2.234	1.737
A (%) ; A^e (%)	15.60	6.50	24.91	9.98	8.92	3.81
p-type Si Case 2						
μ_{max}/μ_o; μ^e_{max}/μ_o	2.662	1.867	3.069	1.962	2.416	1.797
μ_{min}/μ_o; μ^e_{min}/μ_o	2.114	1.694	2.103	1.689	2.122	1.697
A (%) ; A^e (%)	22.96	9.73	37.37	14.94	12.96	5.73

TABLE VII

	$(11\bar{2}0)+5°$	$(11\bar{2}0)$	$(11\bar{2}0)-5°$
Case 1			
$(\alpha_1-\alpha_2)=-.72\times10^{-6}/°C$			
$(T_1+T_2)/2$	-1.19666×10^{10}	-1.1987×10^{10}	-1.19272×10^{10}
$(T_1-T_2)/2$	$+0.25722\times10^{9}$	$+0.12332\times10^{9}$	-0.004171×10^{9}
T_6	$+0.69159\times10^{9}$	$+0.51312\times10^{9}$	$+0.35984\times10^{9}$
Case 2			
$(\alpha_1-\alpha_2)=-1.08\times10^{-6}/°C$			
$(T_1+T_2)/2$	-1.197500×10^{10}	-1.1987×10^{10}	-1.19197×10^{10}
$(T_1-T_2)/2$	$+0.31262\times10^{9}$	$+0.18499\times10^{9}$	$+0.06398\times10^{9}$
T_6	$+0.94029\times10^{9}$	$+0.76968\times10^{9}$	$+0.62468\times10^{9}$

TABLE VIII

	$(11\bar{2}0)+5°$		$(11\bar{2}0)$		$(11\bar{2}0)-5°$	
n-type Si Case 1						
μ_{max}/μ_o	1.0147		1.0250		1.0625	
μ_{min}/μ_o	.9636		.9612		.9127	
$\theta_{\mu_{max}}$	101.82		38.24		30.46	
$A(\%)$	5.15		6.42		15.16	
n-type Si Case 2						
μ_{max}/μ_o	1.0099		1.0422		1.0762	
μ_{min}/μ_o	.9707		.9465		.9008	
$\theta_{\mu_{max}}$	79.55		38.24		31.96	
$A(\%)$	3.95		9.63		17.75	
p-type Si Case 1						
μ_{max}/μ_o; μ^e_{max}/μ_o	3.624	2.063	2.8510	1.9141	2.6495	1.8637
μ_{min}/μ_o; μ^e_{min}/μ_o	1.872	1.593	2.2195	1.7323	2.2265	1.7347
$\theta_{\mu_{max}}$	120.97		128.24		186.15	
$A(\%)$; $A^e(\%)$	63.75	25.68	24.91	9.97	17.35	7.16
p-type Si Case 2						
μ_{max}/μ_o; $\mu^e_{max}\ \mu_o$	3.945	2.110	3.0694	1.962	2.6210	1.856
μ_{min}/μ_o; $\mu^e_{min}\ \mu_o$	1.808	1.563	2.1030	1.689	2.2318	1.737
$\theta_{\mu_{max}}$	122.30		128.24		161.90	
$A(\%)$; $A^e(\%)$	74.29	29.74	37.37	14.94	16.04	6.65

TABLE IX

Mode I Epitaxy, $(001)Si//(01\bar{1}2)Al_2O_3$

X	θ(Deg)	N-type Si			P-Type Si					
		μ_{max}/μ_o	μ_{min}/μ_o	A(%)	μ_{max}/μ_o	μ^e_{max}/μ_o	μ_{min}/μ_o	μ^e_{min}/μ_o	A(A)	A^e(%)
0.0	0.0	0.730	0.665	9.3	1.067	1.065	1.059	1.057	0.7	0.7
0.1247	10.0	0.749	0.672	10.8	1.163	1.150	1.058	1.056	9.4	[illegible]
0.2574	20.0	0.815	0.701	14.9	1.501	1.396	1.088	1.084	31.9	25.2
0.4082	30.0	0.934	0.752	21.5	2.326	1.768	1.190	1.173	64.6	40.5
0.5933	40.0	1.047	0.831	23.0	3.636	2.065	1.431	1.351	87.0	41.8
0.8427	50.0	1.053	0.927	12.7	3.424	2.030	1.901	1.606	57.2	23.3
1.0	54.7	1.040	0.947	9.3	3.024	1.953	2.102	1.689	35.9	14.5
1.2247	60.0	1.070	0.911	16.0	3.300	2.008	1.896	1.604	54.0	22.4
1.9427	70.0	1.142	0.812	33.7	5.091	2.233	1.362	1.304	115.5	52.5
2.0	70.5	1.145	0.808	34.5	5.212	2.244	1.343	1.291	118.0	53.9
4.0102	80.0	1.180	0.754	44.1	7.434	2.376	1.121	1.114	147.5	72.3
1000.	90.0	1.184	0.741	46.0	8.286	2.409	1.057	1.055	154.7	78.2

TABLE X

Mode II, (111)Si//(1124)$A\ell_2O_3$ & (221)Si//(1122)$A\ell_2O_3$

		N-Type Si			P-Type Si					
X	θ(Deg)	μ_{max}/μ_o	μ_{min}/μ_o	A(%)	μ_{max}/μ_o	μ^e_{max}/μ_o	μ_{min}/μ_o	μ^e_{min}/μ_o	A(%)	A^e(%)
0.0	0.0	0.714	0.714	0.0	1.057	1.056	1.057	1.056	0.0	0.0
0.1247	10.0	0.736	0.719	2.3	1.133	1.124	1.063	1.061	6.3	5.8
0.2574	20.0	0.806	0.738	8.8	1.414	1.340	1.090	1.086	25.8	20.9
0.4082	30.0	0.920	0.781	16.4	2.086	1.683	1.173	1.159	56.0	36.9
0.5933	40.0	1.023	0.857	17.7	3.195	1.987	1.374	1.313	79.7	40.9
0.8427	50.0	1.011	0.966	4.5	3.187	1.986	1.794	1.557	56.0	24.2
1.0	54.7	1.024	0.962	6.3	2.659	1.866	2.112	1.693	22.9	9.7
1.2247	60.0	1.088	0.894	19.6	2.585	1.846	2.097	1.687	20.8	9.0
1.9427	70.0	1.193	0.776	42.4	3.896	2.103	1.435	1.354	92.3	43.3
2.0	70.5	1.198	0.771	43.4	3.980	2.114	1.413	1.339	95.2	44.9
4.0102	80.0	1.259	0.703	56.6	5.554	2.270	1.153	1.141	131.2	66.1
1000.	90.0	1.282	0.680	61.3	6.448	2.327	1.075	1.072	142.8	73.8

TABLE XI

Mode III, $(111)Si//(11\bar{2}0)Al_2O_3$

		N-Type Si			P-Type Si					
X	θ(Deg)	μ_{max}/μ_o	μ_{min}/μ_o	A(%)	μ_{max}/μ_o	μ^e_{max}/μ_o	μ_{min}/μ_o	μ^e_{min}/μ_o	A(%)	A^e(%)
0.0	0.0	0.725	0.674	7.4	1.089	1.085	1.036	1.036	4.9	4.6
0.1247	10.0	0.746	0.679	9.4	1.130	1.122	1.083	1.079	4.2	3.9
0.2573	20.0	0.813	0.705	14.2	1.445	1.360	1.111	1.105	26.1	20.7
0.4082	30.0	0.933	0.753	21.3	2.209	1.728	1.208	1.188	58.5	37.0
0.5933	40.0	1.048	0.830	23.2	3.460	2.036	1.446	1.361	82.1	39.7
0.8427	50.0	1.053	0.927	12.7	3.399	2.025	1.911	1.610	56.0	22.8
1.0	54.7	1.042	0.946	9.6	3.066	1.961	2.101	1.689	37.3	14.9
1.2247	60.0	1.071	0.909	16.4	3.385	2.023	1.896	1.604	56.4	23.1
1.9427	70.0	1.147	0.808	34.7	5.357	2.255	1.364	1.306	118.8	53.3
2.0	70.5	1.150	0.804	35.5	5.496	2.266	1.345	1.292	121.4	54.7
4.0102	80.0	1.190	0.747	45.7	8.199	2.406	1.112	1.106	151.9	74.0
1000.	90.0	1.196	0.732	48.1	9.384	2.443	1.054	1.053	159.6	79.5

TABLE XII

Mode IV, (111)Si//(10$\bar{1}$4)$A\ell_2O_3$

X	θ(Deg)	N-Type Si			P-Type Si					
		μ_{max}/μ_o	μ_{min}/μ_o	A(%)	μ_{max}/μ_o	μ^e_{max}/μ_o	μ_{min}/μ_o	μ^e_{min}/μ_o	A(%)	A^e(%)
0.0	0.0	0.712	0.711	0.1	1.0701	1.067	1.046	1.045	2.1	2.1
0.1247	10.0	0.736	0.719	2.4	1.1310	1.122	1.065	1.063	6.0	5.4
0.2574	20.0	0.809	0.740	8.9	1.3801	1.317	1.104	1.099	22.2	18.0
0.4082	30.0	0.923	0.782	16.6	1.9441	1.625	1.196	1.178	47.6	31.9
0.5933	40.0	1.026	0.854	18.3	2.7809	1.897	1.400	1.331	66.0	35.0
0.8427	50.0	1.020	0.956	6.4	2.7940	1.900	1.814	1.566	42.5	19.3
1.0	54.7	1.011	0.974	3.7	2.4145	1.796	2.120	1.696	12.9	5.7
1.2247	60.0	1.071	0.909	16.4	2.5712	1.842	1.974	1.638	26.2	11.7
1.9427	70.0	1.172	0.790	38.9	3.7990	2.089	1.407	1.335	91.8	44.0
2.0	70.5	1.177	0.785	39.9	3.8771	2.100	1.387	1.322	94.6	45.5
4.0102	80.0	1.241	0.714	53.8	5.3583	2.255	1.147	1.137	129.4	65.9
1000.	90.0	1.272	0.685	59.9	6.3041	2.319	1.074	1.071	141.7	73.6

TABLE XIII

Mode V, (111)Si//(111)$MgA\ell_2O_4$

X	θ(Deg)	N-Type Si			P-Type Si					
		μ_{max}/μ_o	μ_{min}/μ_o	A(%)	μ_{max}/μ_o	μ^e_{max}/μ_o	μ_{min}/μ_o	μ^e_{min}/μ_o	A(%)	A^e(%)
0.0	0.0	0.715	0.715	0.0	1.057	1.055	1.057	1.055	0.0	0.0
0.1247	10.0	0.738	0.721	2.4	1.127	1.119	1.066	1.063	5.6	5.1
0.2574	20.0	0.810	0.741	8.9	1.375	1.313	1.104	1.098	21.9	17.8
0.4082	30.0	0.925	0.783	16.5	1.892	1.602	1.201	1.182	44.7	30.2
0.5933	40.0	1.029	0.853	18.6	2.530	1.830	1.415	1.340	56.5	30.9
0.8427	50.0	1.030	0.946	8.5	2.422	1.799	1.826	1.572	28.0	13.4
1.0	54.7	0.993	0.993	0.0	2.116	1.694	2.116	1.694	0.0	0.0
1.2247	60.0	1.041	0.937	10.5	2.518	1.827	1.775	1.547	34.6	16.6
1.9427	70.0	1.115	0.837	28.5	3.482	2.039	1.331	1.282	89.4	45.6
2.0	70.5	1.118	0.832	29.2	3.537	2.048	1.315	1.270	91.6	46.9
4.0102	80.0	1.157	0.774	39.7	4.452	2.171	1.121	1.114	119.5	64.3
1000.	90.0	1.171	0.753	43.4	4.884	2.215	1.061	1.059	128.6	70.6

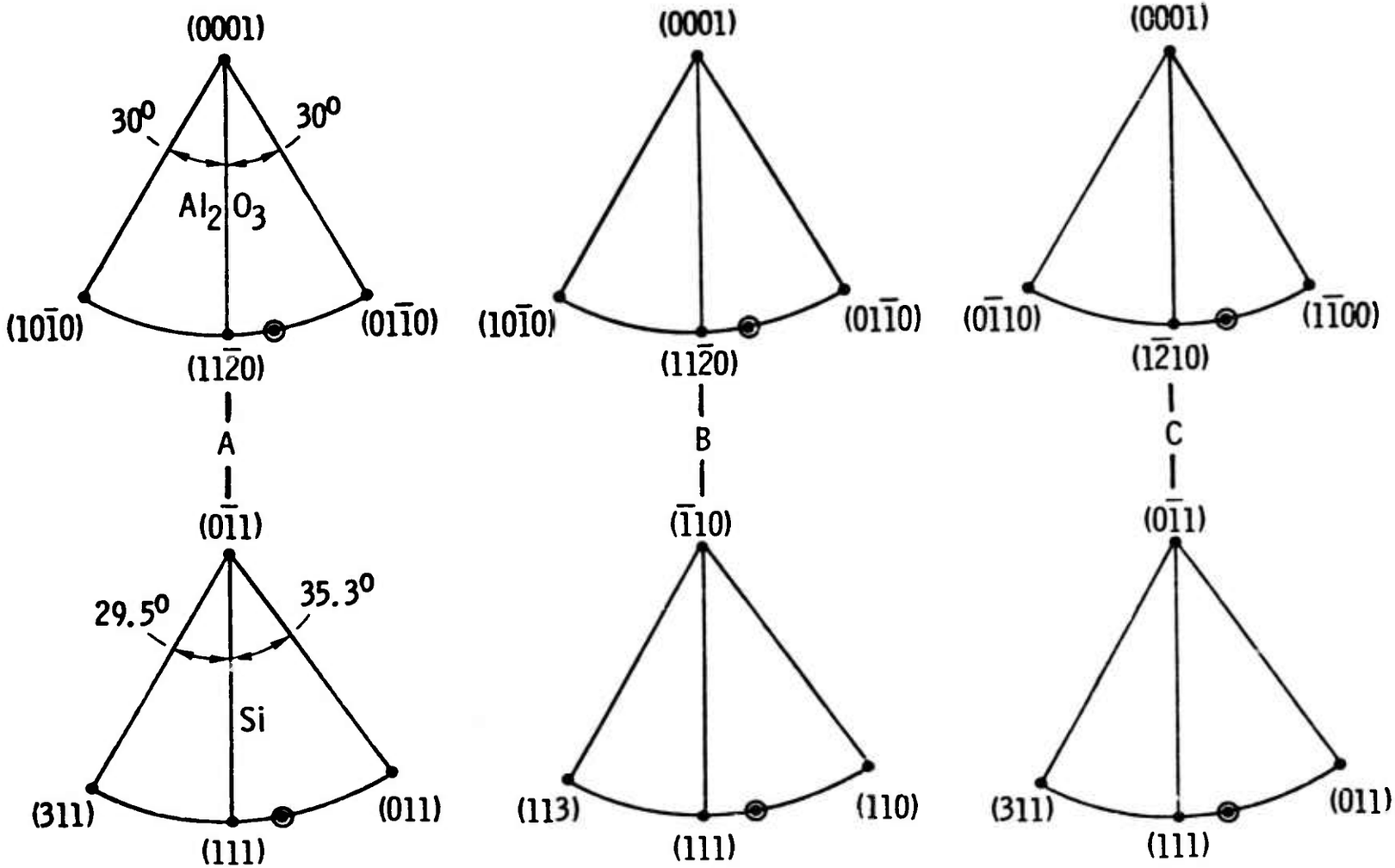
(0001)
30°
30°
Al_2O_3
(10$\bar{1}$0)
(01$\bar{1}$0)
(11$\bar{2}$0)
A
(0$\bar{1}$1)
29.5°
35.3°
Si
(311)
(011)
(111)
(0001)
(10$\bar{1}$0)
(01$\bar{1}$0)
(11$\bar{2}$0)
B
($\bar{1}$10)
(113)
(110)
(111)
(0001)
(0$\bar{1}$10)
(1$\bar{1}$00)
(1$\bar{2}$10)
C
(0$\bar{1}$1)
(311)
(011)
(111)

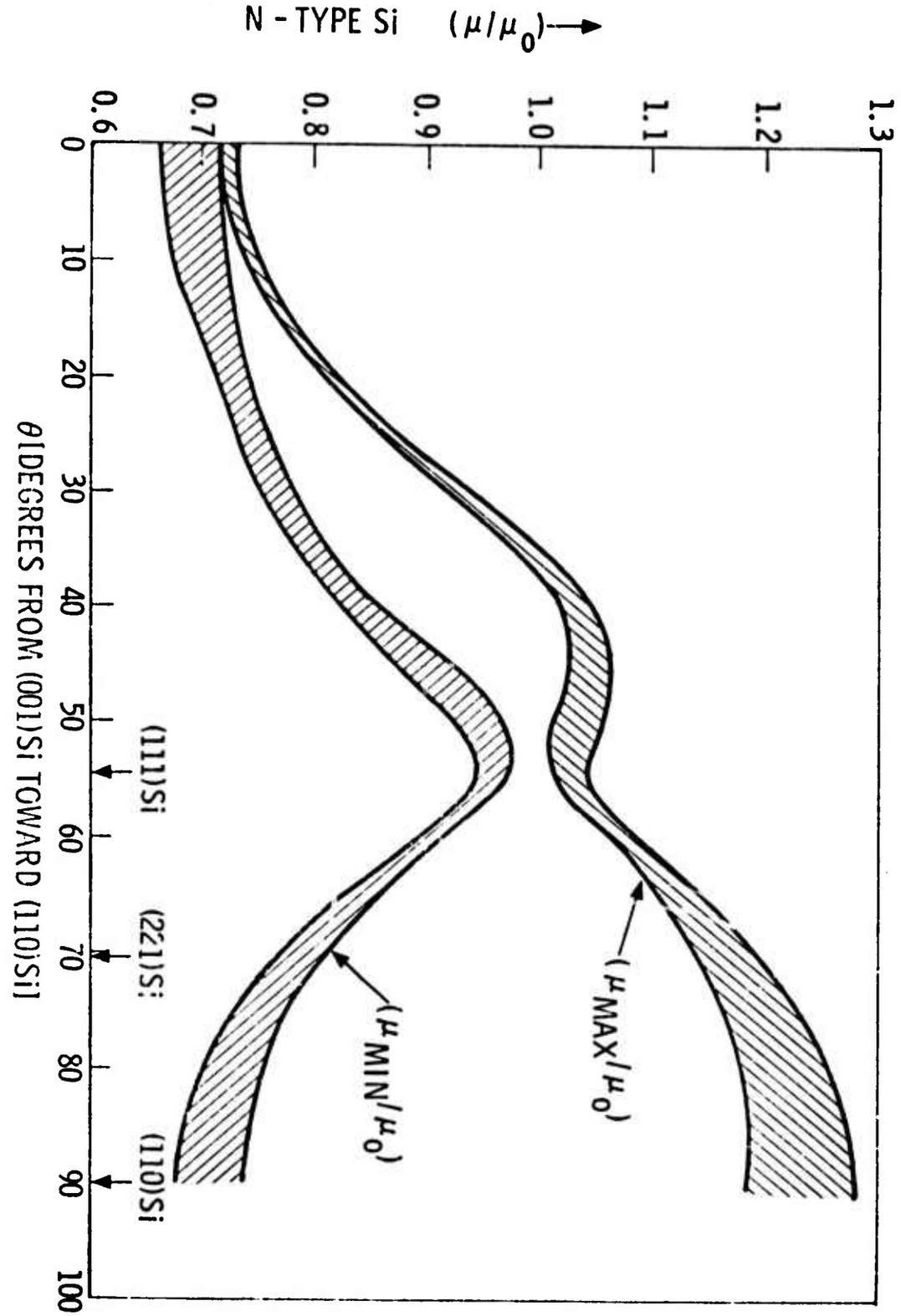
N - TYPE Si (μ/μ_0)
0.6
0.7
0.8
0.9
1.0
1.1
1.2
1.3
0
10
20
30
40
50
60
70
80
90
100
θ IDEGREES FROM (001)Si TOWARD (110)Si]
IS(110)Si
IS(221)Si
IS(111)Si
(μ_{MIN}/μ_0)
(μ_{MAX}/μ_0)

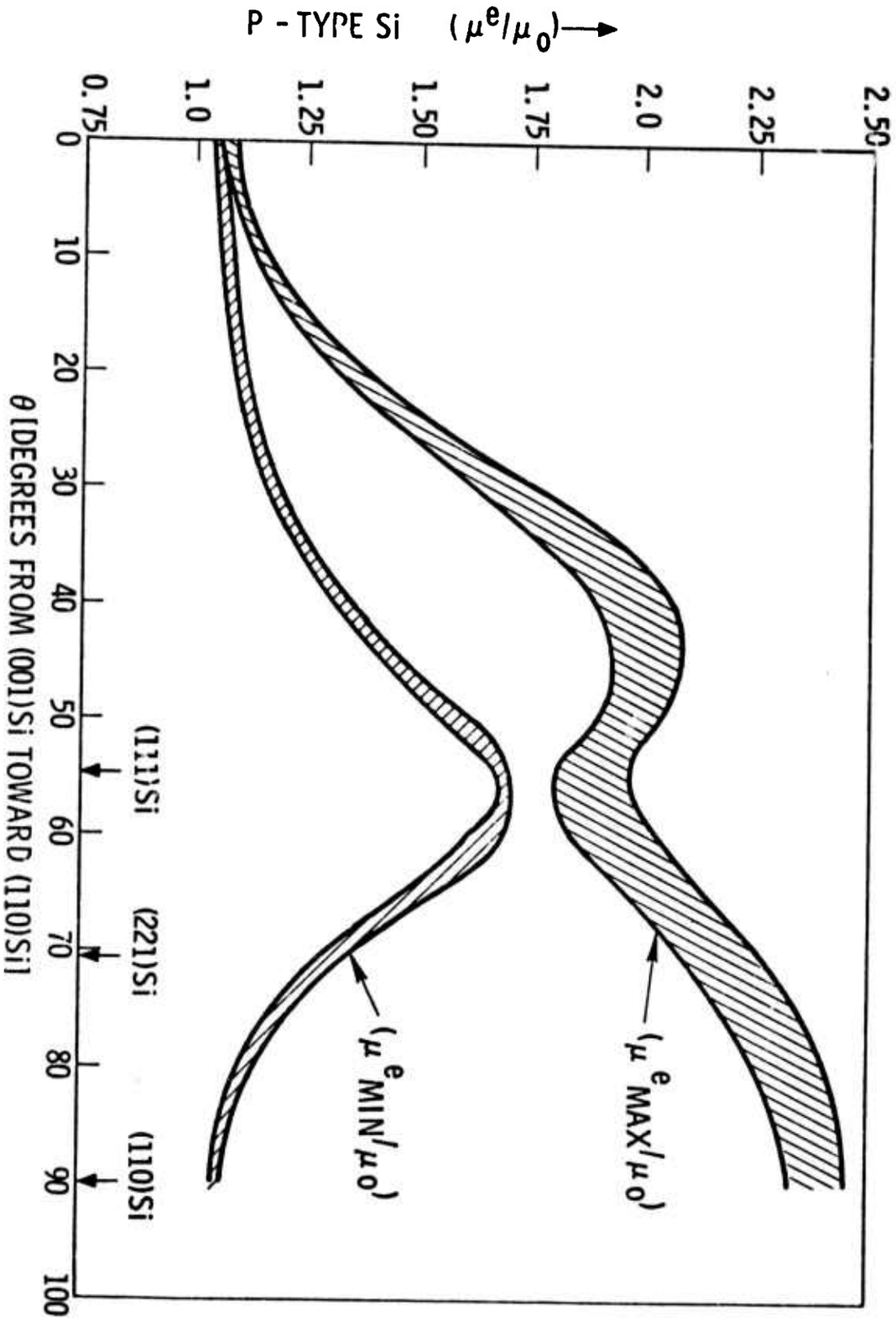
P - TYPE Si (μ^e/μ_0)
2.50
2.25
2.0
1.75
1.50
1.25
1.0
0.75
0
10
20
30
40
50
60
70
80
90
100
θ [DEGREES FROM (001)Si TOWARD (110)Si]
(111)Si
(221)Si
(110)Si
(μ^e_{MAX}/μ_0)
(μ^e_{MIN}/μ_0)

APPENDIX 5

BIBLIOGRAPHY

ELECTRON MICROSCOPE IN SITU NUCLEATION AND GROWTH STUDIES

Introduction

A search of the technical literature involving the electron microscopic in situ observation of the nucleation and growth of thin films has been performed. The resultant bibliography, it is hoped, includes all previous research of interest to someone undertaking such a task. Pertinent literature in all major electron microscopy conferences listed in section G has been included, as well as numerous articles from the general scientific literature. Insofar as is possible for someone in the physical sciences on a limited time budget, the biological literature was searched for information on hydration or environmental chambers. All articles encountered concerning auxiliary pumping systems or improvement of the contamination rate were included, primarily in section E20-39. The author would appreciate information concerning any pertinent article not included.

To date, no one has yet examined in situ the nucleation and growth of a thin solid film from a gaseous, molecular phase onto an electron transparent substrate. In particular, the excellent works of Pashley et al, and Poppa (references C1-C8 and D1-D11) refer specifically to physical vapor deposition, not chemical vapor deposition. The experiments listed in section B concern either (a) oxidation of a thin film, (b) growth of solid whiskers from pyrolysis of a gaseous phase, or (c) decomposition of a solid phase into a different solid phase plus a gaseous phase. None concern the growth of a thin solid film from the pyrolysis of a gaseous phase, an in situ experiment which the author is undertaking. The references cited have been valuable chiefly for their collective wealth of ideas and experimental techniques.

BIBLIOGRAPHY: ELECTRON MICROSCOPE IN SITU
NUCLEATION AND GROWTH STUDIES

A. Experimental Techniques: Chemical Vapor Deposition and Gas Reactions

A1. H. Hashimoto, T. Naiki, T. Eto, K. Fujiwara, M. Watanabe, and Y. Nagatama, p 181 in reference G2 (6th Int'l, Kyoto, 1966), "Specimen Chamber for Observing the Reaction Process with Gas at High Temperature."

A2. H. Hashimoto, T. Naiki, T. Eto, and K. Fujiwara, Japan. J. Appl. Phys. 7, 946 (1968). "High Temperature Gas Reaction Specimen Chamber for an Electron Microscope."

A3. H. Hashimoto, K. Tanaka, and E. Yoda, Japan. J. Electronmicroscopy 6, 8 (1958). "A Specimen Treating Device at High Temperature for the Electron Microscope."

A4. T. Ito and K. Hiziya, Japan. J. Electronmicroscopy 6, 4 (1958). "A Specimen Reaction Device for the Electron Microscope and its Applications." (JEM) See also Reference B5.

A5. T. Gabor and J. M. Blocher, J. Electrochem. Soc. 114, 214C (1967). (Abstract only, see reference B8 for details.) "In-Situ Transmission Electron Microscopic Study of Crystal Growth by Chemical Vapor Deposition."

A6. U. Valdre, p 131 in reference G11 (27th EMSA, St. Paul, 1969). "Special Specimen Holders for a High Voltage Electron Microscope."

A7. H. Hashimoto and T. Naiki, J. Appl. Phys. 37, 3936 (1966) (24th EMSA). "High Temperature Gas Reaction Specimen Chamber" (Abstract only, see references A1 and A2).

A8. G. Shimaoka, J. Phys. Soc. Japan 17, 306 (1962). Suppl. B11, Proc. International Conf. on Magnetism and Crystallography, Vol. II. "Electron Diffraction Specimen Holder for the Study of Gas-Metal Reaction at Elevated Temperature."

A9. J. R. Fryer, Siemens Review XXV (2nd Special Issue) 13, (1968). "The Direct Observation of Gas-Solid Reactions Inside the Electron Microscope." (Siemens, see also reference A14).

A10. D. L. Allinson, p 169 in reference G1 (7th Int'l, Grenoble, 1970). "Environmental Cell for Use in a High Voltage Electron Microscope."

A11. J. C. Mills and A. F. Moodie, Rev. Sci. Inst. 39, 962 (1968). "Multi-purpose High Resolution Stage for the Electron Microscope."

A12. J. Escaig and C. Sella, Compt. Rend. 268, 532 (1969). "Nouvelle Micro-chambre Pour Observation en Microscopie Électronique a Haute Température et sous Atmosphère Controlée."

A13. J. Escaig, Compt. Rend. 262, 538 (1966). "Porte-objet Permettant L'Observation au Microscope Électronique de Spécimens Placés dan une Atmosphère Contrôlée."

A14. J. R. Fryer, Ph.D. Thesis, U. Glasgow (1969). "Heated Gas Reaction Chamber for Siemens Electron Microscope."

A15. P. Sung, Rev. Sci. Inst. 42, 1731 (1971). "Hot Stage and Environmental Cell on a High Voltage Electron Microscope."

A16. G. Dalmai-Imelik and C. Leclercq, p 359 in reference G1. (7th Int'l, Grenoble, 1970). "Etude de L'Evolution de Catalyseurs au cours de leur Preparation et de Reactione Catalytiques."

A17. J. Escaig and C. Sella, p 177 in reference G2 (6th Int'l, Kyoto, 1966). "Cellule Porte-Objet Permettant L'Observation de Specimen Chauffes Sous Atmosphere Contrôlée."

A18. J. L. Kenty, p 624 in reference G15 (30th EMSA, Los Angeles, 1972). "Preliminary EM6 Modifications for In Situ Chemical Vapor Deposition."

A19. P. R. Swann, in reference G17 (5th European, Manchester, 1972). "Side Entry Single Tilt Specimen Holders for Heating and Stress Corrosion Crac ing of Electron Microscope Specimens."

A20. D. L. Allinson, A. W. O. Gosnold and M. S. Loveday, in reference G17 (5th European, Manchester, 1972). "Modified Environmental Cell for use in a High Voltage Electron Microscope."

A21. G. L. Price and J. A. Venables, in reference G17 (5th European, Manchester, 1972). "Apparatus for In Situ Nucleation Studies in the T.E.M."

A22. P. R. Swann and N. J. Tighe, p 436 in reference G17 (5th European, Manchester, 1972). (See also ref E36) "Voltage and Pressure Dependence of the Electron Transmission through Various Gases."

B. Results: Chemical Vapor Deposition and Gas Reactions

B1. H. Hashimoto and M. Ishii, p 515 in reference G2 (6th Int'l, Kyoto, 1966). "Metallic Oxide Crystals Grown in Heated Thin Films of Copper and α-Brass."

B2. H. Hashimoto, T. Naiki, T. Eto, and K. Fujiwara, p. 495 in reference G2 (6th Int'l, Kyoto, 1966). "Electron Cinematographic Observations of Whisker Growth of Molybdenum Oxides and Copper."

B3. H. Hashimoto, K. Tanaka, K. Kobayashi, S. Shimadzu, T. Naiki and M. Mannami, p 477 in reference G4 (4th Int'l, Berlin, 1958). "Cinematographic Study of the Growth Process of Oxide Crystals in the Electron Microscope."

B4. H. Hashimoto, A. Kumao, T. Eto, and K. Fujiwara, J. Crystal Growth 7, 113 (1970). "Drops of Oxides on Tungsten Oxide Needles and Nuclei of Dendritic Crystals."

B5. K. Hiziya, H. Hashimoto, M. Watanabe, and K. Mihama, p 80 in reference G4 (4th Int'l, Berlin, 1958). "Gas Reaction on the Specimen."

B6. H. Hashimoto, T. Naiki, M. Mannami, and K. Fujita, Structure and Property of Thin Films, Ed. C. A. Neugebauer, J. B. Newkirk, and D. A. Verymilyea (Wiley, New York, 1959), p 71. "Electron Microscope Study by Cine Film on the Formation of Thin Oxide Films."

B7. T. Gabor and J. M. Blocher, J. Appl. Phys. 40, 2696 (1969). "In-Situ Electron Microscopic Study of the Growth of Iron Whiskers by Chemical Vapor Depositions."

B8 T. Gabor and J. M. Blocher, J. Vac. Sci. Technol. 6, 73 (1969). "Non-equilibrium Chemical Reactivity of Polycrystalline Iron Foils."

B9. T. Gabor and J. M. Blocher, J. Vac. Sci. Technol. 6, 815 (1969). Errata: J. Vac. Sci. Technol. 6, 969 (1969). "In-Situ Transmission Electromicroscopic Study of Crystal Growth by Chemical Vapor Deposition."

B10. R. K. Hart and J. K. Maurin, p 539 in reference G2 (6th Int'l, Kyoto, 1966). "Growth of Oxide Nuclei on Iron."

B11. R. F. W. Pease, A. N. Broers, and R. A. Ploc, p 389 in reference G6 (6th Int'l, Kyoto, 1966) (3rd European, Prague, 1964). "Scanning Electron Microscopy of the Growth and Subsequent Sectioning of Sputtering of Iron Oxide Films."

B12. S. A. Jansson, p 73 in reference G6 (3rd European, Prague, 1964). "Continuous Observation in the Electron Microscope of the Oxidation of 20 Cr-35Ni Stainless Steel."

B13. G. Shimaoka, J. Electrochem. Soc. 110, 1177 (1963). "Structure of Oxide Films Formed on Individual Crystal Grains of Stainless Steel."

B14. J. Escaig and C. Sella, p 241 in reference G5 (4th European, Rome, 1968). "Application d'une Nouvelle Cellule à Atmosphere Controlee à l'etude de Quelques Problemes d'Oxydation et de Depot par Decomposition Thermique en Phase Vapeur."

B15. J. Escaig and C. Sella, Compt. Rend. 271, 84 (1970). "Nucleation of Croissance Epitaxique des Couches de Fer Préparées par Décomposition Thermique de $Fe(CO)_5$."

B16. N. Sasaki and R. Ueda, p 479 in reference G4 (4th Int'l, Berlin, 1958). "Electron Microscopic and Diffraction Study on the Progress of Reduction of Tungsten Trioxide."

B17. N. Sasaki and R. Ueda, p 463 in reference G9 (3rd Int'l, London, 1954). "The Electronmicroscopic and Micro-diffraction Observation In Situ of Changes in Solids (Reduction of MoO_3)."

B18. R. K. Hart and J. K. Maurin, Surface Science 20, 285 (1970). "The Nucleation and Growth of Oxide Islands on Aluminum."

B19. F. S. Feates, H. Morley, and P. S. Robinson, p 295 in reference G1 (7th Int'l, Grenoble, 1970). "Controlled Atmosphere Electron Microscopy."

B20. F. S. Feates, P. S. Harris, R. T. K. Baker, p 357 in reference G1 (7th Int'l, Grenoble, 1970). "Catalytic Oxidation of Graphite by Continuous Electron Microscopic Observation."

B21. R. S. Gordon and W. D. Kingery, J. Amer. Ceram. Soc. 49, 654 (1966) and 50, 8 (1967). "Thermal Decomposition of Brucite: I, Electron and Optical Microscope Studies; II, Kinetics of Decomposition in Vacuum."

B22. J. F. Goodman, Proc. Roy. Soc. A247, 346 (1958). "The Decomposition of Magnesium Hydroxide in an Electron Microscope."

B23. P. L. Burnett, W. R. Mitchell, and C. L. Houck, p 446 in reference G12 (26th EMSA, New Orleans, 1968). "Observations of the Thermal Decomposition of Brucite."

B24. L. Ponsolle, G. Wrobel, D. Debut, and J. C. Mutte, p 355 in reference G1 (7th Int'l, Grenoble, 1970). "Enregistrement Cinematographique de Reactions Chemiques Solide-Gaz Suives au Microscope Electronique."

B25. C. A. English and J. A. Venables, p 362 in reference G17 (5th European, Manchester, 1972). "The Use and Advantages of a Pressure Cell in Studying Thin Films of Condensed Gases."

B26. J. A. Venables, p 344 in reference G17 (5th European, Manchester, 1972). "In Situ Experiments in Electron Microscopes."

B27. H. Hashimoto, A. Kumao, T. Etoh, K. Fujiwara, M. Maeda, p 461 in reference G1 (7th Intl, Grenoble, 1970). "Electron Microcinematographic Observations of Nucleation of Dendritic Tungsten Oxide Crystals by VLS Mechanism."

C. Experimental Techniques: Physical Vapor Deposition

C1. U. Valdre, E. A. Robinson, D. W. Pashley, M. J. Stowell, and T. J. Law, J. Phys. 3E, 501 (1970). "An Ultra-High Vacuum Electron Microscope Specimen Chamber for Vapor Deposition Studies."

C2. D. W. Pashley, M. J. Stowell, E. A. Robinson, T. J. Law, and U. Valdre, p 387 in reference G5 (4th European, Rome, 1968). "An UHV Specimen Chamber and Its Application to the Direct Study of Epitaxial Growth."

C3. U. Valdre, D. W. Pashley, E. A. Robinson, M. J. Stowell, K. J. Routledge, and R. Vincent, p 155 in reference G2 (6th Int'l, Kyoto, 1966). "An Ultra-High Vacuum Specimen Chamber with Facilities for Growing Thin Films."

C4. R. D. Moorhead and H. Poppa, p 116 in reference G11 (27th EMSA, St. Paul, 1969). "An Ultrahigh Vacuum Specimen Chamber for In-Situ Electron Microscopy of Vapor Deposition Processes."

C5. H. Poppa, Phil. Mag. 7, 1013 (1962). "Sputtering Experiments Inside the Electron Microscope."

C6. H. Poppa, p GG14 in reference G3 (5th Int'l, Philadelphia, 1962). "In-Situ Epitaxy Studies."

C7. H. Poppa, J. Vac. Sci. Technol. 2, 42 (1965). "Progress in the Continuous Observation of Thin Film Nucleation and Growth Processes by Electron Microscopy."

C8. H. Poppa, Trans. Ninth Annual Symposium of the American Vacuum Society, Ed. G. H. Bancroft (MacMillan), New York, 1962), p 21. "A Method for High Resolution Studies of Thin Film Growth."

C9. D. N. Braski, J. Vac. Sci. Technol. 7, 164 (1970). "High Vacuum Evaporation Stage for an Electron Microscope."

C10. D. N. Braski, J. R. Gibson, and E. H. Kobisk, Rev. Sci. Inst. 39, 1806 (1968). "Ultrahigh Vacuum Electron Microscope."

C11. C. W. B. Grigson, W. C. Nixon, and F. Tothill, p 157 in reference G2 (6th Int'l, Kyoto, 1966). "An Ultra High Vacuum Transmission Electron Microscope (EM6)."

C12. F. C. S. Tothill, W. C. Nixon, and C. W. B. Grigson, p 229 in reference G5 (4th European, Rome, 1968). "Ultrahigh Vacuum Modification of an AEI-EM6 Electron Microscope for Studies of Nucleation in Evaporated Films."

C13. A. E. Curzon and K. Kimoto, J. Sci. Inst. 40, 601 (1962). "An Evaporator for Use in an Electron Microscope (JEM 6A)."

C14. A. Barna, P. B. Barna, and J. F. Pōcza, Vacuum 17, 219 (1967). "Design of a New Vacuum Deposition Specimen Holder for an Electron Microscope Operating at 10^{-8} torr (JEM 6A)."

C15. F. Gronland, p 257 in reference G5 (4th European, Rome, 1968). "Electron Diffraction in High Vacuum."

D. Results: Physical Vapor Deposition

D1. M. J. Stowell, T. J. Law, and J. Smart, Proc. Roy. Soc. (London) A318, 231 (1970). "The Growth Structure, Melting, and Solidification of Lead Deposits on Molybdenite and Carbon Substrates.

D2. M. J. Stowell and T. J. Law, phys. stat. sol. 25, 139 (1968). "The Growth and Defect Structure of Gold Films Formed on Molybdenite in Ultra-High Vacuum."

D3. D. W. Pashley and M. J. Stowell, p 487 in reference G2 (6th Int'l, Kyoto, 1966). "Structural Changes Occurring During the Growth of Evaporated Metal Films."

D4. D. W. Pashley and M. J. Stowell, J. Vac. Sci. Technol. 3, 156 (1966). "Nucleation and Growth of Thin Films as Observed in the Electron Microscope."

D5. M. H. Jacobs, D. W. Pashley, and M. J. Stowell, Phil. Mag. 13, 129 (1966). "The Formation of Imperfections in Epitaxial Gold Films."

D6. D. W. Pashley, M. J. Stowell, M. H. Jacobs, and T. J. Law, Phil. Mag. 10, 127 (1964). "The Growth and Structure of Gold and Silver Deposits Formed by Evaporation Inside an Electron Microscope."

D7. G. A. Bassett, Condensation and Evaporation of Solids, Ed. E. Rutner, P. Goldfinger, and J. P. Hirth (Gordon and Breach, New York, 1962), p 599. "Continuous Electron Microscope Study of Vacuum Evaporated Metal Films,:

D8. D. W. Pashley and M. J. Stowell, p GG 1 in reference G3 (5th Int'l, Philadelphia, 1962). "The Growth of Evaporated Silver Layers Inside an Electron Microscope."

D9. G. A. Bassett, p 270 in reference G7 (2nd European, Delft, 1960). "Continuous Observation of the Growth of Vacuum Evaporated Metal Films."

D10. H. Poppa, Zeit. Naturforsch. 19a, 835 (1964). "In-Situ Studies of Epitaxial Thin Film Growth."

D11. H. Poppa, J. Appl. Phys. 38, 3883 (1967). (See Also National Aeronautics and Space Agency Technical Note D-4506, 1968). "Heterogeneous Nucleation of Bi and Ag on Amorphous Substrates (In-Situ Electron Microscopy)."

D12. A. E. Curzon and K. Kimoto, p 507 in reference G2 (6th Int'l, Kyoto, 1966). "The Condensation of Liquid Lead on Molybdenite in an Electron Microscope."

D13. B. Coopersmith, A. E. Curzon, K. Kimoto, and N. D. Lisgarten, Basic Problems in Thin Film Physics, Ed. R. Niedermayer and H. Mayer (Vandenhoeck and Ruprecht, Gottengen, 1966), p 83. "The Condensation of Lead Inside an Electron Microscope."

D14. T. A. McLaughlan, R. S. Sennett, and G. D. Scott, Canadian J. Research 28A, 530 (1950). "Continuous Observations with the Electron Microscope on the Formation of Evaporated Films of Silver, Gold, and Tin."

D15. A. Barna, P. B. Barna, and J. F. Pōcza, p 445 in reference G1 (7th Int'l, Grenoble, 1970). "Simultaneous Investigation of Structure and Electrical Properties of Vacuum Deposited Thin Films by In-Situ Electron Microscopy."

D16. T. E. Hutchinson, p 376 in reference G12 (26th EMSA, New Orleans, 1968). "In situ Electron Microscope Investigations of the Growth and Structure of Thin Films."

D17. H. Poppa, p 378 in reference G12 (26th EMSA, New Orleans, 1968). "Thin Film Nucleation and Growth Under Controlled Conditions."

D18. E. F. Pōcza, A. Barna, and P. Barna, Basic Problems in Thin Film Physics, Ed. N. Niedermayer and H. Mayer (Vandenhoeck and Ruprecht, Gottingen, 1966) p 153. "Nucleation and Growth Processes in Vacuum Deposited Germanium Films."

D19. T. E. Hutchinson and D. Sherman, U. Minnesota Annual Technical Progress Report III - COO-1790, 3 Jan. 1971; IV - COO-1790 - 4 Jan. 1972, "In Situ Electron Microscope Investigation of the Nucleation and Growth of Sputtered Thin Films."

D20. D. M. Sherman and T. E. Hutchinson, p 516 in reference G10 (28th EMSA, Houston, 1970). "Nucleation and Early Growth of Sputtered Thin Films."

D21. R. D. Moorhead, H. Poppa, p 516 in reference G15 (30th EMSA, Los Angeles, 1972). "In Situ Deposition of Gold on MgO."

D22. H. Sato and S. Shinozaki, J. Vac. Sci. and Technol. 8, 159 (1971). "Morphology of Nuclei and Epitaxial Behavior of Au and Ag on MgO."

D23. H. Sato, S. Shinozaki, and L. J. Cicotte, J. Vac. Sci. and Technol. 6, 62 (1969). "Direct Observation of Epitaxy on MgO."

D24. S. Shinozaki, G. Honjo, and H. Sato, p 505 in reference G2 (6th Int'l, Kyoto, 1966). "Direct Observation of the Epitaxy of Ag on MgO Substrates."

D25. S. Shinozaki and H. Sato, J. Appl. Phys. 43, 701 (1972) "Cleaving of MgO inside an Electron Microscope."

D26. K. Yagi, K. Kobayashi, K. Takayanagi, and G. Honjo, p 439 in reference G1 (7th Int'l, Grenoble, 1970). "In Situ Observation of Epitaxial Growth of Metals and Non-metals."

D27. J. F. Pocza, A. Barna, and P. B. Barna, J. Vac. Sci. Technol. 6, 472 (1969). "Formation Processes of Vacuum Deposited Indium Films and Thermodynamical Properties of Submicroscopic Particles Observed by In Situ Electron Microscopy."

E. (1-19) Related Topics: Gas Inlet Devices

E1. D. W. Pashley and A. E. B. Presland, Phil. Mag. 7, 1407 (1962). "The Movement of Dislocations During the Observation of Metal Films Inside an Electron Microscope."

E2. H. G. Heide, J. Cell Biology 13, 147 (1962). "Electron Microscopic Observation of Specimens Under Controlled Gas Pressure."

E3. H. G. Heide, p 87 in reference G4 (4th Int'l, Berlin, 1958). "Die Objektverschmutzung und ihre Verhütung."

E4. I. G. Stoyanova and G. A. Mikhailovski, Biofizika 4, 483 (1959).

E5. J. L. Williams, K. Heathcote, and E. J. Greer, p 100 in reference G11 (27th EMSA, St. Paul, 1969). "A New 1000 kV Electron Microscope."

E6. I. G. Stojanowa, p 82 in reference G4 (4th Int'l, Berlin, 1958). "Ein Kammer für die Untersuchung von Objekten mit Gasumgebung (A Chamber for the Examination of Objects Surrounded by Gas)."

E7. H. G. Heide, Naturwissenschaften 47, 313 (1960). "Electron Microscopy of Objects Under Atmospheric Pressure or Pressures Which Prevent Drying of Objects."

E8. V. R. Matricardi, G. G. Hausner, and D. F. Parsons, p 542 in reference G10 (28th EMSA, Houston, 1970). "Hydration Chamber for Jeolco 200kv Microscope."

E9. R. C. Moretz, G. D. Hausner, and D. F. Parsons, p 544 in reference G10 (28th EMSA, Houston, 1970). "Studies on Water in the Hydration Chamber of a Modified Electron Microscope."

E10. R. C. Moretz, G. G. Hausner, and D. F. Parsons, p 44 in reference G14 (29th EMSA, Boston, 1971). "New Design for a Differentially Pumped Hydration Chamber for a Siemens 1A."

E11. D. F. Parsons and R. C. Moretz, p 497 in reference G1 (7th Int'l, Grenoble, 1970). "Microscopy and Diffraction of Water in the Electron Microscope."

E12. D. L. Allinson, p 169 in reference G1 vol I (7th Int'l, Grenoble, 1970). "Environmental Cell for Use in a High Voltage Electron Microscope."

E13. A. Fukami, K. Adachi, and M. Katoh, p 263 in reference G2 (6th Int'l, Kyoto, 1966). "On a Study of New Micro Plastic Grid and its Applications."

E14. A. Fukami, T. Etoh, N. Ishihara, M. Katoh, and K. Fujiwara p 171 in reference G1 (6th Int'l, Kyoto, 1966). "Pressurized Specimen Chamber for Electron Microscope."

Preceding page blank

E15. G. Dupouy, F. Perrier, and L. Durrieu, Comptes Rendus 251, 2836 (1960). "L'Observation de la matière vivante au moven d'un microscope électronique fonctionnant sans tres haute tension." (The Observation of Living Material by Means of an Electron Microscope Operating at Very High Voltage.)"

E16. G. Dupouy, F. Perrier, and L. Durrieu, Comptes Rendus 254, 3786 (1962). "L'Observation des objets en milieu gazeur. Application à l'étude de la contamination dans le microscope électronique." (The Observation of Objects in the Midst of GaAs. Application to the Study of Contamination in the Electron Microscope."

E17. P. R. Ward and R. F. Mitchell, p 44 in reference G16 (25th EMAG, 1971). "An Electron Microscope Environmental Specimen Chamber."

E18. A. Fukami and M. Katoh, p 612 in reference G15 (30th EMSA, Los Angeles, 1972). "Construction and Application of Environmental Cell."

E19A. V. R. Matricardi, J. Subjeck, and D. F. Parsons, p 180 in reference G15 (30th EMSA, Los Angeles, 1972). "Hydration Stages - Achievements and Obstacles."

E19B. A. Fukami and K. Adachi, J. Electron Microscopy 14, 112 (1965). "A New Method of Preparation of a Self Perforated Micro Plastic Grid and Its Application."

E19C. A. Fukami, K. Adachi, and M. Katoh, J. Electron Microscopy 21, 99 (1972). "Micro Grid Techniques and Their Contribution to Specimen Preparation Techniques for High Precisions Work."

E. (20-39) Related Topics: Ion Pumping and Residual Gas Analysis

E20. R. E. Hartman, H. Akahori, C. Garrett, R. S. Hartman, and P. L. Ramos, p 80 in reference G11 (27th EMSA, St. Paul, 1969). "A Prototype High Vacuum Electron Microscope."

E21. C. J. Calbick and R. E. Hartman, p 82 in reference G11 (27th EMSA, St. Paul, 1969). "Residual Gas Reaction in the Electron Microscope: II. The Design of a Gas Control Chamber for Quantitative Observations."

E22. J. A. Maliakal, p 78 in reference G11 (27th EMSA, St. Paul, 1969). "Application of Ion Pumps for Electron Microscopes."

E23. R. E. Hartman and R. S. Hartman, p 159 in reference G2 (6th Int'l, Kyoto, 1966). "Residual Gas Analysis in an Ion Pumped Electron Microscope."

E24. R. K. Hart, T. F. Kassner, and J. K. Maurin, p 161 in reference G2 (6th Int'l, Kyoto, 1966). "Residual Gas Analysis in an Auxiliary Pumped Siemens Electron Microscope."

E25. R. E. Hartman and R. S. Hartman, J. Appl. Phys. 37, 3936 (1966). (Abstract only, 24th EMSA). "Conversion of Two Electron Microscopes to High Vacuum Operation."

E26. R. B. Marcus, C. J. Calbick, and T. T. Sheng, Rev. Sci. Inst. 41, 1319 (1970). "Improvements in an Electron Microscope for Clean, Quiet, Vibrationless Operation."

E27. R. B. Marcus, C. J. Calbick, and T. T. Sheng, p 163 in reference G1 (7th Int'l, Grenoble, 1970). "Improvements in an Electron Microscope for Clean, Quiet Vibrationless Operation."

E28. R. E. Hartman and R. S. Hartman, Lab. Investigation 14, 409 (1965). "Elimination of Potential Sources of Contaminating Material."

E29. R. E. Hartman and R. S. Hartman, p 74 in reference G14 (29th EMSA, Boston, 1971). "Residual Gas Reactions in the Electron Microscope: IV. A Factor in Radiation Damage."

E30. R. E. Hartman, R. S. Hartman and P. L. Ramos, p 292 in reference G12 (26th EMSA, New Orleans, 1968). "Residual Gas Reactions in the Electron Microscope: I. Qualitative Observations on the Water Gas Reaction."

E31. D. N. Braski, p 314 in reference G12 (26th EMSA, New Orleans, 1968). "A High Vacuum Electron Microscope."

E32. E. A. Buvinger, p 348 in reference G12 (26th EMSA, New Orleans, 1968). "Background Gas Reduction in the Electron Microscope."

E33. R. K. Hart, T. F. Kassner, and J. K, Maurin, Phil. Mag. 21, 453 (1970). "The Contamination of Surfaces during High Energy Electron Bombardment."

E34. J. R. Parsons and C. W. Hoelke, Can. J. Phys. 44, 2685 (1966). "Electron Microscopic Observation of Atomic Planes and Atomic Positions in Germanium."

E35. G. M. Greene, J. W. Sprys, and C. D. Melvin, p 620 in reference G15 (30th EMSA, Los Angeles, 1972). "Reduction of Contamination Rates in Electron Microscopes."

E36. P. R. Swann and N. J. Tighe, in reference G17 (5th European, Manchester, 1972). "Performance of a Differentially Pumped Environmental Cell in the AEI EM7." See also ref. A27.

E. (40-59) Related Topics: Specimen Heating Stages

E40. A. W. Agar and J. H. Lucas, p E2 in reference G3 (5th Int'l, Philadelphia, 1962). "Use of a New Heating Stage for the Electron Microscope."

E41. J. O. McPartland, p E3 in reference G3 (5th Int'l, Philadelphia, 1962). "A High Temperature Stage for Transmission Electron Microscopy."

E42. N. Takahashi, T. Takeyama, K. Ito, T. Ito, K. Mihama, and M. Watanabe, Japan. J. Electronmicroscopy 4, 16 (156). "High Temperature Furnace for the Electron Microscope (JEM 5)."

E43. N. Sasaki and R. Uyeda, Rev. Sci. Instr. 23, 136 (1952). "A Specimen Treating Adaptor for the Electron Microscope."

E44. I. Okazaki, M. Watanabe, and K. Mihama, p 93 in reference G4 (4th Int'l, Berlin, 1958). "Improvement of the Specimen Heating Device for the Electron Microscope."

E45. K. Itoh, T. Itoh, and M. Watanabe, p 658 in reference G9 (3rd Int'l London, 1954).

E46. M. J. Whelan, p 96 in reference G4 (4th Int'l, Berlin, 1958). "A High Temperature Stage for the Elmiskop I."

E47. W. Loebe, O. Schott and F. Wilko, p 131 in reference G7 (2nd European, Delft, 1960). "Objektheizungseinvichtung zum Elmiskop I (Specimen Heating Stage for the Siemens)."

E48. R. M. Fisher, P. R. Swann, and J. Nutting, p 131 in reference G7 (2nd European, Delft, 1960). "A New Objective Pole-Piece and Specimen Heating Stage for the Elmiskop."

E49. U. Valdre, J. Sci. Instrum. 42, 853 (1965). "A Double Tilting Heating Stage for an Electron Microscope."

E50. U. Valdre, p 165 in reference G2 (6th Int'l, Kyoto, 1966). "A Universal Specimen Stage and Combined Cartridges for an Electron Microscope."

E51. U. Valdre, Il Nuovo Cimento X53B, 157 (1968). "Combined Cartridges and Versatile Specimen Stage for Electron Microscopy.

E52. D. Jones, p 662 in reference G9 (3rd Int'l, London, 1954). "A Specimen Furnace for the Reflection Electron Microscope."

E53. I. W. Sprys and P. C. J. Gallagher, p 312 in reference G12 (26th EMSA, New Orleans, 1968). "A New Hot Stage for the Philips EM200 and its Calibration."

E54. V. Valdrè, p 317 in reference G17 (5th European, Manchester, 1972). "General Considerations on Specimen Stages."

E. (60-79) Related Topics: Cinematography

E60. V. A. Phillips, Phil. Mag. 5, 571 (1960). "Direct Observation of Defects in Evaporated Silver."

E61. R. W. Horne and R. H. Ottewill, p 140 in reference G4 (4th Int'l, Berlin, 1958). "Cinematographic Studies on the Interaction of Electrons with Microcrystals of Silver Iodide."

E62. K. F. Hale, M. H. Brown, and D. L. Allinson, p 297 in reference G1 (7th Int'l, Grenoble, 1970). "Resolution and Contrast Experiments with Various Arrangements of Environmental Cell Windows at High Voltages."

E63. E. Sugata, Y. Nishitani, S. Kaneda, M. Tateishi, and H. Yoloya, p 452 in reference G9 (3rd Int'l, London, 1954). "Fundamental Researches for Observing Specimens in Gas Layers."

E64. F. D. Lugton and C. E. Warble, Rev. Sci. Instr. 41, 1793 (1970). "High Resolution Cinematography at High Temperature in the Electron Microscope."

E65. M. J. Whelan, P. B. Hirsch, R. W. Horne, and W. Bollmann, Proc. Royal Soc. (London) A240, 524 (1957). "Dislocations and Stacking Faults in Stainless Steel."

E66. K. Anderson, P. B. Kenway, p 244 in reference G12 (26th EMSA, New Orleans, 1968). "External Photography of the Microscope Image."

E67. J. W. S. Hearle, D. J. Clarke, B. Lomas, D. A. Reeves, and J. T. Sparrow, p 210 in reference G16 (25th EMAG, 1971). "A Simple Method of Recording Dynamic Events in the SEM Using a 16 mm Camera."

M. Heerschap and R. DeCat, p 170 in reference G17 (5th European, Manchester, 1972). "Direct Filming of Transient Phenomena with a Closed TV Circuit as Viewfinder."

F. Related Topics: Cooling Stages (Partial Listing)

F1. J. A. Venables and D. J. Ball, Proc. Royal Society, London A322, 331 (1971). "Nucleation and Growth of Rare Gas Crystals."

F2. J. A. Venables, Phil. Mag. 21, 147 (1970). "Electron Micrscopy and Diffraction of Solid αN_2."

F3. J. A. Venables, D. J. Ball, and G. J. Thomas, J. Phys. (Sci. Instr.) E1, 121 (1968). "An Electron Microscope Liquid Helium Stage for Use with Accessories."

F4. D. J. Ball and J. A. Venables, p 239 in reference G5 (4th European, Rome, 1968). "The Use of a Pressure Cell for Studying Condensed Gases."

F5. J. A. Venables and D. J. Ball, J. Crystal Growth, 3, 4, 180 (1969). "Microstructure of Condensed Gases."

F6. J. A. Venables, p 175 in reference G2 (6th Int'l, Kyoto, 1966). "A Goniometer Stage for Use at Liquid Helium Temperatures."

F7. J. A. Venables and D. J. Ball, p 333 in reference G2 (6th Int'l, Kyoto, 1966). "Defects in Rare Gas Crystals."

F8. U. Valdre and M. J. Goringe, J. Phys.(Sci. Instr.) E3, 336 (1970). "An Improved Liquid Helium Stage for an Electron Microscope."

F9. U. Valdre and M. J. Goringe, J. Sci. Instr. 42, 268 (1965). "A Liquid Helium Cooled Goniometer Stage for an Electron Microscope."

F10. U. Valdre, p 61 in reference G6 (3rd European, Prague, 1964). (See also references E50 and E51). "A Double Tilting Liquid Helium Cooled Object Stage for the Siemens Electron Microscope."

F11. P. R. Swann, in reference G11 (27th EMSA, St. Paul, 1969). "A Tilting Cold Stage for the AEI EM802."

F12. R. M. J. Cotterill, p 63 in reference G6 (3rd European, Prague, 1964). "A Liquid Helium Stage for the Siemens Elmiskop I."

F13. G. R. Piercy, R. W. Gilbert and L. M. Howe, J. Sci. Instr. 40, 487 (1963). "A Liquid Helium Cooled Finger for the Siemens Electron Microscope."

F14. H. Boersch, O. Boslanjoglo, B. Lischke, H. Niedrig, and L. Schmidt, p 167 in reference G2 (6th Int'l, Kyoto, 1966). "Electron Microscopy with Liquid Helium Cooled Stages."

F15. N. Kitamura, O. N. Srivastava, and J. Silcox, p 169 in reference G2 (6th Int'l, Kyoto, 1966). "A Tilt and Magnetic Stage for Operation at Liquid Helium Temperatures."

F16. H. Watanabe, I. Ishikawa. H. Kojima, and T. Suzuki, p 171 in reference G2 (6th Int'l, Kyoto, 1966). "Liquid Helium Cooled Stage and Its Applications."

F17. C. A. English and J. A. Venables, p 48 in reference G16 (25th EMAG, 1971). "The Design of Pressure Cells for Studying Condensed Gases."

F18. M. Watanabe, F. Okazaki, G. Honjo, and K. Mihamo, p 90 in reference G4 (4th Int'l, Berlin, 1958). "Improvement of the Specimen Cooling Device for the Electron Microscope."

F19. H. G. Heide and K. Urban, p 107 in reference G1 (7th Int'l, Grenoble, 1970). "A Novel Specimen Stage for Temperatures Between 4°K and 300°K.

F20. H. G. Heide, Lab. Investigation 14, 4021/1140 (1965). "Techniques for the Prevention of Contamination of the Object."

F21. O. Bostanjoglo and B. Lischke, Z. Naturforschg 22a, 1620 (1967). "Elektronenmikroskopische Untersuchungen am Kondensierten Wasserstoff, Stickstoff, und Sauerstoff (Electron Microscopy and Diffraction of Solid H_2, N_2 and O_2)."

F22. K. J. Schulze and G. Schimmel, p 173 in reference G2 (6th Int'l, Kyoto, 1966). "Ancillary Devices for the Elmiskop I Enabling Simultaneous Tilting, Rotation, Cooling, and Irradiation with α Particles."

F23. U. Valdre and R. W. Horne, in reference G17 (5th European, Manchester, 1972. "A Freeze Drying and Low Temperature Stage for an Electron Microscope."

F24. B. W. Griffiths, C. A. Mills, and J. A. Venables, in reference G17 (5th European, Manchester, 1972). "A Versatile Liquid Helium Stage for the SEM."

F25. E. M. Horl, in reference G17 (5th European, Manchester, 1972). "Liquid Helium Stage for the SEM."

F26. D. M. Cort and J. W. Steeds, in reference G17 (5th European, Manchester, 1972). "A Liquid Helium Cooled Stage for the SEM."

F27. D. J. Ball and J. A. Venables, p 459 in reference G1 (7th Int'l, Grenoble, 1970). "In Situ Studies of Nucleation and Growth of Condensed Gas Crystals."

G. General References: Electron Microscopy Conferences

G1. Electron Microscopy 1970 (Seventh International Congress on Electron Microscopy, Grenoble, 1970), Ed. P. Favard (Societe Francaise de Microscopie Electronique, Paris 1970), Vol. 1, Methods and General Techniques. Vol. 2, Physics.

G2. Electron Microscopy 1966 (Sixth International Congress for Electron Microscopy, Kyoto, 1966), Edw. R. Uyeda (Maruzen Co., Tokyo, 1966). Vol. 1, Physics.

G3. Electron Microscopy (Fifth International Congress for Electron Microscopy, Philadelphia, 1962), Ed. S. S. Breese, (Academic Press, New York, 1962), Vol. 1, Physics and General Electron Microscopy.

G4. Fourth International Conference on Electron Microscopy (Berlin, 1958), Eds. W. Barqmann, G. Mollenstedt, H. Niehrs, R. Peters, E. Ruska, and C. Wolpers (Springer-Verlag, Berlin, 1960).

G5. Electron Microscopy (Proceedings of the Fourth European Regional Conference, Rome, 1968), Ed. D. A. Bocciarelli (Tipografia Poliglotta Vaticana, Rome, 1968).

G6. Electron Microscopy 1964 (Proceedings of the Third European Regional Conference, Prague, 1964), Ed. M. Titlbach (Publishing House of the Czechoslovak Academy of Sciences, Prague, and The Royal Microscopical Society, London, 1964), Vol. A, Physics.

G7. Proceedings of the (Second) European Regional Conference on Electron Microscopy (Delft 1960),Eds. A. L. Houwink and B. J. Spit (Nederlandse Vereniging voor Electronenmicroscopie, Delft. 1960), Vol. 1, Physics.

G8. Electron Microscopy (Proceedings of the Stockholm (First European Regional Conference, 1956), Eds. F. S. Sjostrand and J. Rhodin (Almquist and Wiksell, Stockholm, 1956).

G9. Third International Conference on Electron Microscopy (London, 1954), Eds. V. E. Cosslett and R. Roso. (Royal Microscopical Society, London, 1954).

G10. Proceedings 28th Annual Meeting Electron Microscopy Society of America. (Houston, 1970) Ed. C. J. Arceneaux (Claitor's Publishing Division, Baton Rouge, 1970).

G11. Proceedings 27th Annual Meeting Electron Microscopy Society of America. (St. Paul, 1969) Ed. C. J. Arceneaux (Claitor's Publishing Division, Baton Rouge, 1969).

G12. Proceedings 26th Annual Meeting Electron Microscopy Society of America. (New Orleans, 1968) Ed. C. J. Arceneaux (Claitor's Publishing Division, Baton Rouge, 1968).

G13. Proceedings 25th Annual Meeting Electron Microscopy Society of America. (Chicago, 1967) Ed. C. J. Arceneaux (Claitor's Publishing Division, Baton Rouge, 1967).

G14. Proceedings 29th Annual Meeting Electron Microscopy Society of America. (Boston, 1971) Ed. C. J. Arceneaux (Claitor's Publishing Division, Baton Rouge, 1971).

G15. Proceedings 30th Annual Meeting Electron Microscopy Society of America. (Los Angeles, 1972) Ed. C. J. Arceneaux (Claitor's Publishing Division, Baton Rouge, 1971).

G16. Proceedings of the 25th Anniversary Meeting of EMAG . Ed. W. C. Nixon (Institute of Physics, London, 1971.)

G17. Fifth European Congress on Electron Microscopy (Manchester, 1972). (The Institute of Physics and the Royal Microscopical Society, London, 1972).

APPENDIX 6

ELECTRON SCATTERING BY GASEOUS ATOMS

The presence of a gas phase near the specimen in an electron microscope causes unwanted electron scattering of the primary beam, resulting in a loss of resolution. More importantly, there is an intensity loss in the transmitted beam and, also, a background-intensity increase and partial destruction of contrast information because of multiply-scattered electrons, i.e., electrons originally scattered out of the primary beam but rescattered into the transmitted beam.

The beam intensity loss due to gas-phase scattering has been calculated and used in determining the upper limits of the gas pressure and gas layer thickness which can be tolerated in an in situ CVD experiment. These two related variables determine the dimensions of that portion of the specimen chamber which contains the substrate and the surrounding reactant gases, and through which the electron beam must pass.

The electron scattering for a single molecule is a function of the electron scattering cross-section σ for the molecule, which varies strongly with the energy of the incident electrons, and the number and distribution of electrons in the molecule. The total cross section for a volume of gas containing N atoms/cm^3 is

$$Q = N\sigma, \tag{1}$$

where Q has the units cm^2/cm^3. For a gas of molecular weight M and pressure P (torr)

$$Q = \frac{\sigma N_o}{M} = \frac{P\sigma N_o}{RT}, \tag{2}$$

where $N_o = 6.025 \times 10^{23}$ molecules/mole and R = 62,400 torr-cm/deg K-mole.

The product Qt determines the amount of scattering, where t is the thickness of gas through which the electron beam passes. The intensity lost from the primary beam, i.e., the beam intensity scattered outside the objective aperature, is

$$I = I_o e^{-Qt} = I_o e^{\frac{-(Pt)\sigma N_o}{RT}}, \tag{3}$$

where I_o is the electron beam intensity incident on the gas region under consideration.

The major uncertainty in Equation (3) is the proper value to use for Q (or σ). Experimental values for Q or σ are known for only a few elements and compounds and do not agree well with theoretical values. The values for SiH_4 and O_2 used for these calculations were obtained as follows. Measured σ values* (for 65KV electrons) for thin solid films of Be, C, SiO, Cr, Ge, Pd, Pt and U were plotted versus the number of electrons per molecule (Z) on a log-log plot. A linear relationship was obtained by least-squares curve fitting, as follows:

$$\sigma = 0.14 \times 10^{18} Z. \qquad (4)$$

Equation (4) can be used to estimate σ for SiH_4, O_2, and other gases of interest if the somewhat doubtful assumption is made that the electron scattering depends linearly on the number of electrons present in the molecule, independent of the number of atomic nuclei present. This assumption is valid to a first approximation only, for it is unlikely that the scattering for Si(Z = 14), for example, is 7/3 times that of C(Z=6) or 14 times that of H(Z=1). Nevertheless, the assumption does permit determination of an interrelationship between the two parameters P and t.

The use of Equation (4) yields $\sigma = 2.5 \times 10^{-18} cm^2$ for SiH_4(Z=18) and $\sigma = 2.2 \times 10^{-18} cm^2$ for O_2(Z=16). These are the best available estimates of σ for these materials but may still be in error.

The intensity loss which can be tolerated in practice before a noticeable resolution loss occurs in the electron microscope is not well known. At higher magnifications the limit to proper focusing is frequently provided by the low intensity of the electron beam, so scattering losses become more severe in that range of operation. An intensity loss of 50% is clearly unacceptable, and a loss of 10% is more likely a reasonable upper limit. An intensity difference of 1% is not noticeable in electron micrographs, so a loss of this magnitude is unimportant. Thus the maximum tolerable intensity loss due to gas-phase scattering appears to be between 1 and 10%.

*C. E. Hall, Introduction to Electron Microscopy (McGraw-Hill, New York, 1953), p. 246.

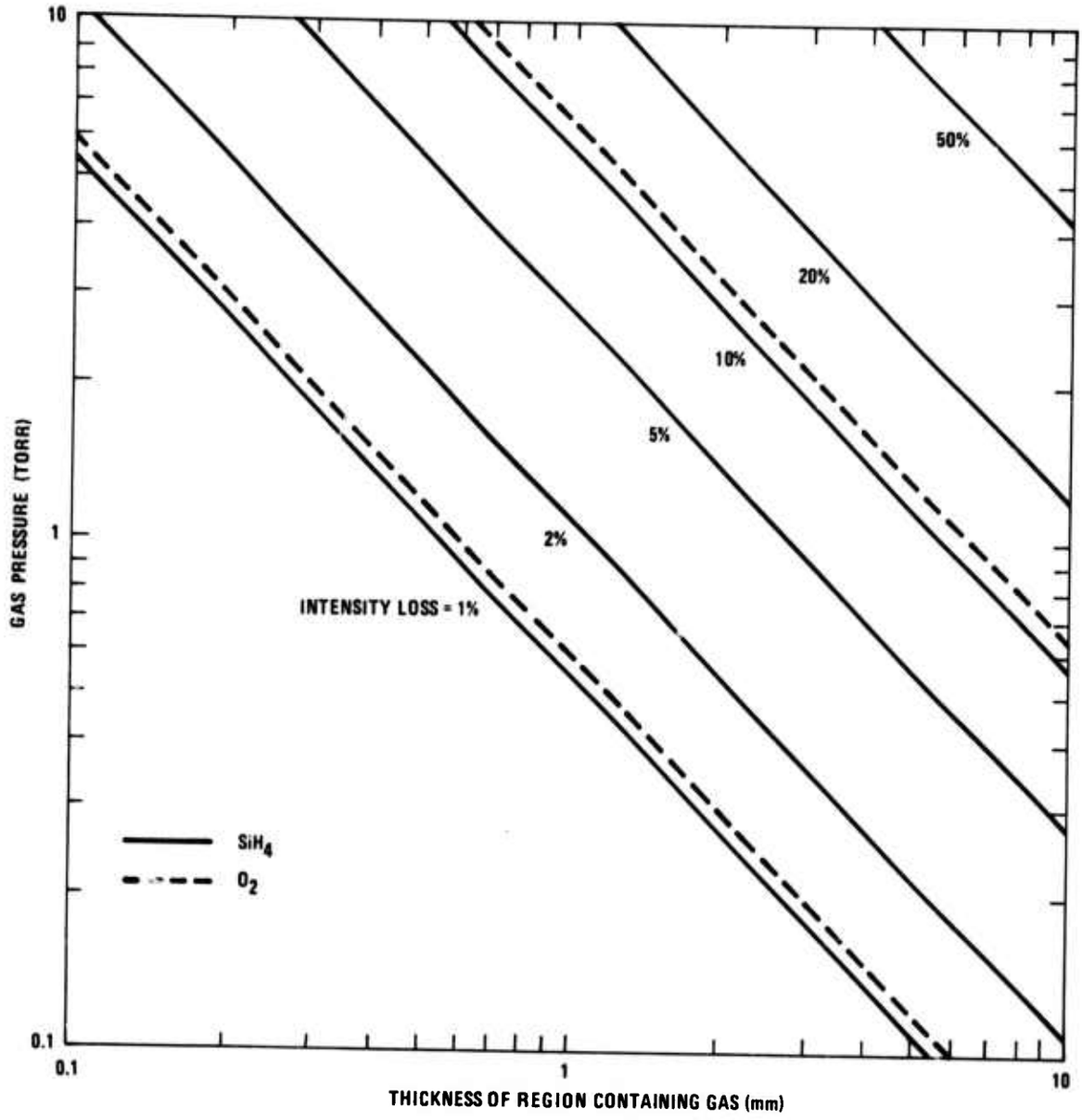

Figure 1. Relationship between Permissible Gas Pressure and Gas Region Thickness for SiH_4 (Solid Lines) and O_2 (Dotted Lines) for Various Electron Beam Intensity Losses[2]

APPENDIX 7

Reprinted from:
"30th Ann. Proc. Electron Microscopy Soc. Amer."
Los Angeles, Calif., 1972. C. J. Arceneaux (ed.).

PRELIMINARY EM6 MODIFICATIONS FOR IN SITU CHEMICAL VAPOR DEPOSITION*

J. L. Kenty

North American Rockwell Corporation, Electronics Group, Anaheim, CA 92803

An AEI EM6 electron microscope is being modified for in situ chemical vapor deposition. The objective is to observe the nucleation and growth kinetics and structure of silicon deposited by SiH_4 gas pyrolysis on substrates of sapphire (single crystal α-Al_2O_3).

An Edwards DCP2 thermoelectrically cooled baffle has been installed using a simple adapter which permitted attachment without drilling or cutting of the EM6 frame or vacuum system. Prior to installation the measured contamination rate was 240Å/min; afterward the contamination rate was less than 100Å/min.

An auxiliary pumping system is mounted to the left rear of the column and attached by a special stainless steel flexible bellows to the pumping port at the rear of the specimen chamber. The auxiliary system has an ultimate presure $<1 \times 10^{-6}$ torr, but the measured pressure in the specimen chamber was no better than 1×10^{-5} torr, due primarily to the high outgassing rate of the beam deflector coil immediately above the specimen chamber. Future modifications planned include completion of the differential pumping system by addition of an impedance tube between the specimen chamber and beam deflector stage and a permanent aperture between the specimen chamber and objective lens.

The bottom of the plate camera has been modified to accept a transmission phosphor screen of aluminized P-11 phosphor material. A 16 mm motion picture camera has been mounted directly below this screen so that sequences of in situ growth may be photographed. Normal operation of the microscope is not affected.

A CVD microchamber, Figure 1, has been constructed which sits in the objective lens at the normal 4 mm focal length position. A new center post, brazed into the extensively modified base of a standard AEI specimen holder, acts as one electrode. The center post contains a 100μm dia. hole which serves as a gas limiting aperture. An outer cylindrical electrode is fastened by screws to a fired lava insulator, which is similarly fastened to the base. A gas-tight seal is obtained by lapping the insulator, base, and outer electrode base flat. Once assembled, the outer electrode need not be disassembled to load the specimen. A removable disc containing a 100μm dia. aperture is held tightly in place by a threaded cap. The specimen is held between two resistively heated 200-mesh stainless steel grids attached to the electrodes by two #80 NM screws. The holder is inverted for loading permitting the specimen and removable aperture to be aligned with the fixed aperture. Gas is admitted to the microchamber through a flexible nickel bellows, flows through the annular space between the electrodes, and exhausts through the apertures. The space between apertures is 2 mm, which at a SiH_4 pressure of 2.9 torr corresponds to a mass thickness of 0.55 μg/cm^2, giving a 10% intensity loss assuming $\sigma = 2.5 \times 10^{-18}$ cm^2.

*This research sponsored by ARPA under Order 1585, monitored by USAMICOM, Redstone Arsenal, AL, under Contract DAAH01-70-C-1311.

Reprinted from:
"30th Ann. Proc. Electron Microscopy Soc. Amer."
Los Angeles, Calif., 1972. C. J. Arceneaux (ed.).

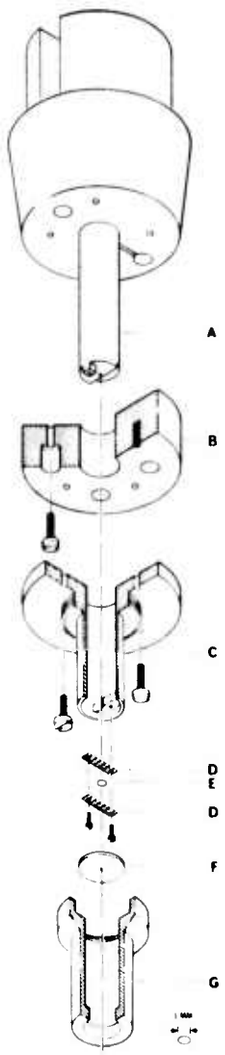

Figure 1. In Situ Chemical Vapor Deposition Microchamber. A, center electrode and gas limiting aperture; B, lava insulator; C, outer electrode; D, heating grids; E, sample; F, removable aperture; G, aperture cap.